METAMORPHISM AT WOODALL SHOALS

IN THE EASTERN BLUE RIDGE,

GEORGIA - SOUTH CAROLINA

by

CHARLES HOWARD FORTNER

(Under the direction of ALBERTO E. PATIÑO-DOUCE)

ABSTRACT

Metamorphic conditions were estimated for the Tallulah Falls Formation in the vicinity of Woodall Shoals on the Chattooga River on the Georgia–South Carolina border. Thermal peak metamorphic conditions of 700ºC, 6.25kbar, and $0.65<a_{H_2O}<1.0$ were estimated using a variety of geothermometers and geobarometers applied to amphibolite, amphibole-garnet-biotite gneiss, and sillimanite-biotite-gneiss. Results from this study confirm Barrovian metamorphism in the eastern Blue Ridge.

INDEX WORDS: Geothermometry, geobarometry, metamorphic conditions, Tallulah Falls Formation, Woodall Shoals, South Carolina, Georgia, eastern Blue Ridge, southern Appalachians, Chattooga River

METAMORPHISM AT WOODALL SHOALS

IN THE EASTERN BLUE RIDGE,

GEORGIA - SOUTH CAROLINA

by

CHARLES HOWARD FORTNER

B.S., The University of Georgia, 1999

A Thesis Submitted to the Graduate Faculty

of The University of Georgia in Partial Fulfillment

of the

Requirements for the Degree

MASTER OF SCIENCE

ATHENS, GEORGIA

2002

METAMORPHISM AT WOODALL SHOALS

IN THE EASTERN BLUE RIDGE,

GEORGIA - SOUTH CAROLINA

by

CHARLES HOWARD FORTNER

Approved:

Major Professor: Alberto E. Patiño-Douce

Committee: Michael F. Roden
Samuel E. Swanson

Electronic Version Approved:

Gordhan L. Patel
Dean of the Graduate School
The University of Georgia
May 2002

CONTENTS

Page

INTRODUCTION

This study quantifies the metamorphic conditions of the Woodall Shoals outcrop along the Chattooga River that forms the Georgia – South Carolina border. The expansive pavement outcrop of fresh rock at Woodall Shoals makes it an ideal location to study the structural and metamorphic history of the southern Appalachians and because of this Hatcher (1989) has even gone so far as to call Woodall Shoals "a Rosetta stone for the...eastern Blue Ridge."

Several thermobarometric studies have focused on the rocks of the Rankin's (1970) Ashe Formation of western North Carolina that correlate with the Acadian aged metamorphic rocks of the Tallulah Falls Formation (Hatcher 1971, 1978, 1999) of which Woodall Shoals is a part. McSween *et al.* (1989) used Fe-Mg exchange between garnet and biotite or garnet and hornblende, NaSi-CaAl exchange between hornblende and plagioclase, and Na-K exchange between alkali feldspar for geothermometry of the Ashe formation. McSween *et al.* (1989) found few assemblages appropriate for geobarometry, thus were only able to calculate pressures for two samples. They found the Ashe to have equilibrated at 600-650°C and 7.5 kbar. Willard and Adams (1994) present pressure and temperature estimates for eclogite, retrograde amphibolite, and adjacent schists of the Ashe that Adams and Trupe (1997) use in the construction of a retrograde *P-T* path from eclogite facies at ~15kbar/750°C to amphibolite facies at 5kbar/575°C. More recently, Bier *et al.* (2000) found temperature of 600-700°C for the Tallulah Falls Formation of the North Carolina Inner Piedmont, but did not report any pressure data.

Eckert *et al.* (1989) calculated temperatures and pressures for the Taconic aged metamorphic rocks of the Wayah granulite metamorphic core located west of Franklin,

NC in the Richard Russell thrust sheet. They chose to use garnet-biotite geothermometry and garnet-aluminosilicate-quartz-plagioclase geobarometry because the assemblages appropriate for other geothermometers and geobarometers did not exist throughout the whole range of metamorphic conditions. They obtained T/P estimates of 585°C, 5.5 kbar at the first sillimanite isograd and ~730-842°C, ~7.5-9.8 kbar in the granulite facies. A related study by Absher and McSween (1985) found that the granulite facies rocks of Winding Stair Gap, N.C., reached temperatures of 750-775ºC and pressures of 6.5-7.0 kbar. Another more recent study of Winding Stair Gap by Moecher (2000) found P-T conditions of 850-900ºC at 9-10 kbar. A study by Chen and Roden (1994) in the Shooting Creek area of North Carolina found maximum temperatures from garnet Fe-Mg partitioning between 430 and 840ºC.

Mineral abbreviations and conventions used in this study are presented in Tables 1.1 and 1.2. The next chapter gives a brief overview of the setting and geologic history of the eastern Blue Ridge and Woodall Shoals. Chapter three contains petrologic descriptions of the samples and chapter four gives mineral chemistry and thermobarometric data. The data are discussed the fifth chapter.

Table 1.1   Mineral abbreviations used in this paper. After Miyashiro (1994).

Abbreviation	Mineral
qtz	Quartz
sill	Sillimanite
opq	Opaque
py	Pyrite
il	Ilmenite
bt	Biotite
ms	Muscovite
plag	Plagioclase
ab	Albite
an	Anorthite
or	Orthoclase
epi	Epidote
zoi	Zoisite
gar	Garnet
grs	Grossular
sps	Spessartine
alm	Almandine
pyr	Pyrope
amph	Amphibole
tsc	Tschermakite
par	Pargasite
hbl	Hornblende
ed	Edenite
rich	Richterite

Table 1.2   Variables, conventions, and constants used in this paper.

Variable	Name	Units
P	Pressure	bar or kilobar (kbar)
T	Temperature	$^\circ$C or K
X	mol fraction	unitless
a	activity	unitless
f	fugacity	unitless
G	Gibbs free energy	kJ/mol
H	enthalpy	kJ/mol
S	entropy	J/mol/K
V	molar volume	J/bar
C_p	heat capacity	J/mol/K

Constant	Name	Value
R	Universal Gas Constant	8.3451 J/mol/K

Convention	Explanation
ΔQ	For reaction [reactants] $\rightleftharpoons$ [products], $\Delta Q = \Sigma Q_{products} - \Sigma Q_{reactants}$
q°_i	Standard state (1bar, 298K) of variable q for a non-fluid component i.

BACKGROUND

2.1 SETTING: GEOGRAPHIC AND GEOLOGIC

The Woodall Shoals outcrop is located on the South Carolina side of the Chattooga River that forms the Georgia-South Carolina border in the USGS Rainy Mountain 7.5' quadrangle and lies within the USDA's Chattooga Wild and Scenic River Corridor. The nearest towns are Clayton, Georgia 12 km northwest of the outcrop (Fig. 2.1) and Westminster, South Carolina 24 km to the southeast.

Geologically, Woodall Shoals lies within the Tallulah Falls thrust sheet of the eastern Blue Ridge province of the Appalachians (Fig. 2.1). The eastern Blue Ridge, like other Appalachian provinces, consists of several stacked thrust sheets bounded by thrust faults to the southeast and the northwest. The Hayesville Fault separates the volcanic, ultramafic, and granitic rocks of the eastern Blue Ridge from the metasedimentary rocks of the western Blue Ridge (Drake *et al.* 1989, Nelson *et al.* 1998) to the northwest, while to the southeast the Brevard Fault Zone separates the eastern Blue Ridge from the high-grade gneisses and migmatites of the Inner Piedmont (Allard and Whitney 1994).

Within the eastern Blue Ridge are four thrust sheets (Fig. 2.1) recognized by Nelson *et al.* (1998). From southeast to northwest they are the Tallulah Falls thrust sheet, Helen thrust sheet, Richard Russell thrust sheet, and the Young Harris thrust sheet. Being structurally highest, the Tallulah Falls thrust sheet is bounded to the southeast by the Brevard Fault Zone and to the northwest by the Dahlonega fault (Nelson *et al.* 1998). Much of the sheet is composed of the Tallulah Falls Formation with the remainder
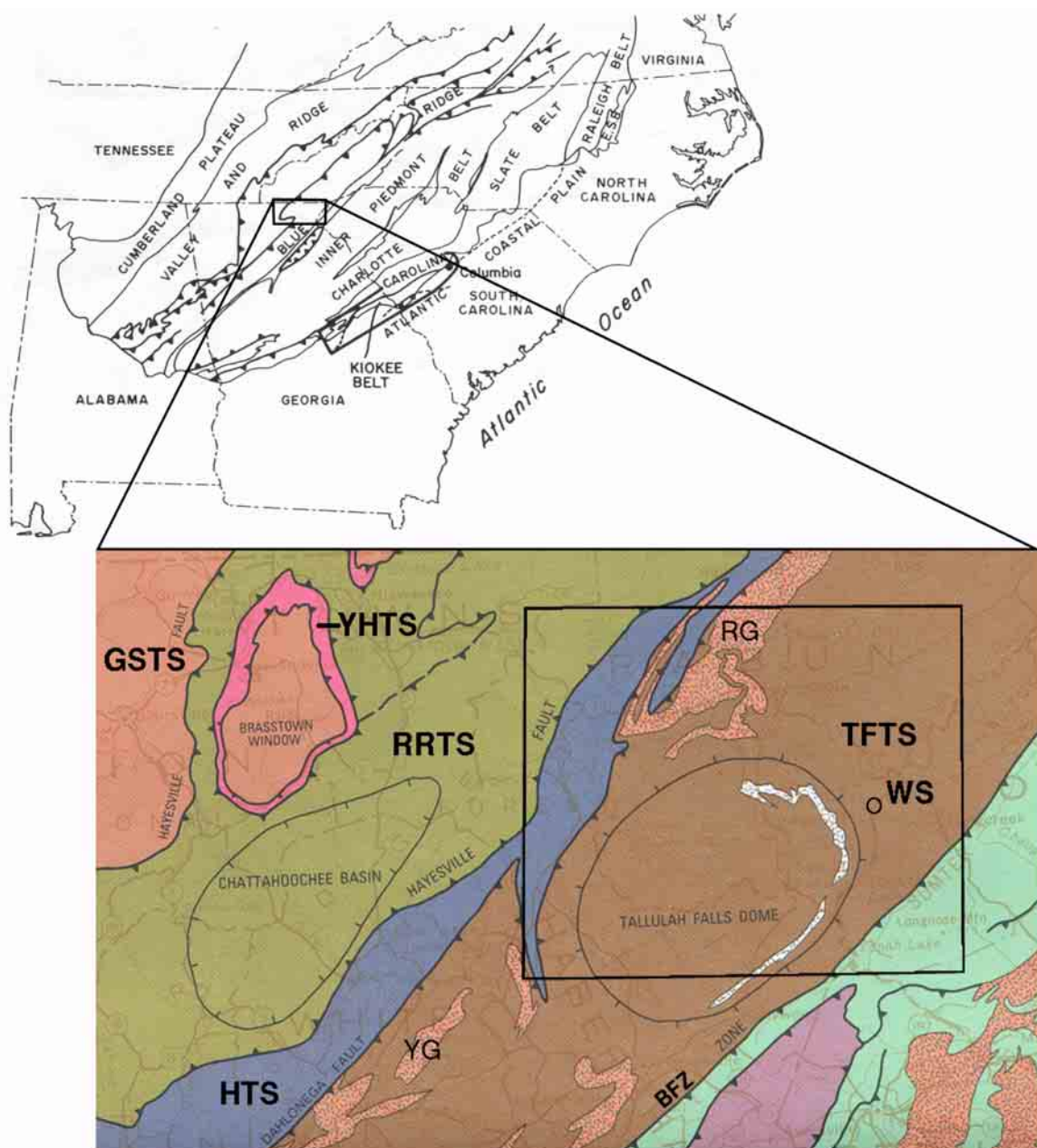
Figure 2.1   Geologic provinces of the southern Appalachians and general geology of the eastern Blue Ridge after Hatcher 1989 and Nelson *et al.* 1998. Abbreviations: WS – Woodall Shoals, YG – Yonah gneiss, RG – Rabun gneiss, BFZ – Brevard Fault Zone, TFTS – Tallulah Falls thrust sheet, HTS – Helen thrust sheet, RRTS – Richard Russell thrust sheet, YHTS – Young Harris thrust sheet, GSTS – Great Smoky thrust sheet. Location of Figure 2 outlined in lower map.
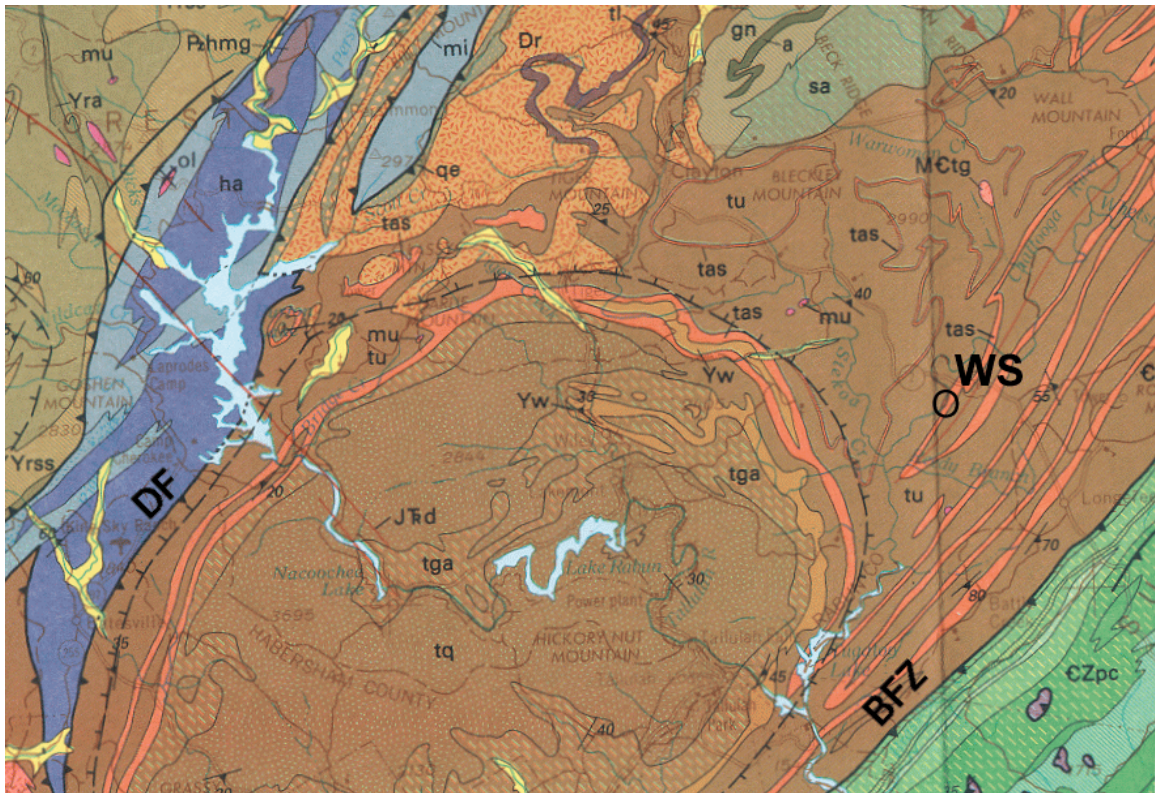
Figure 2.2 Detail of Nelson *et al.*'s (1998) geologic map in the vicinity of Woodall Shoals. Brown and orange units: Tallulah Falls thrust sheet. Blue units: Helen thrust sheet. Tan units: Richard Russell thrust sheet. Green units: Inner Piedmont. Key for the Tallulah Falls Formation and selected Tallulah Falls thrust sheet units: tq – quartzite schist, tga – graywacke schist, tas – garnet-aluminous schist, tl – greywacke-schist-amphibolite, tu – undivided Tallulah Falls Formation, WS – Woodall Shoals, BFZ – Brevard fault zone, DF – Daholnega fault, Dr – Rabun gneiss, Yw – Wiley gneiss.

composed of unnamed amphibolite, biotite gneiss, and mica schist. The Tallulah Falls

Formation consists of four members: 1) a basal metagraywacke-schist-amphibolite unit,

2) an aluminous schist, 3) a metagraywacke-schist, 4) and an upper unit composed of

quartzite schist (Nelson *et al.* 1998, Hopson *et al.* 1989). Woodall Shoals is located in

the aluminous schist member (Fig. 2.2). The Tallulah Falls Formation has been

correlated to the northeast with the rocks of the Ashe Formation of North Carolina

(Rankin 1970) and to the southwest with the rocks of the Sandy Springs Group near

Atlanta (Hatcher 1978). Protoliths of the Tallulah Falls Formation are believed to be

sediments deposited in a fluvial-delta to distal-turbidite environment (Gillon 1982).

2.1 GEOLOGIC HISTORY: DEFORMATION AND METAMORPHISM

All rock units in the eastern Blue Ridge have undergone several episodes of deformation

that include both folding and faulting. The age of deformation can only be determined

through dating metamorphism (Drake *et al.* 1989). Nelson *et al.* (1998) maintain that

there is evidence for at least four deformational events across the eastern Blue Ridge

(Table 2.1) and evidence for as many as six in some places. Hopson *et al.* (1989) agree,

but seem to believe evidence for the fifth and sixth events are more widespread than put

forth by Nelson *et al.* (1998). Moreover, Hopson *et al.* (1989) cite work by Hatcher and

Butler (1979) that documents up to seven phases of deformation. Both Hopson *et al.*

(1989) and Nelson *et al.* (1998) agree on most of the features of the first four folding

events:

F_1 Rootless, recumbent to reclined, isoclinal intrafolial folds that trend NE. Hopson

      et al. (1989) note that these occur as folds in amphibolite boudins and are rarely

      observed.

F_2 Steep to recumbent, isoclinal folds that have a well-developed axial planar S_2

      foliation defined by platy minerals. These are the major folds present in the

      eastern Blue Ridge and trend generally NE and plunge gently NE or SW. This

      generation may be related to the metamorphic peak during the Taconic orogeny,

Table 2.1   Timeline of thermal and deformational events in the southern
Appalachians after Nelson *et al.* (1998), Hopson *et al.* (1989), Hatcher *et
al.* (1989).

Alleghanian	Doming via duplexing. Brittle movement along Dahlonega fault and Brevard Fault Zone.
	$F_4 - F_6$ events?
	Tallulah Falls thrust sheet emplaced on Helen thrust sheet via the Dahlonega fault. Intrusion of Rabun gneiss (~374 Ma?). Creation of F_3 deformational features.
Acadian	Tallulah Falls thrust sheet metamorphosed during the Acadian M_2 event.
	Russell and Young Harris thrust sheets thrust along the Hayesville fault over the Helen thrust sheet during or after Taconic metamorphism (M_1) generating F_2 deformation. Metamorphic peak reached with formation of granulites
Taconic	Young Harris thrust sheet emplaced within Richard Russell thrust sheet.
	Helen thrust sheet emplaced on the western Blue Ridge (Great Smoky thrust sheet). F_1 event (?).
Mid to late Proterozoic	Deposition of the shallow-water sediments (Great Smoky thrust sheet) on the North American craton, deposition of deep-water pelitic sediments and related volcanics that would become the eastern Blue Ridge.

but work by Dallmeyer (1988) shows that it may actually be related to the Acadian orogeny. Disagreements arise as to whether this folding event was syn- or post-metamorphic. Hopson *et al.* (1989) maintain that it is syn-metamorphic (M_1), while Nelson *et al.* (1998) and Drake *et al.* (1989) assert that it is post-metamorphic (M_1).

F_3 Upright to slightly inclined, tight to isoclinal, conjugate fold pairs that refold F_2 folds. Axial-planar S_3 crenulations are sometimes present in the hinges of the folds. The conjugate folds that Nelson *et al.* (1998) see trend NE and NW. Both parties (Hopson *et al.* 1989, Nelson *et al.* 1998) agree that this stage was post-metamorphic (M_2), but before the rocks completely cooled.

F_4 Both parties agree that this fold generation is sparsely developed, but Hopson *et al.* (1989) believe these to only be crenulations, while Nelson *et al.* (1998) believe this generation to be gentle, upright folds and warps that trend NE.

F_5, F_6 Hopson *et al.* (1989) define these generations as open folds, with F_5 folds trending NE and F_6 folds trending NW. Hatcher (1999) points out that these generations form dome and basin interference patterns visible at Woodall Shoals.

The mid- to upper-amphibolite grade rocks (Nelson *et al.* 1998) of the Tallulah Falls thrust sheet are thrust over the lower-amphibolite grade rocks of the Helen thrust sheet via the Dahlonega fault. Hopson *et al.* (1989) point out that the fault must be post-peak-metamorphic because no migmatite is seen in the Helen thrust sheet, while Nelson *et al.* (1998) maintain that ductile and brittle deformation along the fault, indicated by the presence of mylonites and button schists, shows that the fault was in motion shortly after the metamorphic peak and continued through cooling, dating the fault as Acadian or younger. Hatcher (1999) agrees, pointing out that the fault cuts the 375 Ma Rabun pluton.

The Tallulah Falls dome, located approximately 7 km to the west of Woodall Shoals, is a conspicuous structural feature within the eastern Blue Ridge. Nelson *et al.*

(1998) believe it results from interference patterns generated by superposed folding, but offers no explanation as to which fold generation resulted in refolding. Based on seismic reflection data from the Appalachian Ultradeep Core Hole Project, other workers dispute Nelson *et al.*'s conclusion, favoring a model that involves Alleghanian duplexing of underlying rocks to form the Tallulah Falls dome (Hatcher *et al.* 1989, Hopson *et al.* 1989). According to this model, as a sheet is thrust over a ramp the footwall locks and is broken into horses within a duplex structure, causing an arch to form and manifest itself on the surface as a window if breached or dome if unbreached (Hatcher *et al.* 1989). Later work by Hatcher (1999) is less conclusive, speculating that the Tallulah Falls dome may either be a macroscopic analogue of the F_5/F_6 boudins seen at Woodall Shoals or a result of duplexing.

Metamorphism in the eastern Blue Ridge generally attained the amphibolite facies, with the exception of a few granulite facies rocks in the Wayah metamorphic core near Franklin, NC (Hopson *et al.* 1989, Nelson *et al.* 1998, Eckert *et al.* 1989). The Tallulah Falls thrust sheet has kyanite zone rocks along its boundary with the Brevard Fault Zone and in the Tallulah Falls dome (Hopson *et al.* 1989, Nelson *et al.* 1998), with the remaining portions of the thrust sheet generally in the first sillimanite zone. The Helen thrust sheet is generally lower grade than the surrounding sheets and contains rocks ranging in metamorphic grade from the garnet to staurolite-kyanite zones (Nelson *et al.* 1998). Most rocks in the Richard Russell and Young Harris thrust sheets are in the sillimanite zone, with the exception of granulites near Franklin, North Carolina (Hopson *et al.* 1989).

Age of metamorphism across the eastern Blue Ridge varies. Two metamorphic events, one during the Taconic orogeny (M_1) and one during the Acadian orogeny (M_2), are believed to have taken place. Although the existence of an Acadian event in the southern Appalachians is now generally accepted, it is a relatively new idea and there is ongoing debate regarding its relation to the deformational and crystallization events. Dallmeyer (1988) found $^{40}Ar/^{39}Ar$ amphibole plateau ages between 322 and 328 Ma for

the Tallulah Falls thrust sheet, dating post-metamorphic cooling through ~500°C as Late Mississippian to Early Pennsylvanian (Acadian). The Helen thrust sheet shows similar cooling ages (Dallmeyer 1988). Nelson *et al.* (1998) cite unpublished U-Pb zircon ages of T.W. Stern indicating the last metamorphic event in the Tallulah Falls thrust sheet to be no older than 373 to 351 Ma. These data indicate metamorphism of Acadian age (M_2) in the Tallulah Falls and Helen thrust sheets. Metamorphic ages of approximately 470 Ma for Winding Stair Gap in the Richard Russell thrust sheet (Moecher 2000) dates metamorphism in that thrust sheet to the Taconic orogeny (M_1).

The Rabun gneiss, north of the Tallulah Falls dome (Fig 2.2), is a coarse grained microcline-plagioclase gneiss that contains multiple foliations and xenoliths with an even earlier foliation (Hatcher 1999). The Rabun gneiss intruded the Tallulah Falls Formation, was beheaded by the Dahlonega fault, and finally the fault was refolded (Hatcher 1999, Nelson *et al.* 1989). Miller *et al.* (1998) dated the crystallization age of the Rabun gneiss as 374 Ma (U-Pb). Hatcher (1999) speculates that the Rabun was intruded and deformed during the Acadian orogeny. Because of their structural and lithological similarities, Hopson *et al.* (1989) correlate the Rabun granite with Gillon's (1982) Yonah gneiss to the southwest (Fig. 2.1).

Little is known about the metamorphism and petrology in the immediate area of Woodall Shoals. Hatcher *et al.* (1983) produced a large-scale map of the outcrop with rock unit descriptions, described the structure in detail in several publications (Hatcher 1989, 1999, just to name two), and mapped the kyanite-sillimanite isograd, but beyond this the metamorphic and petrologic details remain uninvestigated.

CHAPTER 3

SAMPLING, PETROGRAPHY, MINERAL COMPOSITIONS

3.1 SPECIMEN SAMPLING

Samples for this study were collected from the Woodall Shoals outcrop and from

outcrops north and south of Woodall Shoals along the Chattooga River. The freshest

exposures were in the river valley, but thick underbrush and steep terrain made collection

along the river difficult. Samples were obtained from Woodall Shoals, Bull Sluice near

the US 76 bridge to the north, and from an unnamed locality to the south (Figs. 3.1, 3.2).

Given its large expanse of pavement outcrop, Woodall Shoals was the starting point for

sampling. Using Hatcher *et al.*'s (1983) large-scale map of the outcrop and lithologic

descriptions, approximately one dozen samples containing garnet, amphibole, and/or

biotite (i.e., samples that could be used to estimate metamorphic conditions) were

collected. Outcrop near the US 76 bridge on the Chattooga River was abundant, although

useful lithologies were not. Three samples were taken. Sampling south of Woodall

Shoals proved more difficult as access to the river was impossible, much of the exposed

rock at the accessible points was highly weathered, and useful lithologies were in short

supply. Four samples were collected from this area.

3.2 PETROGRAPHIC ANALYSIS

The samples were examined and those that seemed to have the lowest variance

assemblages were thin sectioned and polished. Thin sections were cut parallel to the

dominant foliation. Six samples had useful assemblages. The dominant synmetamorphic

S_2 foliation described by Hopson *et al.* (1989) is the primary foliaton in all samples.

Some samples also preserve the weakly developed S_3 foliation (Hopson *et al.*1989) noted

below as a weak secondary foliation. Short petrographic characterizations are presented

13
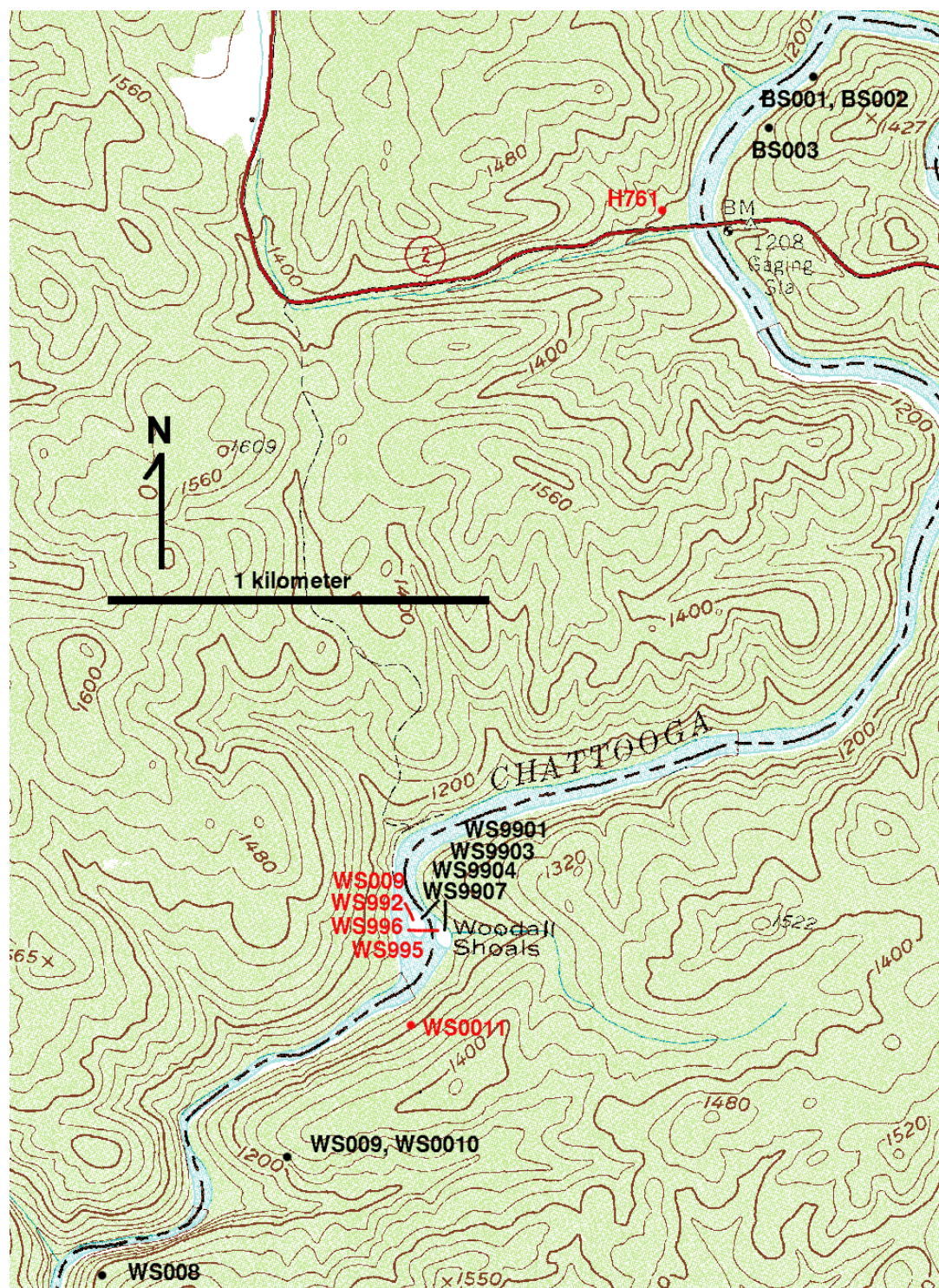
Figure 3.1   Detail of the USGS Rainy Mountain 7.5' quadrangle showing sampling locations. Red text indicates samples used in this study. Lower right corner UTM coordinates are 3851090m.N., 289500m.E.
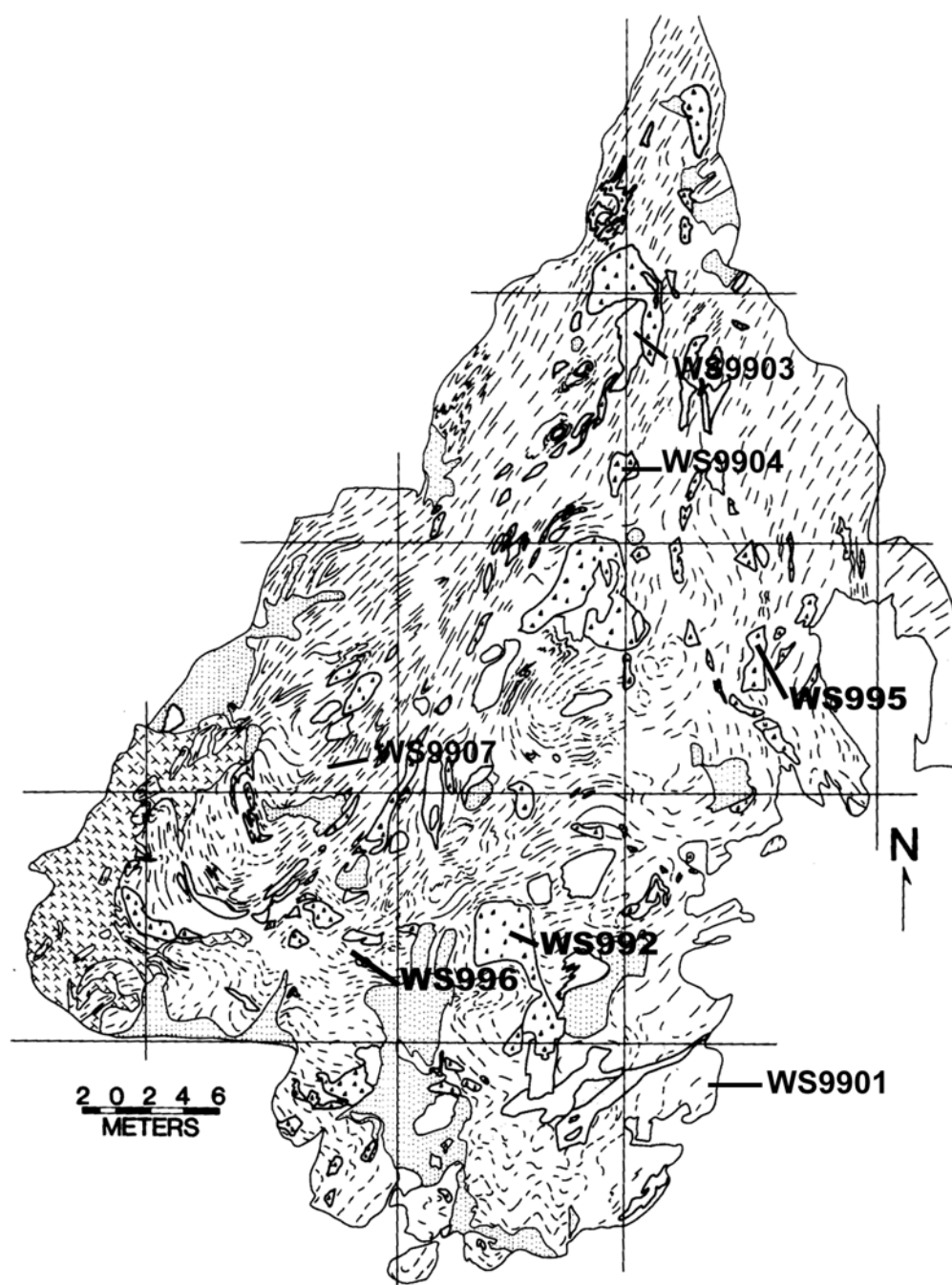
Figure 3.2   Detailed map of the Woodall Shoals outcrop from Hatcher (1989) showing sampling locations. Chattooga River flows along the left edge of the outcrop. Sample WS009 is ~10m north of the map area along the Chattooga River. Cross hatch- late pegmatite, form lines- biotite gneiss, small triangles- amphibolite boudins, unpatterned- foliated gneiss and pegmatite, fine stipple- recent sand.

Table 2.1   Volume percent modal analyses of samples used in this study. 600 points were counted for each thin section using an automatic stage. Opaque minerals are not distinguished. Entries of "x" denote that the phase is present in minor amounts.

	WS0011	H76-1	WS995	WS009	WS996	WS992
amph	55.3	71.2	64.8		3.8	32.2
bt			0.6	20.3	20	15.3
gar	1.3			3	6.2	0.5
plag	16.8	5	9.6	2	18	12
zoi	6.2	3.5	2	0.1	4.5	1.3
ep	x		x		x	
sill				0.8		
qtz	16.6	16	18.3	47.6	42.3	36.6
opq	1.3	4	2.6	0.1	5.2	1.8
sph	2.3		1.6			
ms	x			1.8	x	x
chl	x		0.6		x	0.2
zir		0.3				

below and full petrographic descriptions can be found in Appendix A. Modal analyses
are given in Table 2.1

Sample WS0011 is an amphibolite collected south of Woodall Shoals (Fig. 3.1)
with the assemblage amph + qtz + plag + zoi + gar + ms + sph + il + py (Fig 3.3). A
moderately developed penetrative fabric (S_2) is defined by aligned amphibole grains. No
evidence of secondary foliations (S_3) is present.   Amphiboles are generally subhedral
and possess small quartz and epidote inclusions. Quartz and feldspar are closely
associated and are present together throughout the thin section with interlobate grain
boundaries. Although some areas are slightly richer in feldspar and quartz, no distinct
banding is present. Zoisite is common, occurring as euhedral crystals with distinct cores
in many of the smaller grains. Yellow-green pleochroic epidote has ragged grain
boundaries and occurs in small patches. Although rare, garnet is present as anhedral
crystals with many quartz, feldspar, and epidote inclusions.

Sample H76-1 from north of Woodall Shoals (Fig. 3.1) is an amphibolite
containing hbl + plag + qtz + ep + il (Fig. 3.4). A well-developed penetrative fabric (S_2)
is defined by amphibole alignment and quartz ribbons. Quartz occurs in small grains
throughout the sample and as ribbons with polygonal to interlobate internal grain
boundaries. Subgrains are visible in some ribbons. Most plagioclase grains are
polysynthetically twinned and have an internal network of cracks. Some crack networks
are completely lined with epidote while others are free of any alteration material. Zoisite
occurs as small, euhedral grains distributed throughout the sample. Anhedral imenite is
distributed across H76-1.

Sample WS995, along with all samples that follow, is from the Woodall Shoals
outcrop (Fig. 3.1). WS995 is an amphibolite containing amph + plag + qtz + bt + ep + il
+ chl + sph (Fig 3.5). It has two non-penetrative fabrics: a well-developed fabric (S_2)
defined by subhedral amphiboles and a weak fabric (S_3) defined by cross-cutting biotite.
Chlorite replacement of biotite is common. With a single exception, the biotite grains cut
across the amphibole fabric at a high (>40°) angle. Zoisite is found in the primary
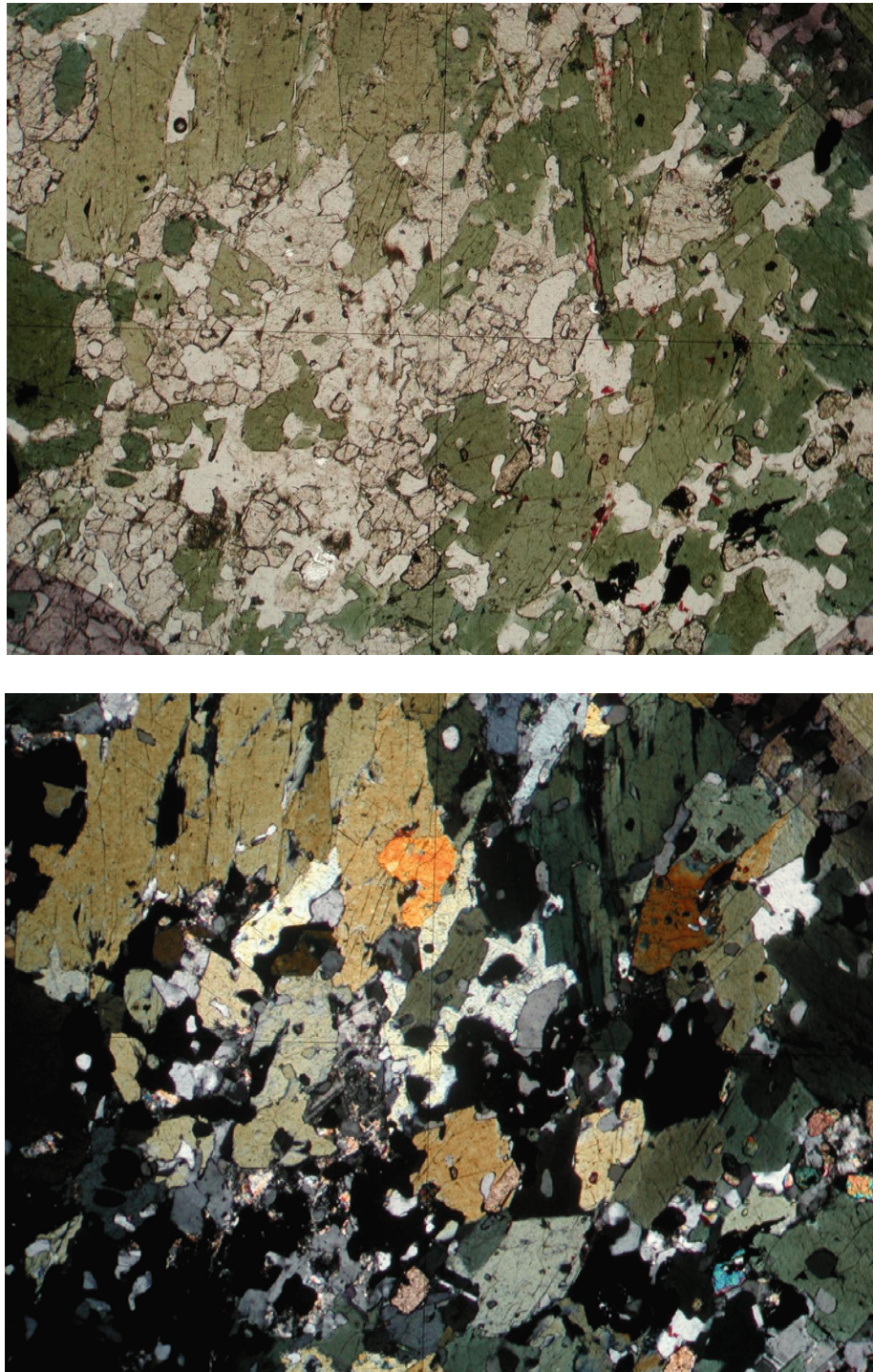
Figure 3.3   Photomicrographs of WS0011 showing anhedral
garnet (high relief mineral) and aligned amphibole
(green mineral). Top: plane polarized light. Bottom:
cross polarized light. Width of view is 5mm.
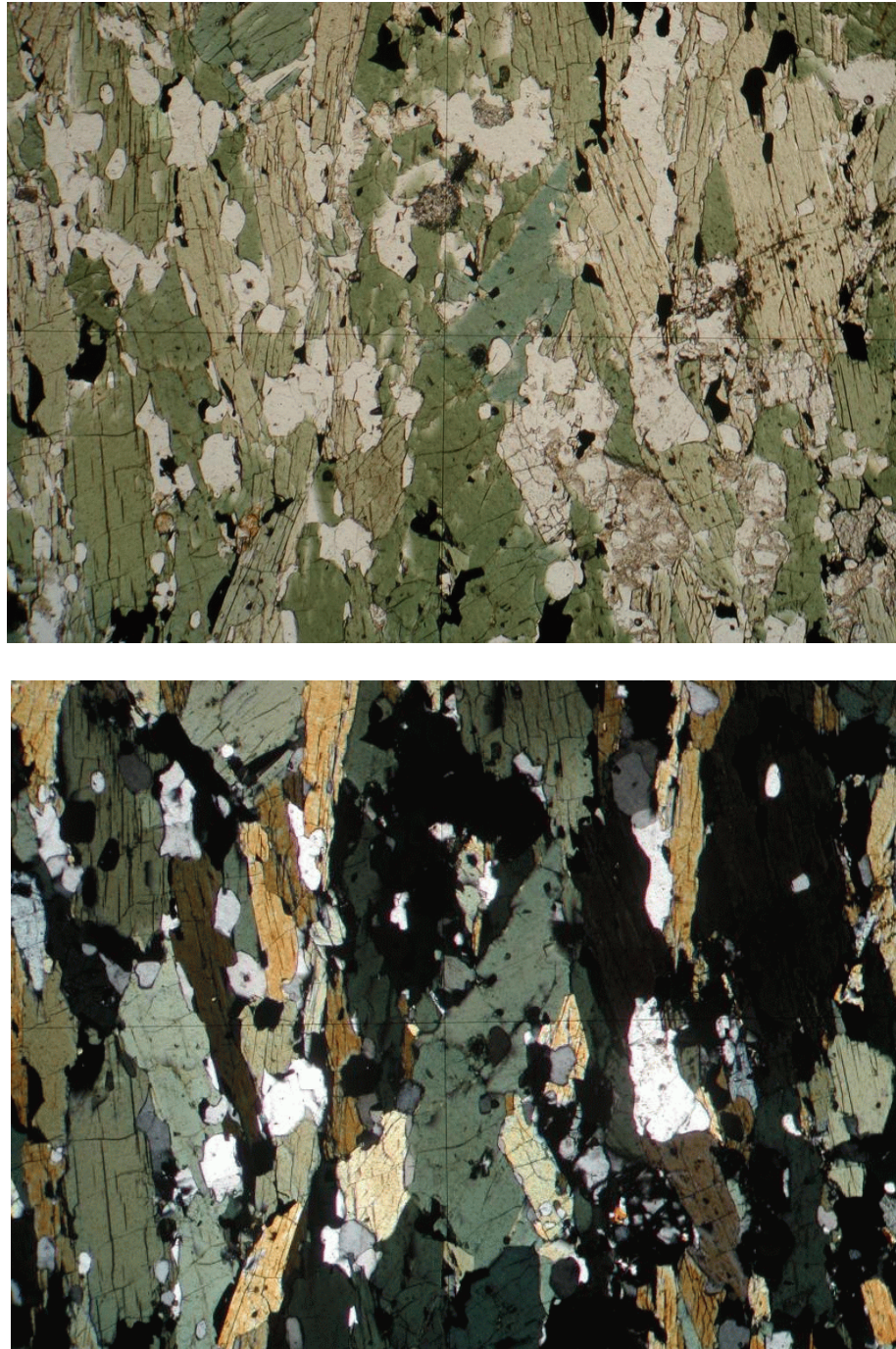
Figure 3.4   Photomicrographs of sample H76-1 showing the well developed fabric defined by amphibole (green mineral).   Top: plane polarized light. Bottom: cross polarized light. Width of view is 5mm.

Figure 3.5   Photomicrographs of sample WS995. Amphibole (green mineral) defines the primary fabric. Note the cross-cutting biotite grain on the right. Top: plane polarized light. Bottom: cross polarized light. Width of view is 5mm.

foliation and is distributed throughout the sample as small, euhedral to subhedral grains. Epidote is associated with chlorite replacement of biotite in the seconday foliation. Sphene is always associated with ilmenite, either forming total or partial mantles around anhedral ilmenite grains.

WS009 is a garnet-biotite gneiss with the assemblage qtz + plag + bt + gar + sill + ms + ep + il (Fig. 3.6). Both primary and secondary fabrics are defined by fine-grained, brown-red pleochroic biotite. The weak secondary fabric is defined by a few cross-cutting biotite grains approximately $50°$ from the primary fabric. There is no grain-size distinction between the two fabrics. Inequigranular quartz grains are dispersed throughout the sample as single crystals and as elongate aggregates, but ribbons that span the length of the thin section are not present. Lobate grain boundaries, subgrains, and sweeping extinction are common among quartz grains in this sample. Many plagioclase crystals are twinned and have sweeping extinction. Alteration of plagioclase is uncommon, but a few crystals have fine-grained epidote and/or muscovite growths around their rims. Garnet is present as euhedral to subhedral crystals. Inclusions are not found in all garnets, but when present are mainly quartz and feldspar. Biotite inclusions are rare. The lack of passive inclusions (biotite) makes exact determination of garnet growth difficult, but since they show no signs of post-growth strain they are taken to be post-tectonic. Euhedral sillimanite is present in the primary fabric.

WS996 is a hornblene-garnet-biotite gneiss containing two fabrics. The primary fabric (S_2) is defined by biotite and to a lesser extent by amphibole. Cross-cutting biotite crystals show the weaker secondary fabric (S_3) at $\geq 40°$ from the primary foliation. Amphiboles are subhedral to anhedral and inclusions are uncommon. Biotite crystals show dark brown pleochroism, with some chlorite replacement. Subhedral to anhedral garnets have many inclusions, mainly of quartz and feldspar and lesser amounts of amphibole, biotite, and ilmenite. The primary fabric is deflected around and is preserved by inclusions in some garnets, so they are believed to be syntectonic with respect to the primary foliation. Due to the weak nature of the secondary fabric, the relationship of the
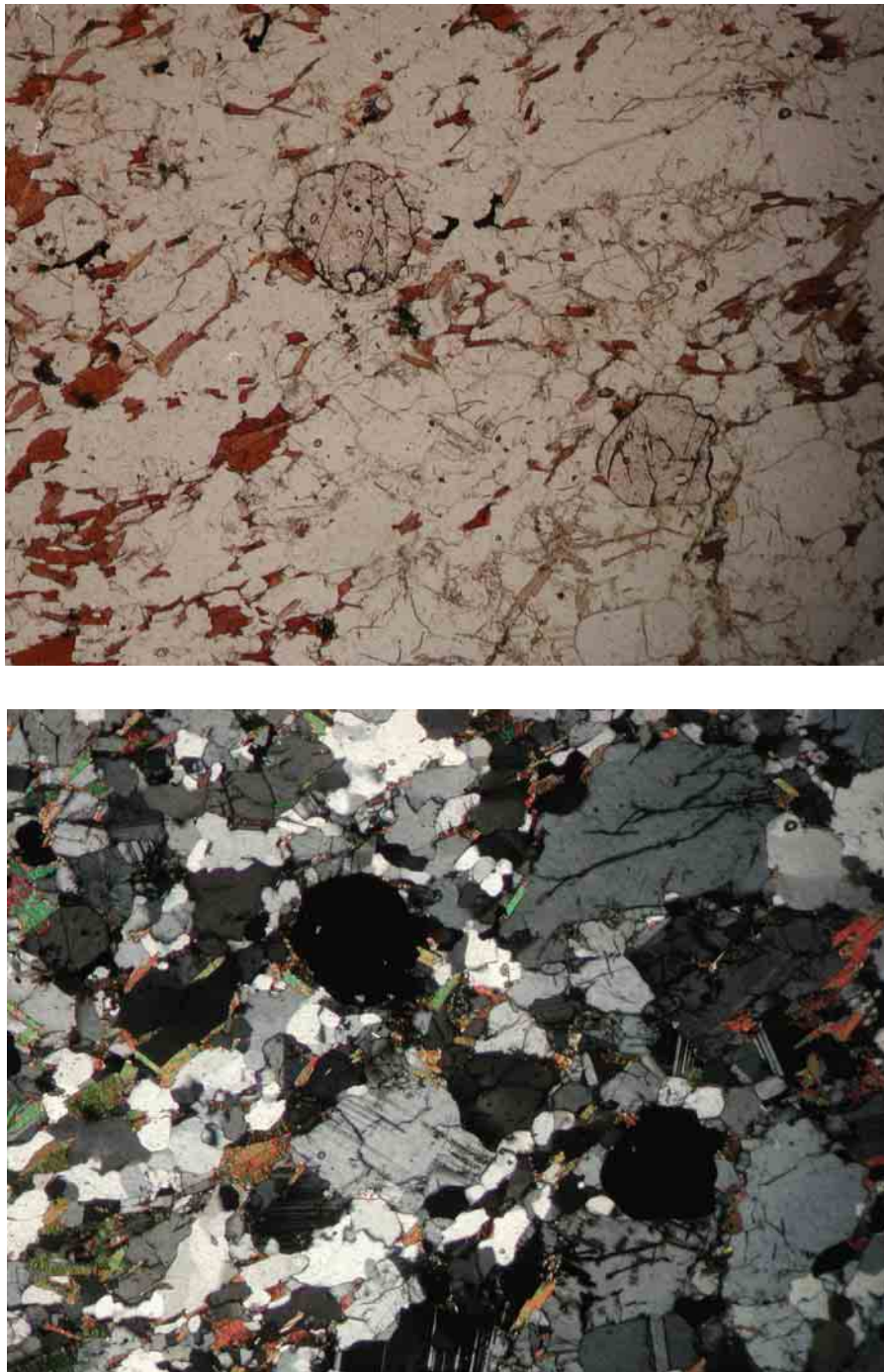
Figure 3.6   Photomicrographs of sample WS009. Note the primary foliation defined by red-brown biotite trending lower left to upper right. Careful observation of the left half of the photos will reveal small cross cutting biotite grains of the secondary foliation. The two high relief minerals are garnet. Top: plane polarized light. Bottom: cross polarized light. Width of view is 5mm.
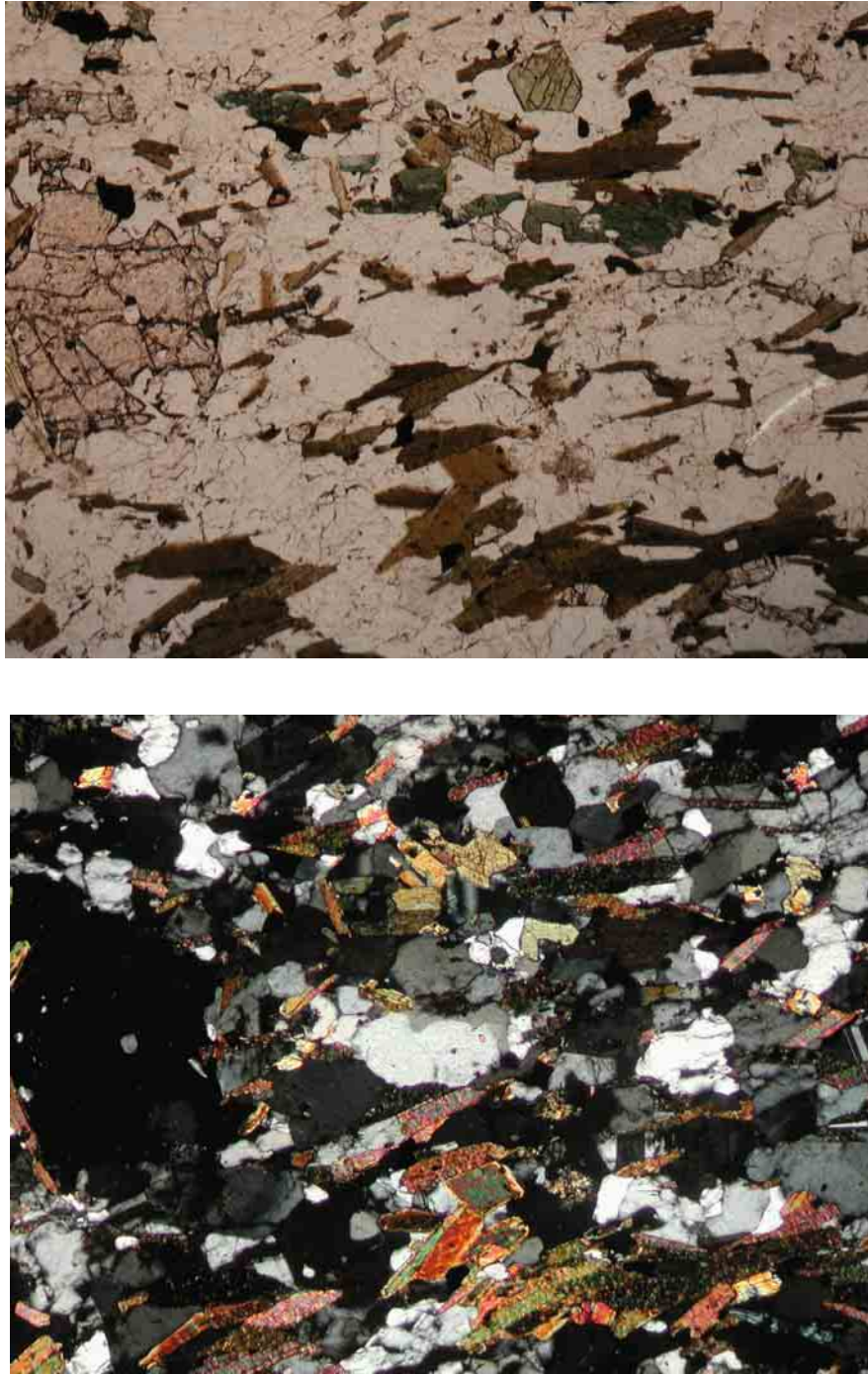
Figure 3.7   Photomicrograph of sample WS996. Primary foliation is defined by biotite. Large grain on the left is garnet and a small amphibole grain is right of center near the top of the photo. Top: plane polarized light. Bottom: cross polarized light. Width of view is 4mm.
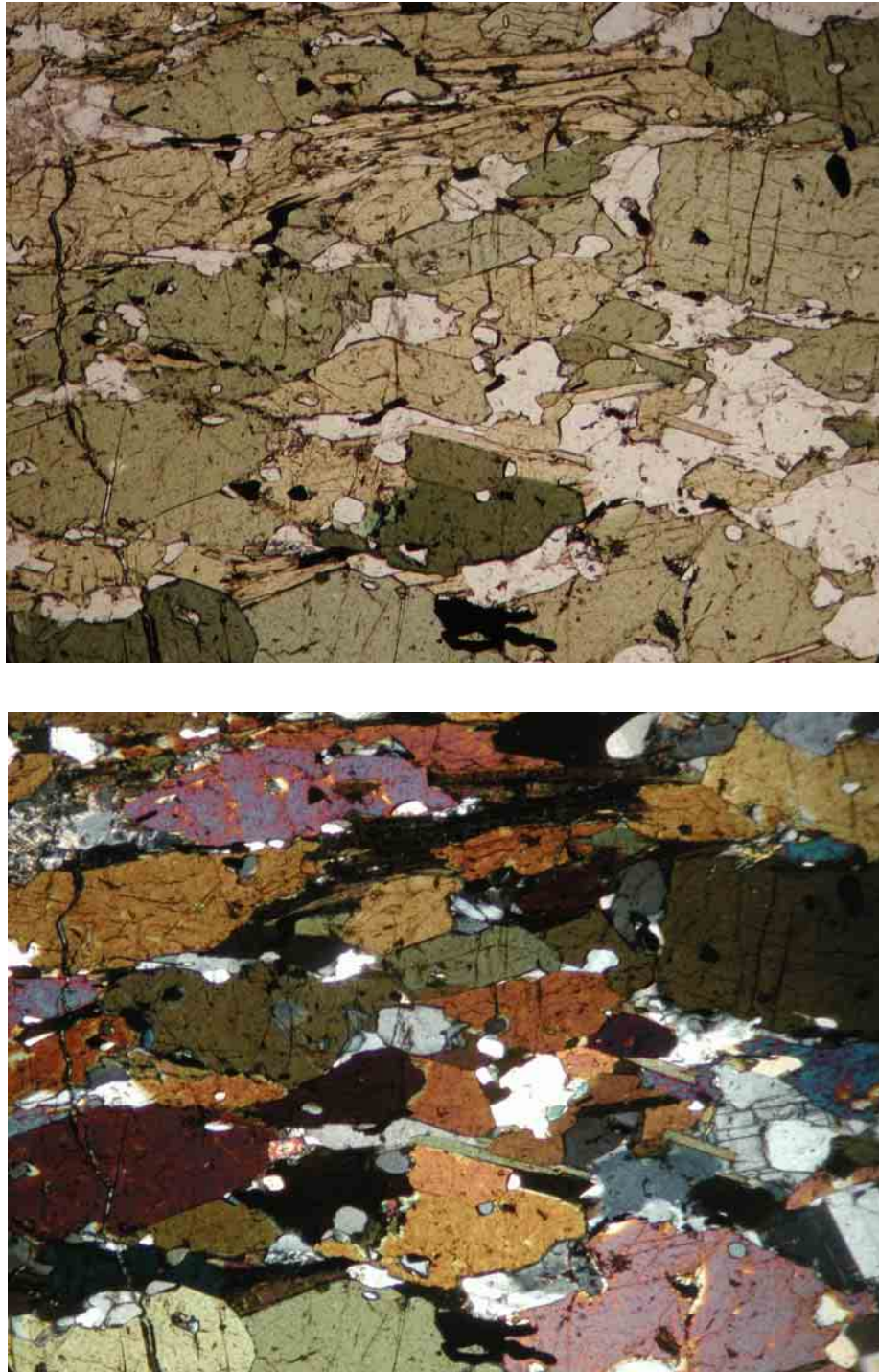
Figure 3.8   Photomicrograph of sample WS992. Well-developed foliation defined by amphibole (large green-brown grains) and biotite (small brown grains). Top: plane polarized light. Bottom: cross polarized light. Width of view is 5mm.

garnets to it could not be determined. However, no strong deformation took place after garnet growth as they show no signs of anisotropy. The matrix is chiefly composed of inequigranular quartz and plagioclase. Quartz occurs as crystals with rounded polygonal to lobate boundaries and undulatory extinction in the larger crystals. Plagioclase crystals are small and subhedral with some twinning and partial seritization in some crystals. Zoisite is distributed across the sample as small, euhedral to subhedral grains. No epidote is present.

The amphibole-biotite gneiss WS992 (Fig 3.8) is composed of amph + bt + plag + qtz + gar + ep + il. A strong penetrative fabric (S_2) is defined by amphibole, biotite, and quartz ribbons. Amphiboles are euhedral to subhedral with few inclusions. All biotite has a dark brown pleochroic scheme and has been slightly chloritized along cleavage planes. Plagioclase occurs in the matrix as equigranular crystals. Many plagioclase crystals are twinned and have sweeping extinctions. Replacement of plagioclase by white mica is present, but very minimal. Quartz is found in both the matrix and in ribbons. Quartz in both occurrences is inequigranular with polygonal to rounded polygonal boundaries. Subgrains have developed in some larger grains. Syntectonic garnet is present in the sample as a single anhedral crystal with abundant inclusions of quartz, plagioclase, and biotite. The fabric is deflected around the garnet and is preserved within by biotite inclusions. Epidote is found throughout the sample in small euhedral to subhedral crystals. Ilmenite occurs as acicular to anhedral crystals dispersed across the sample.

3.3 MINERAL COMPOSITIONS

Electron microprobe analysis was carried out with a JEOL 8600 Superprobe with an accelerating voltage of 15KeV and a beam current of 10nA. To minimize element migration, an unfocused (10μm) beam and 20 second count time were used for Na analyses, while a focused (1μm) beam and 10 second count time were used for analysis of all other elements. Calibration throughout this study was accomplished using the same set of appropriate silicate and oxide standards, and raw count data were reduced to oxide

weight percent using the Armstrong algorithm (JEOL program). Based on standards

analyses, weight percent oxide analyses vary an average of 2% from the accepted value

for elements present in concentrations greater than 3.0 oxide wt% and between 8% and

10% for elements present in concentrations less than 3.0 oxide wt%. In order to

minimize errors in computed pressure and temperature, points for analysis were chosen

so that they would be physically close to each other, usually near grain boundaries of

adjacent minerals appropriate for thermobarometry. Cores of crystals and their

inclusions were also analyzed in some instances where the possibility of seeing a change

in pressure and temperature during crystal growth existed. A general overview of

mineral compositions is presented below and individual mineral analyses are tabulated in

the next chapter.

All minerals analyzed for this study are from the primary (S_2) foliation. Because

the secondary foliation (S_3) was poorly developed and contained no assemblages useful

for thermobarometry it was not considered for analysis. Garnets (Fig. 3.9) from WS009

fell in the range Alm_{71-67} Pyr_{1-2} Grs_{9-8} Sps_{8-4} , while garnets from samples WS996,

WS0011, and WS992 had compositions in the range Alm_{61-51} Pyr_{20-9} Grs_{29-16} Sps_{10-2}.

Garnet oxide weight percent analyses were recalculated on a 12 oxygen basis and all Fe

was assumed to be Fe^{2+}. Except for samples H761 and WS0011, plagioclase

compositions were generally in the range of An_{38} – An_{50}. As Figure 3.10 shows, H761

and WS0011 plagioclase compositions were markedly different from the other samples

with highly anorthitic compositions near An_{83}. Plagioclase oxide weight percent analyses

were recalculated on a 16 oxygen basis. Amphiboles were pargasitic with Si pfu between

6.5 and 7 and the A site mostly filled by Na and K (Fig. 3.11). Amphibole weight

percent analyses tabulated in the next chapter were recalculated on a 23 oxygen basis and

all Fe was assumed to be Fe^{2+}. Biotite Mg/Fe ratios are almost constant throughout all

lithologies (Fig 3.12) and biotite Al^{iv} contents vary between 0.2 and 1.45 pfu. Biotite

oxide weight percent analyses were recalculated on an 11 oxygen basis with all Fe

assumed to be Fe^{2+}. Zoisite oxide weight percent analyses were recalculated on a 12.5 oxygen basis.

With the exception of the anhedral garnets in WS0011 and WS992, all mineral assemblages in the primary fabric (S_2) are taken to be equilibrium assemblages. Grain boundaries are straight and no reaction coronas or embayed grains are present. A few exceptions are instances of chlorite growing along cleavage planes in biotite as noted above, and instances of sphene mantling ilmenite in two samples. Grains exhibiting any sort of alteration were not used in this study. No chemical zoning is observed in biotite or garnet and zoning in amphibole and plagioclase occurs only in a few cases. Inclusions in larger grains of garnet and amphibole are common, but none show a sieve texture or appear to be growing at the expense of their host.
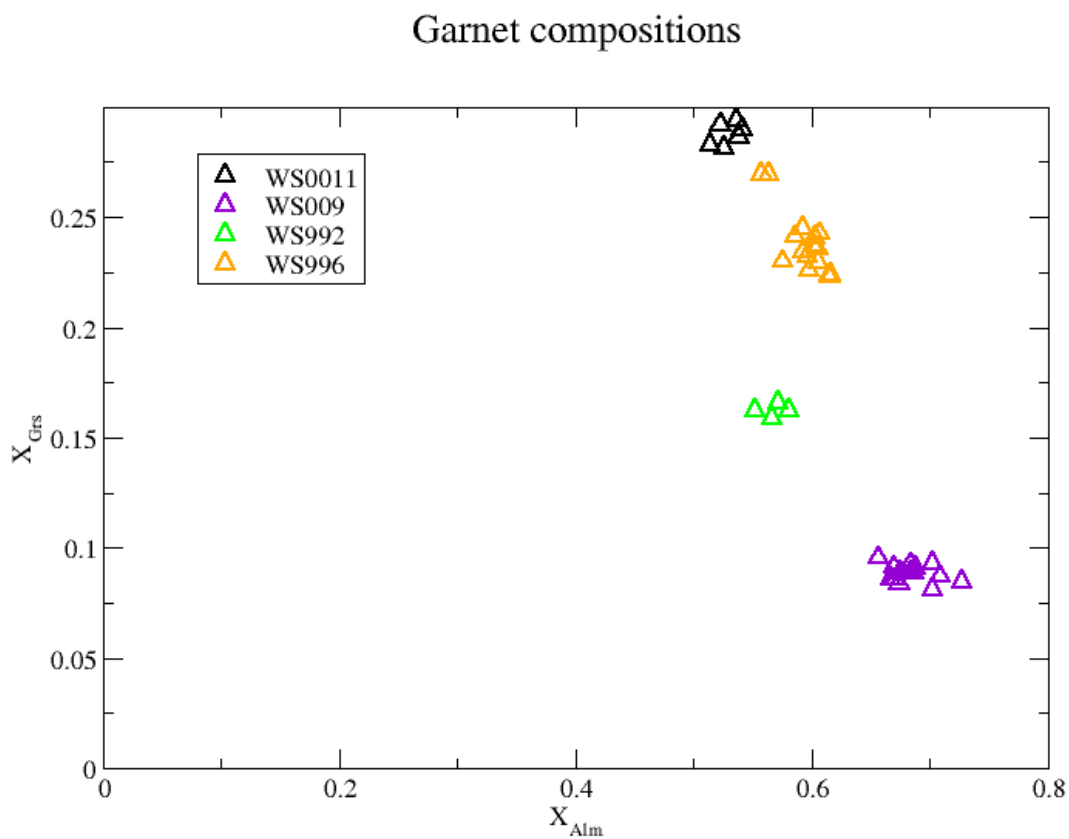
Figure 3.9   Garnet compositions from this study.

Plagioclase compositions
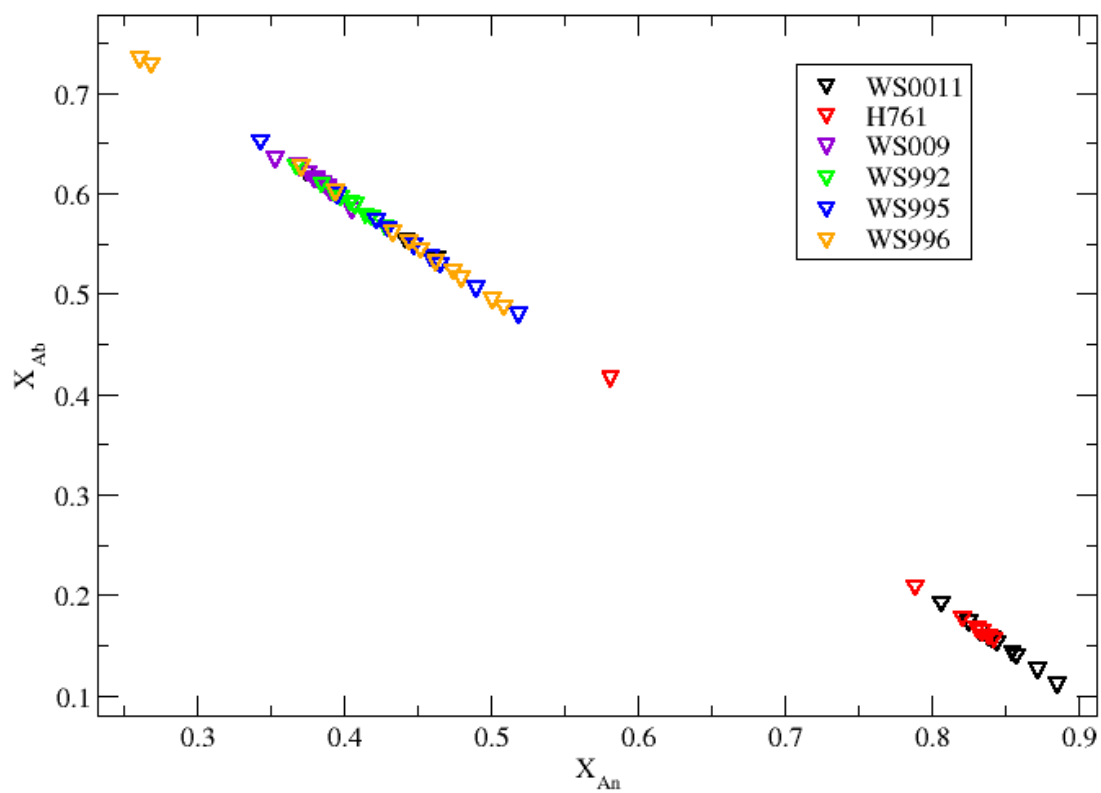
Figure 3.10   Plagioclase compositions from this study.
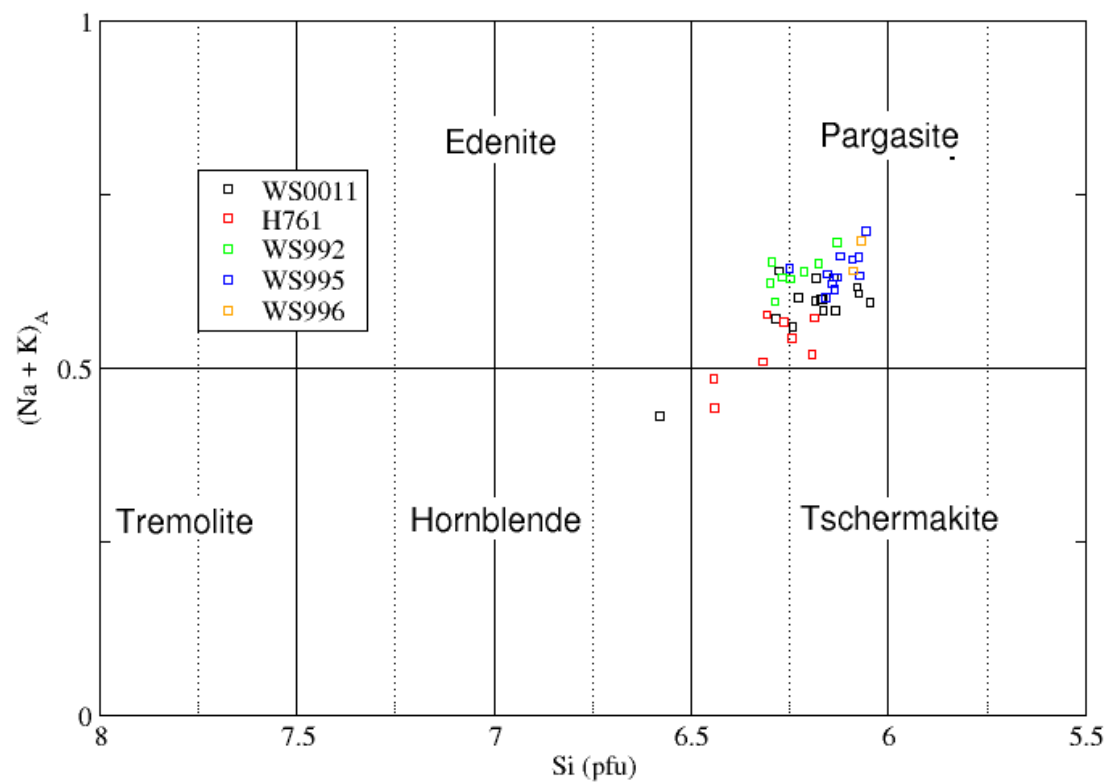
Figure 3.11   Amphibole compositions from this study showing Na + K in the A site and Si in the tetrahedral site. Classification after Deer *et al.* (1992).
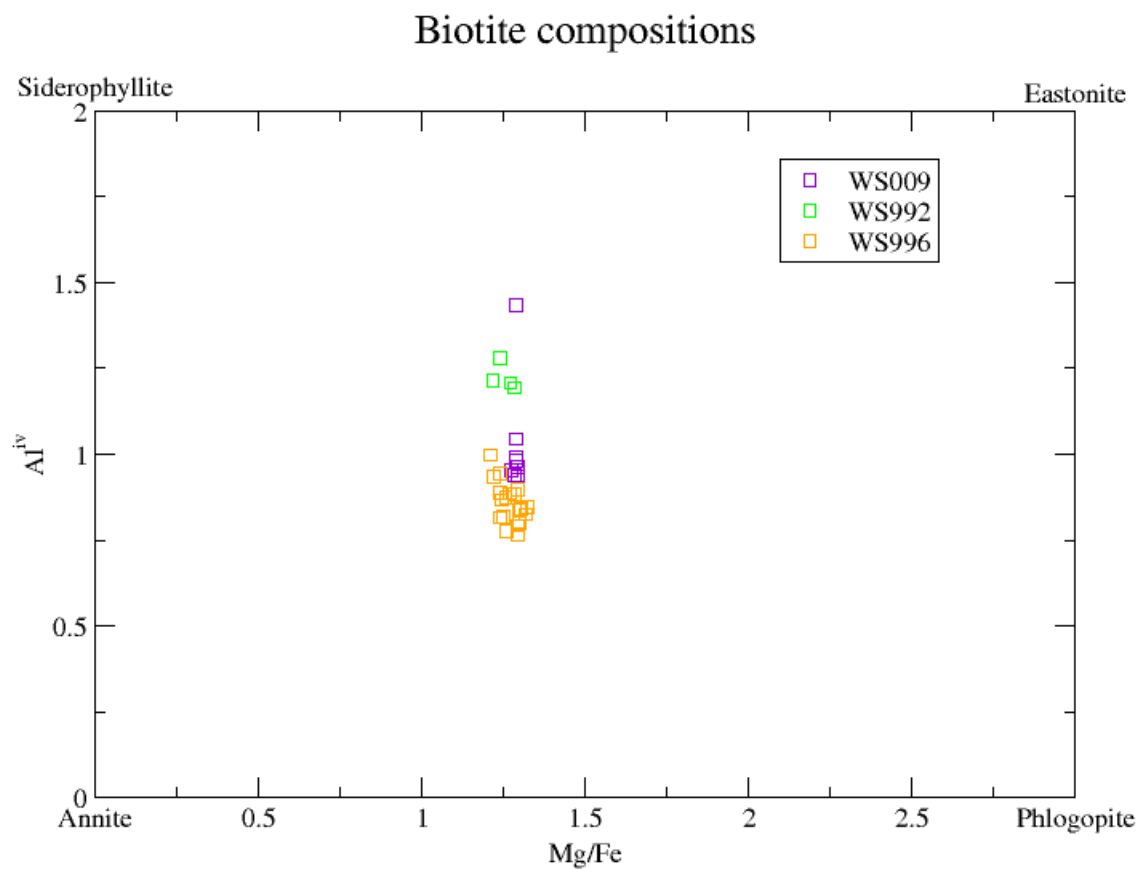
Figure 3.12   Biotite compositions from this study. Classification after Guidotti (1984).

CHAPTER 4

ESTIMATION OF METAMORPHIC CONDITIONS

4.1 SILLIMANITE BEARING BIOTITE-GARNET GNEISS: WS009

WS009 is the only sample in this study that contains an aluminosilicate, and because of this it plays an important role that will become clear later. Three phases were analyzed with the electron probe micro-analyzer to determine their compositions: garnet, plagioclase, and biotite. Results for these minerals are tabulated in Table 4.1, 4.2, and 4.3, respectively. Core and rim analyses were determined by grain geometry and are noted in the tables throughout this chapter where appropriate. The point labeling scheme throughout the chapter follows the form of: ZZ#b, where ZZ is an abbreviation for the mineral (G for garnet, HBL for amphibole, and so on), # is the grain number, and b (if present) distinguishes different points. Sillimanite and quartz were assumed to have end-member compositions.

Activity Models

Garnet activities were computed using Berman's (1990) quaternary Ca-Mg-Fe-Mn model, where the activity of component i is expressed as:

$$a_i = (X_i \cdot \gamma_i)^3 \tag{4.1}$$

with X the mole fraction, γ the activity coefficient, and where γ of the mth component is given:

$$nRT\ln\gamma_m = \sum_1^p W_{ijk}(Q_m X_i X_j X_k / X_m - 2X_i X_j X_k) \tag{4.2}$$

where n is the number of sites where mixing occurs, p is equal to the number of excess parameters needed for a given system, each W refers to $W_G = W_H - TW_S + PW_V$, and Q_m

Table 4.1   Garnet compositions for sample WS009. Stoichiometry recalculated from oxide wt% on a 12 oxygen basis. Table continued on next page.

Label	G1a	G2a	G3a	G3b	G4b	G5a	G6	G7a
Location	rim	rim	rim	rim	core	core	core	core
SiO_2	36.94	36.77	36.66	37.14	36.77	37.03	35.90	36.92
TiO_2	0.00	0.00	0.09	0.00	0.00	0.00	0.00	0.00
Al_2O_3	20.84	20.69	21.10	21.19	21.16	20.83	21.30	21.46
MgO	5.19	3.02	3.76	4.37	5.21	5.14	4.67	4.77
FeO	31.23	31.62	30.86	30.85	29.87	30.72	31.59	30.97
CaO	3.02	3.03	3.25	3.17	3.39	3.09	3.22	3.16
MnO	1.95	3.65	3.39	2.96	1.96	2.17	2.14	2.21
Cr_2O_3	0.00	0.00	0.00	0.00	0.00	0.00	0.00	0.00
Total	99.24	98.86	99.11	99.70	98.47	98.99	98.85	99.50
Si	2.96	2.99	2.96	2.97	2.96	2.97	2.91	2.95
Al^4	0.04	0.01	0.04	0.03	0.04	0.03	0.09	0.05
Al^6	1.93	1.97	1.97	1.97	1.96	1.95	1.94	1.97
Cr	0.00	0.00	0.00	0.00	0.00	0.00	0.00	0.00
Ti	0.00	0.00	0.01	0.00	0.00	0.00	0.00	0.00
Fe	2.09	2.15	2.08	2.06	2.01	2.06	2.14	2.07
Mn	0.13	0.25	0.23	0.20	0.13	0.15	0.15	0.15
Mg	0.62	0.37	0.45	0.52	0.62	0.62	0.56	0.57
Ca	0.26	0.26	0.28	0.27	0.29	0.27	0.28	0.27
X_{alm}	0.67	0.71	0.68	0.68	0.66	0.67	0.68	0.68
X_{sps}	0.04	0.08	0.08	0.07	0.04	0.05	0.05	0.05
X_{py}	0.20	0.12	0.15	0.17	0.20	0.20	0.18	0.19
X_{gr}	0.08	0.09	0.09	0.09	0.10	0.09	0.09	0.09

Table 4.1 continued

Label	G7b	G7c	G7d	G8a	G8b	G5b	G20a	G20b
Location	core	rim	rim	rim	rim	rim	core	rim
SiO_2	36.96	36.73	36.62	36.78	36.67	36.57	36.97	36.74
TiO_2	0.00	0.00	0.00	0.00	0.00	0.00	0.00	0.00
Al_2O_3	21.64	21.24	21.48	21.78	21.52	21.34	21.45	21.20
MgO	5.18	3.70	3.98	4.83	3.25	2.61	4.66	3.20
FeO	31.62	32.05	31.54	31.14	32.26	32.27	30.42	31.34
CaO	3.16	3.23	3.25	3.31	3.34	2.93	3.04	2.83
MnO	2.25	3.89	2.99	2.45	3.53	3.66	2.64	3.93
Cr_2O_3	0.00	0.00	0.00	0.00	0.00	0.00	0.00	0.00
Total	100.88	100.92	99.88	100.28	100.59	99.43	99.18	99.33
Si	2.92	2.93	2.94	2.92	2.94	2.96	2.96	2.97
Al^4	0.08	0.07	0.06	0.08	0.06	0.04	0.04	0.03
Al^6	1.94	1.93	1.97	1.97	1.97	2.00	1.99	1.99
Cr	0.00	0.00	0.00	0.00	0.00	0.00	0.00	0.00
Ti	0.00	0.00	0.00	0.00	0.00	0.00	0.00	0.00
Fe	2.09	2.14	2.12	2.07	2.16	2.19	2.04	2.12
Mn	0.15	0.26	0.20	0.16	0.24	0.25	0.18	0.27
Mg	0.61	0.44	0.48	0.57	0.39	0.32	0.56	0.39
Ca	0.27	0.28	0.28	0.28	0.29	0.25	0.26	0.25
X_{alm}	0.67	0.69	0.69	0.67	0.70	0.73	0.67	0.70
X_{sps}	0.05	0.08	0.07	0.05	0.08	0.08	0.06	0.09
X_{py}	0.20	0.14	0.15	0.19	0.13	0.10	0.18	0.13
X_{gr}	0.09	0.09	0.09	0.09	0.09	0.08	0.09	0.08

Table 4.2   WS009 plagioclase compositions. Stoichiometry recalculated from oxide
wt% on a 16 oxygen basis. Table continued on next page.

Label	P1a	P1c	P1b	P2a	P2b	P3b	P3c	P4a
Location	rim	core	core	core	core	inclusion	inclusion	core
SiO_2	58.73	57.89	57.99	58.15	58.46	57.80	58.43	57.72
TiO_2	0.00	0.00	0.00	0.00	0.00	0.00	0.01	0.00
Al_2O_3	25.84	26.78	26.49	26.66	26.14	26.01	26.22	26.46
MgO	0.02	0.00	0.00	0.01	0.00	0.00	0.00	0.00
FeO	0.06	0.05	0.15	0.19	0.33	0.22	0.25	0.29
MnO	0.07	0.00	0.04	0.05	0.00	0.00	0.00	0.00
CaO	7.16	7.74	7.80	8.01	7.76	7.67	7.65	8.00
K_2O	0.19	0.09	0.07	0.05	0.03	0.03	0.03	0.03
Na_2O	7.11	6.59	6.99	7.00	7.09	7.17	7.20	6.90
BaO	0.00	0.00	0.00	0.00	0.00	0.00	0.00	0.00
Total	99.17	99.15	99.53	100.13	99.83	98.97	99.88	99.45
Si	5.28	5.21	5.21	5.20	5.24	5.23	5.23	5.19
Al	2.74	2.84	2.80	2.81	2.76	2.77	2.77	2.81
Ti	0.00	0.00	0.00	0.00	0.00	0.00	0.00	0.00
Fe	0.00	0.00	0.01	0.01	0.02	0.02	0.02	0.02
Mn	0.01	0.00	0.00	0.00	0.00	0.00	0.00	0.00
Mg	0.00	0.00	0.00	0.00	0.00	0.00	0.00	0.00
Ca	0.69	0.75	0.75	0.77	0.74	0.74	0.73	0.77
Na	1.24	1.15	1.22	1.21	1.23	1.26	1.25	1.20
K	0.02	0.01	0.01	0.01	0.00	0.00	0.00	0.00
Ba	0.00	0.00	0.00	0.00	0.00	0.00	0.00	0.00
X_{an}	0.35	0.39	0.38	0.39	0.38	0.37	0.37	0.39
X_{ab}	0.64	0.60	0.62	0.61	0.62	0.63	0.63	0.61
X_{or}	0.01	0.01	0.00	0.00	0.00	0.00	0.00	0.00

Table 4.2 continued

Label	P4b	P5b	P6a	P20a	P20b
Location	rim	rim	rim	rim	core
SiO_2	57.98	58.67	57.92	59.21	58.29
TiO_2	0.00	0.00	0.00	0.00	0.00
Al_2O_3	26.42	26.76	26.73	26.41	26.98
MgO	0.00	0.00	0.00	0.00	0.00
FeO	0.24	0.11	0.20	0.16	0.11
MnO	0.00	0.03	0.00	0.03	0.00
CaO	8.02	7.99	7.96	7.98	8.49
K_2O	0.04	0.07	0.06	0.04	0.16
Na_2O	7.17	6.89	7.10	7.00	6.76
BaO	0.01	0.00	0.00	0.00	0.00
Total	99.87	100.56	99.98	100.83	100.79
Si	5.20	5.21	5.19	5.24	5.18
Al	2.79	2.80	2.82	2.76	2.82
Ti	0.00	0.00	0.00	0.00	0.00
Fe	0.02	0.01	0.02	0.01	0.01
Mn	0.00	0.00	0.00	0.00	0.00
Mg	0.00	0.00	0.00	0.00	0.00
Ca	0.77	0.76	0.76	0.76	0.81
Na	1.25	1.19	1.23	1.20	1.16
K	0.00	0.01	0.01	0.00	0.02
Ba	0.00	0.00	0.00	0.00	0.00
X_{an}	0.38	0.39	0.38	0.39	0.41
X_{ab}	0.62	0.61	0.62	0.61	0.59
X_{or}	0.00	0.00	0.00	0.00	0.01

Table 4.3   WS009 matrix biotite rim compositions. Stoichiometry recalculated from oxide wt% on an 11 oxygen basis and all Fe is assumed to be Fe^{2+}.

Label	BT1b	BT1a	BT1c	BT5c	BT6a	BT6b	BT8a	BT13a	BT13b
SiO_2	35.52	36.23	36.40	36.51	35.76	36.37	35.99	34.98	35.04
TiO_2	1.94	3.03	2.78	1.25	3.35	3.29	3.11	2.42	2.47
Al_2O_3	18.36	18.74	18.41	18.33	18.27	18.35	18.45	17.73	18.04
MgO	10.59	10.07	10.23	14.08	10.09	10.23	10.37	10.60	10.53
FeO	19.09	19.16	19.15	17.49	18.30	19.45	19.20	18.10	17.66
CaO	0.07	0.00	0.16	0.14	0.06	0.09	0.00	0.06	0.05
MnO	0.03	0.09	0.05	0.00	0.07	0.10	0.06	0.00	0.00
K_2O	8.94	9.11	8.84	7.20	8.51	8.14	8.24	8.92	9.46
Na_2O	0.18	0.19	0.22	0.41	0.23	0.19	0.21	0.29	0.08
BaO	0.16	0.31	0.25	0.13	0.24	0.28	0.27	0.19	0.26
F	0.00	0.58	0.23	0.54	0.25	0.32	0.34	0.00	0.00
Cl	0.04	0.03	0.02	0.04	0.03	0.03	0.04	0.00	0.00
Total	94.91	97.32	96.62	95.88	95.04	96.70	96.15	93.29	93.59
Si	2.71	2.70	2.72	2.71	2.71	2.72	2.70	2.71	2.71
Al^4	1.29	1.30	1.28	1.29	1.29	1.28	1.30	1.29	1.29
Al^6	0.36	0.35	0.35	0.32	0.34	0.33	0.34	0.33	0.35
Ti	0.11	0.17	0.16	0.07	0.19	0.18	0.18	0.14	0.14
Fe	1.22	1.20	1.20	1.09	1.16	1.21	1.21	1.17	1.14
Mn	0.00	0.01	0.00	0.00	0.00	0.01	0.00	0.00	0.00
Mg	1.20	1.12	1.14	1.56	1.14	1.14	1.16	1.22	1.21
Ca	0.01	0.00	0.01	0.01	0.01	0.01	0.00	0.01	0.00
Na	0.03	0.03	0.03	0.06	0.03	0.03	0.03	0.04	0.01
K	0.87	0.87	0.84	0.68	0.82	0.78	0.79	0.88	0.93
Ba	0.00	0.01	0.01	0.00	0.01	0.01	0.01	0.01	0.01

counts the number of subscripts, $i\, j\, k$, equal to $m.$ A full expansion of γ for each endmember and further explanations about the activity models can be found in Appendix C. It is important to note that garnet activity coefficients are functions of composition, temperature, and pressure.

Fuhrman and Lindsley's (1988) ternary feldspar model was used to estimate plagioclase activities. Their model involves an Al-avoidance configurational entropy term (ideal activity) multiplied by a pressure and temperature dependent expression of excess free energy of mixing. Details can be found in Appendix C.

Biotite activities were calculated with Patiño Douce *et al.*'s (1993) activity model. This model computes composition dependent exchange component coefficients for Mg, Fe^{2+}, Al, and Ti in the octahedral layer. The specifics of the activity model are discussed in Appendix C.

Thermobarometry

If we combine mineral compositions, mineral activity calculations, standard state properties for the minerals of interest, and some well-chosen equilibrium equations for an equilibrium assemblage we should be able to deduce the pressure and temperature at which the minerals equilibrated. Three such equations appropriate for the assemblage present in WS009 are:

$$3(An)_{plag} \rightleftharpoons (Gross)_{gar} + 2Sill + Qtz \qquad (4.3)$$

$$(Al_2Mg_{-3})_{bt} + (Pyr)_{gar} \rightleftharpoons 2Sill + Qtz \qquad (4.4)$$

$$(Alm)_{gar} + (Phl)_{bt} \rightleftharpoons (Pyr)_{gar} + (Ann)_{bt} \qquad (4.5)$$
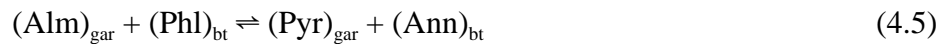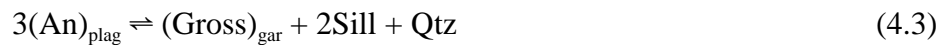
These equations were obvious choices for WS009 because they are appropriate for the assemblage and include mineral phases with well-calibrate thermodynamic properties and solution models. Another consideration in choosing equations for thermobarometry is their $\Delta S/\Delta V$ (dP/dT) slopes. Since pressure and temperature of equilibrium are estimated on the basis of intersections of the equilibrium equations in *P-T* space, lines that cross with very small angles between them present a higher uncertainty in calculated pressure and temperature because a small change in one variable causes a large change in the

other. Conversely, lines that cross at angles close to 90° have smaller uncertainties in pressure and temperature because changing one variable would change the other very slightly (or not at all if the intersection angle is 90°). Equation 4.3, also known as GASP (Garnet, Aluminosilicate, Silica, Plagioclase), has a dP/dT slope of 13.0498 bar/K. Equation 4.4 has a dP/dT slope of 167.9645 bar/K, and equation 4.5 has a dP/dT slope of -16.4146 bar/K.

The method for calculating equilibrium conditions (and hence P and T at equilibrium) of any equilibrium involving only solid phases is essentially the same: solve the equation for heterogenous chemical equilibrium:

$$\Delta G_r^{T,P} = \Delta H_r^o + \int_{298}^{T} \Delta c_p \partial T - T(\Delta S_r^o + \int_{298}^{T} \frac{\Delta c_p}{T} \partial T) + (P-1)\Delta V_r^o + RT\ln K = 0 \qquad (4.6)$$

ΔG is the Gibbs free energy of the reaction at the P and T of interest. Changes in enthalpy, ΔH; entropy, ΔS; molar volume, ΔV; and heat capacity, Δc_p, are known standard state properties taken from Berman (1988). R is the universal gas constant. By fixing one variable, P for equilibria with large dP/dT slopes (thermometers) or T for equilibria with small dP/dT slopes (barometers), the other can be found by letting it vary so that $\Delta G_r^{P,T} = 0$. By doing this iteratively over a range of P or T, the phase boundary of the reaction can be plotted in P–T space. When we can find two equilibrium equations for an assemblage and plot them in P-T space, the intersection of the equations gives the pressure and temperature at equilibrium. Due to uncertainties in standard state properties, analytical errors in mineral composition data, and disequilibrium a third equation is used to check the P and T found from the intersection of the first two equilibria. In a system where the standard state properties and mineral compositions were precisely and accurately known and equilibrium was perfect these three curves would intersect at a point. In reality they rarely form a point, rather they intersect to form an area which can
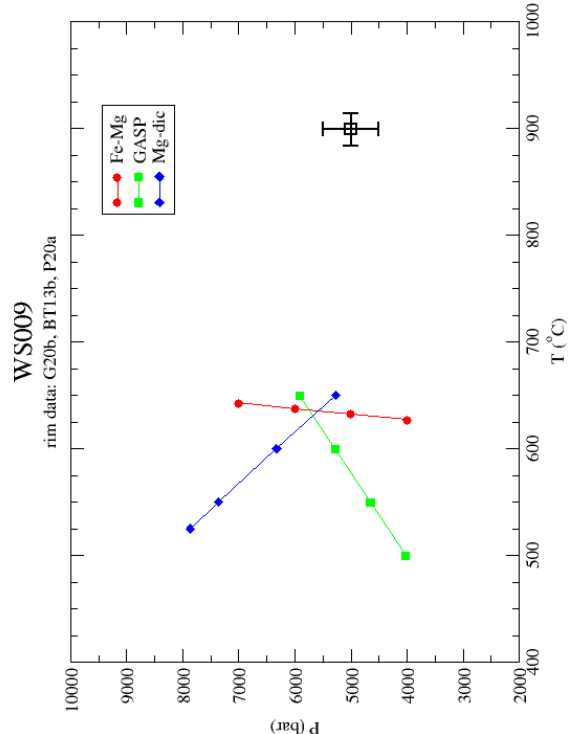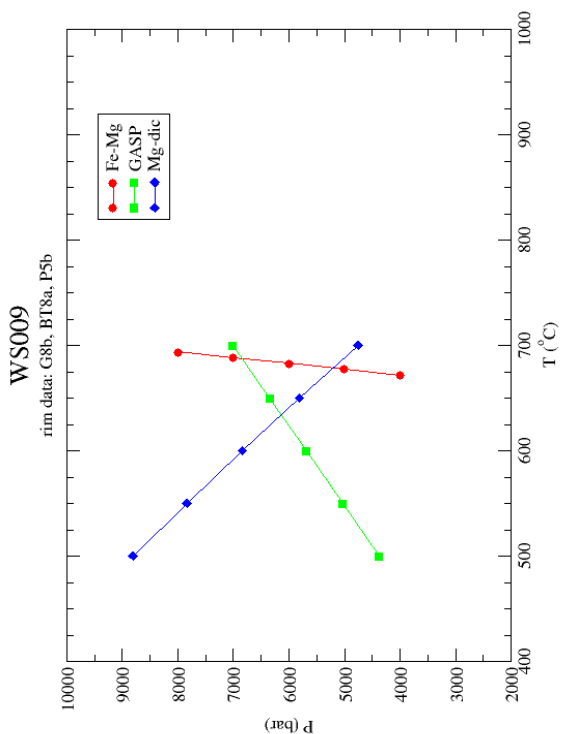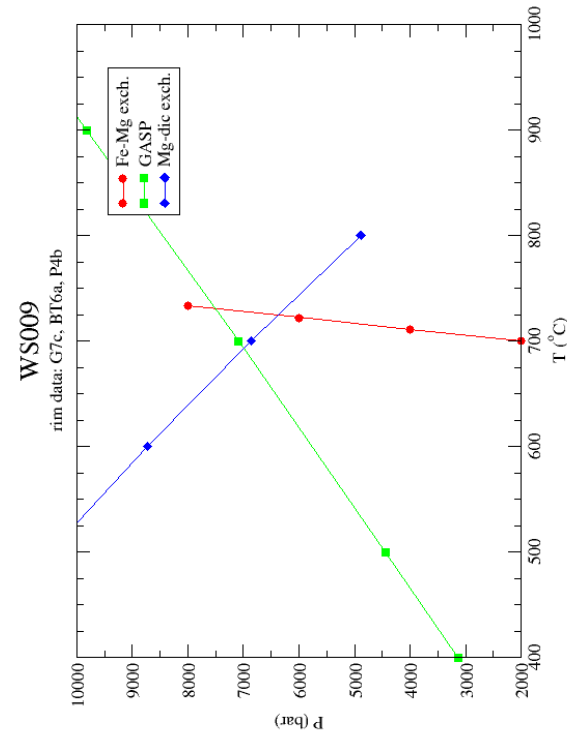
Figure 4.1

Plots of equations 4.3 (GASP), 4.4 (Mg-dic exch.), and 4.5 (Fe-Mg exch.) for sample WS009. All mineral analyses are from rims of adjacent crystals. Specific analysis labels are indicated in title of plots. Error bars for equilibria shown in lower left panel from Patiño *et al.*(1993).

be used to gage the quality of the computed pressure and temperature, where a smaller area suggests a more accurate estimate of P and T at equilibrium (Fig 4.1).

4.2 BIOTITE-AMPHIBOLE-GARNET GNEISSES: WS992, WS996

Five phases in samples WS992 and WS996 were analyzed with the electron probe micro-analyzer to determine their compositions: garnet, plagioclase, biotite, amphibole, and epidote. Analyses for each mineral in these two samples are presented in Tables 4.4 through 4.13. Quartz was assumed to be pure SiO_2. Stoichiometries were recalculated from oxide weight percent on a 12 oxygen basis for garnet, a 16 oxygen basis for plagioclase, an 11 oxygen basis for biotite, a 23 oxygen basis for amphibole, and a 12.5 oxygen basis for epidote.

Therombarometry and Activity Models

Activity models for garnet, plagioclase, and biotite are the same as for the previous sample, WS009. Epidote activity is addressed below in relation to minimum pressure determinations. Temperatures were determined using equation 4.5 where appropriate and Holland and Blundy's (1994) amphibole–plagioclase thermometers:

$$(Ed)_{amph} + 4Qtz \rightleftharpoons (Tr)_{amph} + (Ab)_{plag} \tag{4.7}$$

$$(Ed)_{amph} + (Ab)_{plag} \rightleftharpoons (Ric)_{amph} + (An)_{plag} \tag{4.8}$$
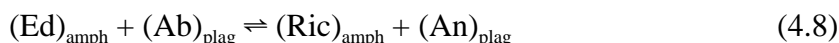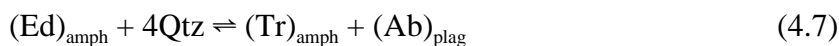
Being thermometers, both equations have very steep dP/dT slopes, 293.58 bar/K for equation 4.7 and 100.46 bar/K for equation 4.8. Holland and Blundy (1994) combined each equation with a ferric iron recalculation and site allocation scheme for amphibole along with a plagioclase activity model to produce a single expression of temperature for each thermometer as a function of pressure, plagioclase composition, and amphibole composition. These thermometers are in a sense free standing because they do not rely on external activity models. Results of applying equations 4.5, 4.7, and 4.8 to WS992 and WS996 are presented in Figures 4.2 and 4.3. Full details for these thermometers can be found in Appendix A.

No equilibria appropriate for direct determination of pressure could be found in WS992 or WS996, although an appropriate equilibria for calculating minimum pressure

Table 4.4   Garnet compositions for sample WS992. Stoichiometry recalculated from oxide wt% on a 12 oxygen basis.

Label	G1a	G2	G2a	G3
Location	rim	rim	rim	rim
SiO_2	37.59	37.31	37.69	36.78
TiO_2	0.00	0.00	0.00	0.00
Al_2O_3	21.35	21.26	21.23	20.95
MgO	4.58	5.66	5.56	4.01
FeO	26.85	27.23	26.37	27.70
CaO	6.09	5.97	6.05	6.05
MnO	4.15	3.11	3.68	5.02
Cr_2O_3	0.00	0.14	0.00	0.00
Total	100.61	100.69	100.59	100.52
Si	2.96	2.93	2.96	2.93
Al^4	0.04	0.07	0.04	0.07
Al^6	1.95	1.89	1.92	1.90
Cr	0.00	0.02	0.00	0.00
Ti	0.00	0.00	0.00	0.00
Fe	1.77	1.79	1.73	1.85
Mn	0.28	0.21	0.24	0.34
Mg	0.54	0.66	0.65	0.48
Ca	0.51	0.50	0.51	0.52
X_{alm}	0.57	0.57	0.55	0.58
X_{sps}	0.09	0.07	0.08	0.11
X_{py}	0.17	0.21	0.21	0.15
X_{gr}	0.17	0.16	0.16	0.16

Table 4.5　　Garnet compositions for sample WS996. Stoichiometry recalculated from oxide wt% on a 12 oxygen basis. Continued on next page.

Label	G1a	G2a	G2b	G2c	G3a	G3b	G3c	G4b	G1d
Location	core				rim	rim	rim	core	
SiO_2	36.46	36.83	37.00	36.35	36.97	37.03	37.44	36.98	36.97
TiO_2	0.11	0.06	0.00	0.00	0.00	0.00	0.05	0.00	0.00
Al_2O_3	20.37	20.87	21.02	20.23	20.87	20.74	20.80	20.95	20.98
MgO	2.79	2.92	3.36	2.61	2.98	2.98	3.14	3.62	3.14
FeO	26.32	28.27	28.36	25.81	27.50	27.97	27.29	26.43	27.96
CaO	9.83	8.37	8.64	9.73	8.88	8.73	8.42	8.25	7.90
MnO	2.80	2.49	1.45	3.30	2.20	1.94	2.34	2.46	1.67
Cr_2O_3	0.00	0.03	0.00	0.00	0.00	0.00	0.00	0.03	0.00
Total	98.68	99.84	99.85	98.08	99.43	99.43	99.47	98.73	98.62
Si	2.95	2.95	2.95	2.96	2.96	2.97	2.99	2.97	2.98
Al^4	0.05	0.05	0.05	0.04	0.04	0.03	0.01	0.03	0.02
Al^6	1.90	1.92	1.93	1.91	1.94	1.93	1.95	1.95	1.97
Cr	0.00	0.01	0.00	0.00	0.00	0.00	0.00	0.01	0.00
Ti	0.01	0.00	0.00	0.00	0.00	0.00	0.00	0.00	0.00
Fe	1.78	1.89	1.89	1.76	1.84	1.88	1.82	1.77	1.88
Mn	0.19	0.17	0.10	0.23	0.15	0.13	0.16	0.17	0.11
Mg	0.34	0.35	0.40	0.32	0.36	0.36	0.37	0.43	0.38
Ca	0.85	0.72	0.74	0.85	0.76	0.75	0.72	0.71	0.68
X_{alm}	0.56	0.61	0.60	0.56	0.59	0.60	0.59	0.58	0.62
X_{sps}	0.06	0.05	0.03	0.07	0.05	0.04	0.05	0.05	0.04
X_{py}	0.11	0.11	0.13	0.10	0.11	0.11	0.12	0.14	0.12
X_{gr}	0.27	0.23	0.24	0.27	0.25	0.24	0.23	0.23	0.22

Table 4.5 continued

Label	G5a	G5c	G6a	G23a	G23b	G24a	G25
Location	rim			rim	core	rim	
SiO_2	37.14	37.33	37.01	37.47	37.47	36.81	37.56
TiO_2	0.00	0.00	0.00	0.00	0.00	0.00	0.00
Al_2O_3	21.56	21.65	21.73	20.94	21.22	20.79	20.86
MgO	3.42	3.40	3.49	2.66	3.31	3.57	3.59
FeO	29.47	27.63	29.13	27.11	27.59	27.75	29.37
CaO	8.36	8.41	9.09	8.71	8.49	8.18	8.35
MnO	1.62	1.86	1.01	3.21	1.46	1.81	1.24
Cr_2O_3	0.00	0.13	0.00	0.00	0.00	0.00	0.00
Total	101.63	100.42	101.48	100.15	99.59	98.96	101.01
Si	2.92	2.94	2.91	2.98	2.98	2.96	2.97
Al^4	0.08	0.06	0.09	0.02	0.02	0.04	0.03
Al^6	1.92	1.96	1.92	1.95	1.97	1.93	1.91
Cr	0.01	0.02	0.00	0.01	0.00	0.00	0.00
Ti	0.00	0.00	0.00	0.00	0.00	0.00	0.00
Fe	1.94	1.82	1.91	1.80	1.83	1.87	1.94
Mn	0.11	0.12	0.07	0.22	0.10	0.12	0.08
Mg	0.40	0.40	0.41	0.32	0.39	0.43	0.42
Ca	0.70	0.71	0.77	0.74	0.72	0.70	0.71
X_{alm}	0.62	0.60	0.61	0.59	0.60	0.60	0.62
X_{sps}	0.03	0.04	0.02	0.07	0.03	0.04	0.03
X_{py}	0.13	0.13	0.13	0.10	0.13	0.14	0.13
X_{gr}	0.22	0.23	0.24	0.24	0.24	0.23	0.22

Table 4.6 WS992 plagioclase compositions. Stoichiometry recalculated from oxide wt% on a 16 oxygen basis.

Label	P5a	P5b	P6a	P6b	P7a	P1a	P1b	P3	P4
Location	core	rim	core	rim	inc.	rim	rim	rim	rim
SiO_2	57.75	58.35	57.89	59.13	57.67	58.78	58.09	57.69	57.63
TiO_2	0.00	0.00	0.02	0.00	0.00	0.00	0.00	0.00	0.00
Al_2O_3	27.24	27.14	26.67	26.38	27.40	27.17	27.60	27.32	27.13
MgO	0.00	0.00	0.00	0.02	0.00	0.00	0.00	0.00	0.02
FeO	0.10	0.21	0.00	0.27	0.36	0.07	0.18	0.34	0.43
MnO	0.00	0.00	0.00	0.00	0.00	0.00	0.00	0.00	0.00
CaO	8.58	7.96	8.64	7.65	8.22	8.24	8.22	8.42	8.74
K_2O	0.09	0.08	0.06	0.07	0.06	0.07	0.05	0.03	0.06
Na_2O	6.62	6.97	6.58	7.21	6.65	6.83	6.96	6.73	6.40
BaO	0.00	0.00	0.00	0.00	0.00	0.00	0.11	0.00	0.00
Total	100.42	100.77	99.89	100.73	100.38	101.20	101.24	100.63	100.45
Si	5.15	5.18	5.19	5.25	5.14	5.19	5.14	5.14	5.14
Al	2.86	2.84	2.82	2.76	2.88	2.83	2.88	2.87	2.85
Ti			0.00	0.00			0.00	0.00	0.00
Fe	0.01	0.02		0.02	0.03	0.00	0.01	0.03	0.03
Mn	0.00	0.00			0.00	0.00	0.00	0.00	0.00
Mg				0.00					0.00
Ca	0.82	0.76	0.83	0.73	0.79	0.78	0.78	0.80	0.84
Na	1.14	1.20	1.14	1.24	1.15	1.17	1.19	1.16	1.11
K	0.01	0.01	0.01	0.01	0.01	0.01	0.01	0.00	0.01
Ba		0.00	0.00				0.00	0.00	0.00
X_{an}	0.42	0.39	0.42	0.37	0.40	0.40	0.39	0.41	0.43
X_{ab}	0.58	0.61	0.58	0.63	0.59	0.60	0.60	0.59	0.57
X_{or}	0.01	0.00	0.00	0.00	0.00	0.00	0.00	0.00	0.00

Table 4.7   WS996 plagioclase compositions. Stoichiometry recalculated from oxide wt% on a 16 oxygen basis. Continued on next page.

Label	P5	P14	P14b	P7a	P7b	P8a	P8b	P9a	P9b
Locatio		core	rim	core	rim	core	rim	rim	core
SiO_2	56.94	55.53	56.67	54.64	58.39	55.49	61.09	56.02	56.39
TiO_2	0.00	0.00	0.00	0.00	0.00	0.00	0.00	0.00	0.00
Al_2O_3	27.54	28.66	28.36	28.45	26.36	27.98	24.43	28.39	27.60
MgO	0.02	0.00	0.00	0.00	0.02	0.01	0.00	0.00	0.00
FeO	0.00	0.00	0.00	0.19	0.26	0.26	0.20	0.00	0.11
MnO	0.00	0.00	0.00	0.01	0.07	0.00	0.00	0.00	0.00
CaO	9.11	10.73	9.84	10.47	7.58	9.47	5.38	9.47	8.93
K_2O	0.04	0.05	0.06	0.05	0.03	0.02	0.06	0.08	0.06
Na_2O	6.26	5.68	5.85	5.72	7.08	5.77	8.36	6.02	6.40
BaO	0.03	0.00	0.00	0.00	0.00	0.01	0.00	0.06	0.06
Total	100.04	100.72	100.84	99.54	99.79	98.99	99.55	100.09	99.57
Si	5.10	4.97	5.04	4.95	5.23	5.03	5.45	5.03	5.08
Al	2.91	3.02	2.97	3.04	2.78	2.99	2.57	3.00	2.93
Ti	0.00	0.00	0.00	0.00	0.00	0.00	0.00	0.00	0.00
Fe	0.01	0.00	0.00	0.01	0.02	0.02	0.02	0.00	0.01
Mn	0.00	0.00	0.00	0.00	0.01	0.00	0.00	0.00	0.00
Mg	0.00	0.00	0.00	0.00	0.00	0.00	0.00	0.00	0.00
Ca	0.87	1.03	0.94	1.02	0.73	0.92	0.51	0.91	0.86
Na	1.09	0.99	1.01	1.01	1.23	1.01	1.44	1.05	1.12
K	0.00	0.01	0.01	0.01	0.00	0.00	0.01	0.01	0.01
Ba	0.00	0.00	0.00	0.00	0.00	0.00	0.00	0.00	0.00
X_{an}	0.44	0.51	0.48	0.50	0.37	0.48	0.26	0.46	0.43
X_{ab}	0.55	0.49	0.52	0.50	0.63	0.52	0.74	0.53	0.56
X_{or}	0.00	0.00	0.00	0.00	0.00	0.00	0.00	0.00	0.00

Table 4.7 continued

Label	P10	P11	P12
Location	core	rim	
SiO_2	56.10	60.93	58.05
TiO_2	0.00	0.03	0.00
Al_2O_3	27.95	24.64	27.12
MgO	0.00	0.01	0.00
FeO	0.08	0.17	0.14
MnO	0.06	0.00	0.08
CaO	9.41	5.50	8.12
K_2O	0.05	0.03	0.04
Na_2O	6.27	8.25	6.86
BaO	0.11	0.00	0.00
Total	100.02	99.57	100.43
Si	5.04	5.43	5.17
Al	2.96	2.59	2.85
Ti	0.00	0.00	0.00
Fe	0.01	0.01	0.01
Mn	0.00	0.00	0.01
Mg	0.00	0.00	0.00
Ca	0.91	0.53	0.77
Na	1.09	1.43	1.18
K	0.01	0.00	0.00
Ba	0.00	0.00	0.00
X_{an}	0.45	0.27	0.39
X_{ab}	0.55	0.73	0.60
X_{or}	0.00	0.00	0.00

Table 4.8   WS992 matrix biotite rim compositions. Stoichiometry recalculated from oxide wt% on an 11 oxygen basis with all Fe assumed to be Fe^{2+}.

Label	BT1a	BT1b	BT2	BT2a
SiO_2	37.27	35.87	36.43	36.17
TiO_2	2.09	2.05	2.43	2.36
Al_2O_3	17.44	17.24	17.06	17.14
MgO	12.28	12.29	12.29	12.17
FeO	18.03	18.36	17.12	17.97
CaO	0.13	0.10	0.03	0.04
MnO	0.09	0.30	0.19	0.12
K_2O	7.86	8.97	8.46	9.57
Na_2O	0.00	0.00	0.00	0.00
BaO	0.26	0.18	0.18	0.29
Total	95.64	95.56	94.37	96.03
Si	2.78	2.72	2.76	2.73
Al^4	1.22	1.28	1.24	1.27
Al^6	0.31	0.25	0.28	0.25
Ti	0.12	0.12	0.14	0.13
Fe	1.13	1.16	1.08	1.13
Mn	0.01	0.02	0.01	0.01
Mg	1.37	1.39	1.39	1.37
Ca	0.01	0.01	0.00	0.00
Na	0.03	0.03	0.03	0.03
K	0.75	0.87	0.82	0.92
Ba	0.01	0.01	0.01	0.01
Total	7.72	7.85	7.76	7.85

Table 4.9 WS996 matrix biotite compositions. Stoichiometry recalculated from oxide wt% on an 11 oxygen basis with all Fe assumed to be Fe^{2+}. Blank entries denote elements not analyzed. Continued on the next two pages.

Label	BT1a	BT2a	BT3a	BT3b	BT3c	BT4a	BT5a	BT5b	BT1b
SiO_2	35.86	36.52	35.65	35.87	34.61	37.12	36.84	36.73	34.64
TiO_2	2.61	1.31	1.64	1.93	2.13	1.61	2.44	2.24	2.21
Al_2O_3	17.28	17.97	17.31	17.62	17.10	18.10	18.22	18.39	18.44
MgO	9.27	10.56	9.61	9.47	9.35	10.96	9.68	9.75	8.86
FeO	21.32	20.17	20.91	20.71	21.78	19.58	19.47	20.06	19.75
CaO	0.02	0.08	0.36	0.10	0.19	0.05	0.09	0.18	0.11
MnO	0.00	0.21	0.09	0.00	0.13	0.10	0.13	0.10	0.00
K_2O	8.76	7.36	8.81	8.21	8.11	7.08	9.06	8.26	9.04
Na_2O	0.17	0.15	0.19	0.18	0.18	0.20	0.26	0.29	0.25
BaO	0.90	0.48	0.34	0.69	0.73	0.51	0.91	0.77	0.19
Cl	0.07	0.06	0.05	0.07	0.08	0.07	0.05	0.04	0.04
Total	96.33	94.85	94.93	94.90	94.35	95.35	97.13	96.81	93.53
Si	2.74	2.78	2.75	2.76	2.70	2.79	2.76	2.75	2.70
Al^4	1.26	1.22	1.25	1.24	1.30	1.21	1.24	1.25	1.30
Al^6	0.29	0.39	0.32	0.35	0.28	0.39	0.37	0.38	0.39
Ti	0.15	0.08	0.09	0.11	0.13	0.09	0.14	0.13	0.13
Fe	1.36	1.28	1.35	1.33	1.42	1.23	1.22	1.26	1.29
Mn	0.00	0.01	0.01	0.00	0.01	0.01	0.01	0.01	0.00
Mg	1.06	1.20	1.11	1.09	1.09	1.23	1.08	1.09	1.03
Ca	0.00	0.01	0.03	0.01	0.02	0.00	0.01	0.01	0.01
Na	0.03	0.02	0.03	0.03	0.03	0.03	0.04	0.04	0.04
K	0.85	0.71	0.87	0.81	0.81	0.68	0.87	0.79	0.90
Ba	0.03	0.01	0.01	0.02	0.02	0.02	0.03	0.02	0.01
Total	7.77	7.71	7.82	7.75	7.80	7.67	7.75	7.72	7.79

Table 4.9 continued

Label	BT8b	BT9b	BT10a	BT7c	BT3d	BT12a	BT20	BT20a
SiO_2	35.72	35.24	35.35	35.92	34.39	34.94	35.22	35.09
TiO_2	2.26	1.88	1.95	1.84	1.77	2.60	1.65	1.60
Al_2O_3	18.00	18.22	18.12	17.43	17.64	17.36	17.52	17.57
MgO	10.01	9.87	9.94	10.29	9.85	9.31	10.06	9.80
FeO	20.18	20.96	21.17	19.41	21.30	20.95	20.26	20.00
CaO	0.05	0.04	0.05	0.07	0.22	0.00	0.08	0.08
MnO	0.13	0.00	0.08	0.17	0.17	0.16	0.15	0.00
K_2O	8.82	8.80	8.28	8.48	8.06	8.65	8.40	8.19
Na_2O	0.27	0.11	0.20	0.20	0.25	0.27	0.27	0.20
BaO	0.82	0.71	0.70	0.80	0.42	0.93	0.81	0.74
Cl								
Total	96.26	95.84	95.83	94.61	94.07	95.18	94.43	93.29
Si	2.71	2.70	2.70	2.76	2.68	2.70	2.73	2.74
Al^4	1.29	1.30	1.30	1.24	1.32	1.30	1.27	1.26
Al^6	0.32	0.34	0.33	0.34	0.30	0.29	0.33	0.36
Ti	0.13	0.11	0.11	0.11	0.10	0.15	0.10	0.09
Fe	1.28	1.34	1.35	1.25	1.39	1.36	1.31	1.31
Mn	0.01	0.00	0.01	0.01	0.01	0.01	0.01	0.00
Mg	1.13	1.13	1.13	1.18	1.15	1.07	1.16	1.14
Ca	0.00	0.00	0.00	0.01	0.02	0.00	0.01	0.01
Na	0.04	0.02	0.03	0.03	0.04	0.04	0.04	0.03
K	0.85	0.86	0.81	0.83	0.80	0.85	0.83	0.82
Ba	0.02	0.02	0.02	0.02	0.01	0.03	0.02	0.02
Total	7.80	7.81	7.79	7.77	7.82	7.80	7.81	7.78

Table 4.9 continued

Label	BT20b	BT21
SiO_2	35.03	34.90
TiO_2	1.76	2.33
Al_2O_3	17.79	17.59
MgO	10.17	10.02
FeO	20.17	21.16
CaO	0.09	0.05
MnO	0.00	0.05
K_2O	8.82	9.04
Na_2O	0.20	0.22
BaO	0.85	0.93
Cl		
Total	94.87	96.30
Si	2.71	2.68
Al^4	1.29	1.32
Al^6	0.32	0.27
Ti	0.10	0.13
Fe	1.30	1.36
Mn	0.00	0.00
Mg	1.17	1.15
Ca	0.01	0.00
Na	0.03	0.03
K	0.87	0.88
Ba	0.03	0.03
Total	7.83	7.85

Table 4.10   Amphibole analyses from sample WS992. Stoichiometry recalculated from oxide wt% on a 23 oxygen basis with all Fe assumed to be Fe^{2+}.

Label	HBL8a	HBL8b	HBL9a	HBL9a	HBL9b	HBL9c	HBL9c	HBL1a
Location	rim	core	rim	rim	core	core	core	rim
SiO_2	40.97	41.49	40.72	41.65	42.03	41.22	41.61	40.10
TiO_2	0.84	0.86	0.54	0.58	0.99	0.77	0.83	0.61
Al_2O_3	14.49	14.62	14.72	14.56	14.04	14.98	13.96	15.20
MgO	9.46	8.99	8.96	9.05	9.65	8.99	9.30	8.30
FeO	17.56	18.06	16.61	16.63	16.91	15.95	16.79	18.18
CaO	11.54	11.64	11.28	11.96	11.37	11.21	11.74	11.46
MnO	0.43	0.36	0.22	0.32	0.34	0.37	0.28	0.42
K_2O	0.92	0.94	0.88	0.77	0.80	0.81	0.86	0.93
Na_2O	1.62	1.59	1.54	1.53	1.62	1.61	1.66	1.69
BaO	0.11	0.08	0.00	0.00	0.00	0.00	0.00	0.00
Total	97.93	98.64	95.52	97.04	97.74	95.91	97.01	96.96
Si	6.18	6.21	6.25	6.29	6.30	6.27	6.30	6.13
Al^4	1.82	1.79	1.75	1.71	1.70	1.73	1.70	1.87
Al^6	0.75	0.79	0.91	0.88	0.78	0.96	0.78	0.87
Ti	0.09	0.10	0.06	0.07	0.11	0.09	0.09	0.07
Fe	2.21	2.26	2.13	2.10	2.12	2.03	2.12	2.32
Mn	0.06	0.05	0.03	0.04	0.04	0.05	0.04	0.05
Mg	2.13	2.01	2.05	2.04	2.16	2.04	2.10	1.89
Ca	1.86	1.87	1.85	1.93	1.83	1.83	1.90	1.88
Na	0.47	0.46	0.46	0.45	0.47	0.47	0.49	0.50
K	0.18	0.18	0.17	0.15	0.15	0.16	0.17	0.18
Ba	0.01	0.00	0.00	0.00	0.00	0.00	0.00	0.00

Table 4.11   Amphibole analyses from sample WS996. Stoichiometry recalculated from oxide wt% on a 23 oxygen basis with all Fe assumed to be Fe^{2+}.

Label	HBL1a	HBL1b
Location	rim	core
SiO_2	39.54	39.13
TiO_2	0.50	0.74
Al_2O_3	15.68	15.56
MgO	6.31	6.23
FeO	21.02	21.28
CaO	11.70	11.11
MnO	0.17	0.25
K_2O	0.98	1.10
Na_2O	1.50	1.55
BaO	0.00	0.00
F	0.00	0.00
Cl	0.07	0.07
Total	97.48	97.01
Si	6.09	6.07
Al^4	1.91	1.93
Al^6	0.94	0.91
Ti	0.06	0.09
Fe	2.71	2.76
Mn	0.02	0.03
Mg	1.45	1.44
Ca	1.93	1.85
Na	0.45	0.47
K	0.19	0.22
Ba	0.00	0.00

Table 4.12   WS992 zoisite analyses. Stoichiometry recalculated from oxide wt% on a
12.5 oxygen basis and all Fe is assumed to be Fe^{2+}.

Label	EP1a	EP1b
Location	rim	core
SiO_2	37.91	38.23
TiO_2	0.14	0.21
Al_2O_3	25.84	26.30
MgO	0.04	0.08
FeO	10.06	9.42
MnO	0.19	0.34
CaO	23.24	23.00
K_2O	0.00	0.00
Na_2O	0.00	0.00
BaO	0.00	0.00
Total	97.46	97.59
Si	3.05	3.06
Al	2.45	2.48
Ti	0.01	0.01
Fe	0.68	0.63
Mn	0.01	0.02
Mg	0.00	0.01
Ca	2.00	1.97
Na		
K	0.00	
Ba	0.00	0.00

Table 4.13   WS996 zoisite analyses. Stoichiometry recalculated from oxide wt% on a
12.5 oxygen basis with all Fe assumed to be Fe^{2+}. Entries are blank for
elements not analyzed.

Label	EP3	EP1	EP2	EP6a	EP6b	EP6b	EP7a	EP8a	EP8b
Location				rim	core	core	rim	rim	core
SiO2	37.71	37.01	32.94	37.49	37.53	37.57	37.92	38.21	32.75
TiO2	0.14	0.11	0.17	0.15	0.16	0.12	0.14	0.09	0.08
Al2O3	24.94	25.37	19.99	25.26	25.46	25.20	25.53	25.44	20.19
MgO	0.00	0.03	0.56	0.06	0.16	0.12	0.06	0.00	0.49
FeO	11.24	10.06	11.25	9.96	10.36	9.12	10.82	10.13	10.83
CaO	23.25	23.13	16.76	23.07	21.83	22.42	23.03	23.50	16.78
MnO	0.14	0.08	0.06	0.15	0.09	0.07	0.27	0.28	0.23
Cr2O3	0.03	0.13	0.00						
K2O	0.00	0.00	0.00	0.00	0.00	0.00	0.00	0.00	0.00
Na2O	0.00	0.00	0.03	0.00	0.03	0.00	0.00	0.00	0.00
Total	97.48	95.91	81.76	96.14	95.66	94.63	97.84	97.68	81.35
Si	3.06	3.03	3.17	3.17	3.07	3.09	3.05	3.07	3.17
Al	2.38	2.45	2.27	2.51	2.46	2.45	2.42	2.41	2.30
Ti	0.01	0.01	0.01	0.01	0.01	0.01	0.01	0.01	0.01
Fe	0.76	0.69	0.91	0.70	0.71	0.63	0.73	0.68	0.88
Mn	0.01	0.01	0.00	0.03	0.01	0.00	0.02	0.02	0.02
Ca	2.02	2.03	1.73	1.65	1.91	1.98	1.99	2.02	1.74
Mg	0.00	0.00	0.08	0.01	0.02	0.01	0.01	0.00	0.07
Cr	0.00	0.03	0.00	0.00	0.00	0.00	0.00	0.00	0.00
Na	0.00	0.00	0.01	0.00	0.01	0.00	0.01	0.00	0.00
K	0.00	0.00	0.00	0.00	0.00	0.00	0.00	0.00	0.00

was available for WS996. The methods and results of minimum pressure calculations are discussed and presented later in this chapter.

4.3 AMPHIBOLITES: WS995, H761, WS0011

Samples WS995, H761, and WS0011, are amphibolites collected at, north of, and south (respectively) of Woodall Shoals (Fig. 3.1). Amphibole and plagioclase were analyzed in all samples (Tables 4.15 to 4.20). Zoisite was analyzed in WS995 (Table 4.22) and WS0011 (Table 4.21). Garnet was present only in WS0011 (Table 4.14).

Activity models and thermobarometry methods are similar to those utilized for samples WS992 and WS996. Activity models include Fuhrman and Lindsley's (1988) model for plagioclase and Berman's (1990) model for garnet. Temperature was determined using Holland and Blundy's (1994) amphibole-plagioclase thermometers (Equns. 4.7 and 4.8). Thermometry results are presented in Figures 4.4 to 4.6. As in samples WS992 and WS996, the amphibolite assemblages did not allow direct barometry so only minimum pressures could be determined.

4.4 MINIMUM PRESSURE CALCULATIONS

Since the assemblages in WS996 and WS0011 precluded direct barometry, minimum pressures were calculated by applying the equilibrium:

$$5(An)_{plag} + (Grs)_{gar} + 2H_2O \rightleftharpoons (Zoi)_{epi} + Qtz \tag{4.9}$$
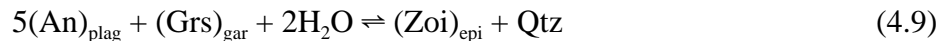
to the Gibbs equation (4.6), in a fashion similar to the technique described above that used equilibria containing only solid constituents. Since this equilibrium (4.9) has both solid and vapor phases, a fugacity term, $RT\ln f$, is added to the heterogenous equilibrium equation (Eqn. 4.6) to take the gas phase into account. We now have three variables, P, T, and f. If there are independent constraints of water fugacity and temperature we can solve for P, using this equilibria as an absolute barometer.

In this study however the only independent constraints are for temperature so we can not compute an absolute pressure, but we can find a minimum pressure. The first step to finding a minimum pressure is to solve the equilibrium equation for f as a function
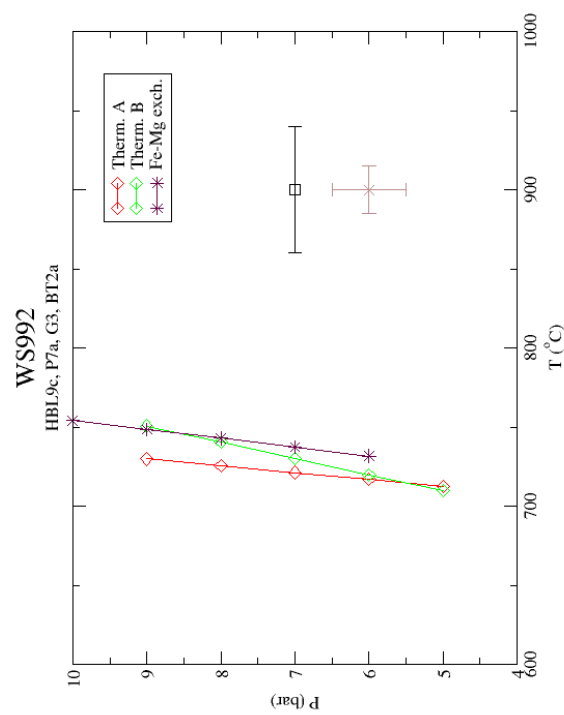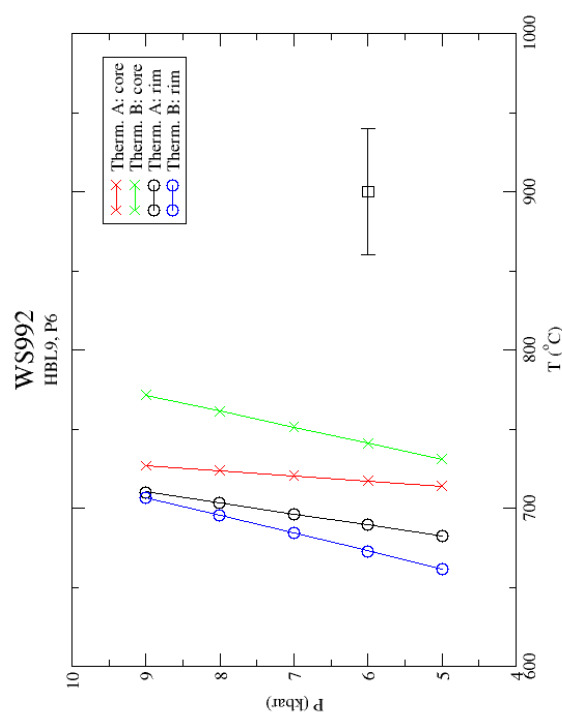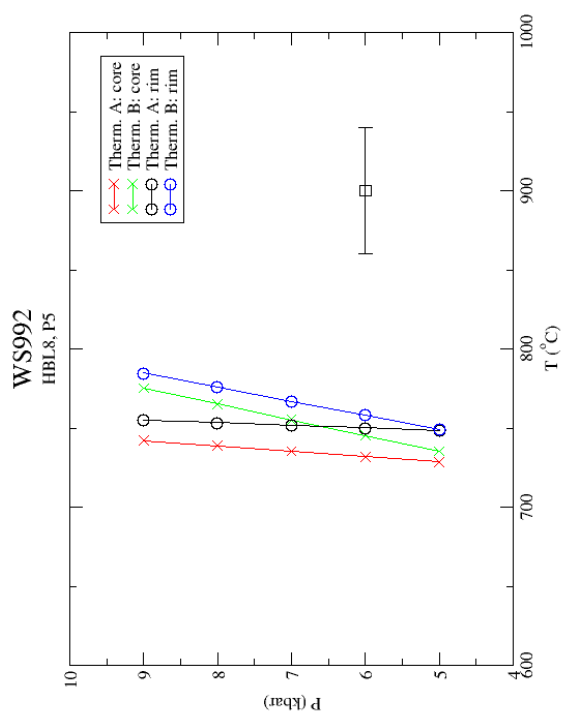
Figure 4.2
Calculated temperatures from WS992. Pressure determinations from these intersections are unreliable because of large dP/dT slopes of all phase boundaries. Black error bars for Therm. A (Ed-Tr) and Therm. B (Ed-Rich) – Holland and Bludy (1994). Brown error bar for Fe-Mg exch. – Patiño Douce *et al.* (1993).
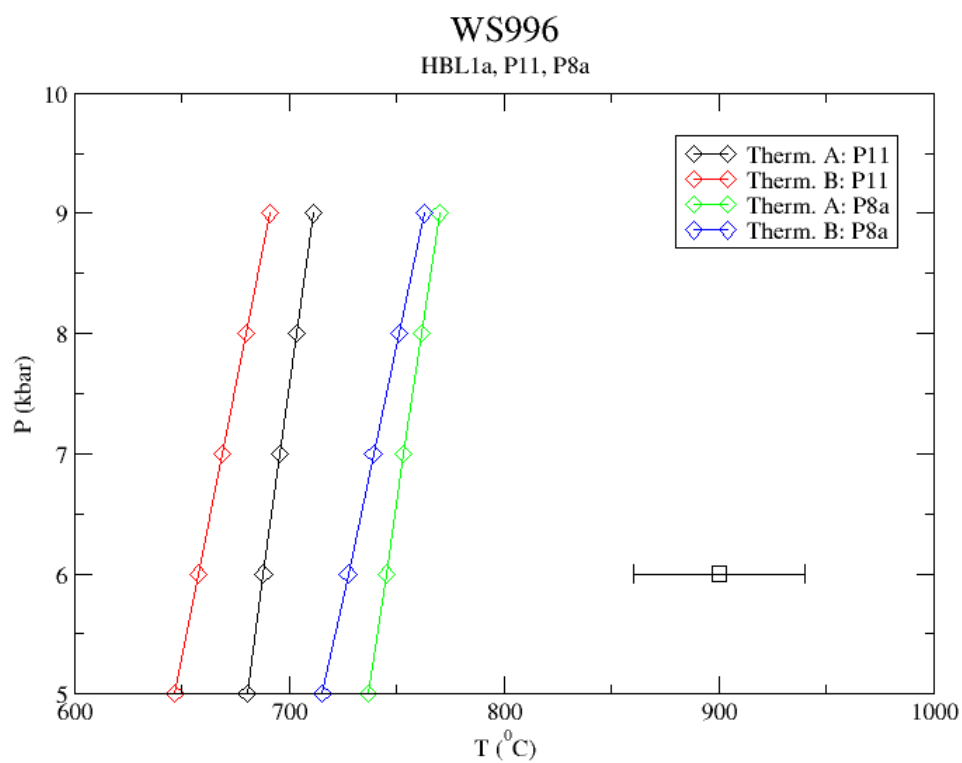
Figure4.3 Cal

Figure 4.3   Calculated temperatures for WS996.   Therm. A (Ed-Tr), Therm.
                    B (Ed-Rich), and error bar from Holland and Blundy (1994).

Table 4.14   WS0011 garnet compositions. Stoichiometry recalculated from oxide wt% on a 12 oxygen basis.

Label	G1a	G1b	G6	G7	G9a	G10a
Location	rim	core	rim	rim	rim	
SiO_2	36.63	36.90	37.29	37.33	37.74	37.68
TiO_2	0.10	0.09	0.08	0.09	0.00	0.07
Al_2O_3	21.59	21.37	21.12	21.37	21.24	21.49
MgO	2.95	2.73	2.38	2.85	2.67	2.51
FeO	25.38	25.12	24.41	24.87	23.85	24.18
CaO	10.62	10.75	10.20	10.33	10.24	10.54
MnO	2.65	3.02	4.63	2.99	4.59	4.06
Cr_2O_3	0.00	0.00	0.00	0.00	0.00	0.00
Total	99.94	100.03	100.19	99.83	100.41	100.52
Si	2.91	2.93	2.96	2.96	2.98	2.97
Al^4	0.09	0.07	0.04	0.04	0.02	0.03
Al^6	1.94	1.93	1.94	1.96	1.95	1.97
Cr	0.00	0.01	0.02	0.00	0.02	0.00
Ti	0.01	0.01	0.00	0.01	0.00	0.00
Fe	1.69	1.67	1.62	1.65	1.57	1.59
Mn	0.18	0.20	0.31	0.20	0.31	0.27
Mg	0.35	0.32	0.28	0.34	0.31	0.30
Ca	0.91	0.91	0.87	0.88	0.87	0.89
X_{alm}	0.54	0.54	0.53	0.54	0.51	0.52
X_{sps}	0.06	0.07	0.10	0.07	0.10	0.09
X_{py}	0.11	0.10	0.09	0.11	0.10	0.10
X_{gr}	0.29	0.29	0.28	0.29	0.28	0.29

Table 4.15   WS0011 plagioclase compostions. Stoichiometry recalculated from oxide wt% on a 16 oxygen basis. Continued on next page.

Label	P1	P2	P3	P4	P10	P11	P12	P13	P3a
Location		rim	rim	rim	rim	rim	rim	rim	rim
SiO_2	46.93	44.85	46.39	58.45	47.78	56.46	46.47	46.13	46.02
TiO_2	0.00	0.00	0.00	0.00	0.00	0.00	0.00	0.00	0.00
Al_2O_3	34.11	31.53	34.06	26.53	34.16	27.76	34.39	35.33	34.41
MgO	0.00	0.00	0.00	0.00	0.00	0.00	0.00	0.00	0.00
FeO	0.10	0.19	0.00	0.13	0.22	0.16	0.14	0.11	0.19
MnO	0.00	0.00	0.00	0.00	0.00	0.00	0.00	0.00	0.00
CaO	16.98	19.78	16.89	7.66	16.49	9.11	17.66	17.89	17.66
K_2O	0.00	0.03	0.00	0.06	0.00	0.04	0.02	0.00	0.00
Na_2O	1.79	1.39	1.75	7.02	2.18	6.32	1.64	1.62	1.42
BaO	0.00	0.00	0.00	0.00	0.00	0.00	0.09	0.00	0.00
Total	99.97	97.84	99.17	99.89	100.85	99.92	100.46	101.17	99.70
Si	4.31	4.27	4.29	5.23	4.35	5.07	4.26	4.20	4.25
Al	3.69	3.53	3.72	2.79	3.66	2.94	3.72	3.79	3.74
Ti	0.00	0.00	0.00	0.00	0.00	0.00	0.00	0.00	0.00
Fe	0.01	0.02	0.00	0.01	0.02	0.01	0.01	0.01	0.01
Mn	0.00	0.00	0.00	0.00	0.00	0.01	0.00	0.00	0.00
Mg	0.00	0.00	0.00	0.00	0.00	0.00	0.00	0.00	0.00
Ca	1.67	2.02	1.68	0.73	1.61	0.88	1.74	1.75	1.75
Na	0.32	0.26	0.31	1.22	0.38	1.10	0.29	0.29	0.25
K	0.00	0.00	0.00	0.01	0.00	0.00	0.00	0.00	0.00
Ba	0.00	0.00	0.00	0.00	0.00	0.00	0.00	0.00	0.00
X_{An}	0.84	0.89	0.84	0.37	0.81	0.44	0.86	0.86	0.87
X_{Ab}	0.16	0.11	0.16	0.62	0.19	0.56	0.14	0.14	0.13
X_{Or}	0.00	0.00	0.00	0.00	0.00	0.00	0.00	0.00	0.00

Table 4.15 continued

Label	P3b	P8a	P9a	P9b
Location	core	rim	rim	
SiO_2	46.69	46.98	56.09	46.57
TiO_2	0.00	0.01	0.00	0.06
Al_2O_3	33.94	33.90	28.23	33.98
MgO	0.00	0.00	0.01	0.00
FeO	0.08	0.08	0.18	0.19
MnO	0.04	0.04	0.03	0.07
CaO	16.86	17.28	9.71	17.22
K_2O	0.03	0.00	0.00	0.01
Na_2O	1.84	2.02	6.21	1.74
BaO	0.00	0.00	0.00	0.12
Total	99.49	100.39	100.45	99.95
Si	4.31	4.31	5.02	4.29
Al	3.69	3.66	2.98	3.69
Ti	0.00	0.00	0.00	0.00
Fe	0.01	0.01	0.01	0.01
Mn	0.00	0.00	0.00	0.01
Mg	0.00	0.00	0.00	0.00
Ca	1.67	1.70	0.93	1.70
Na	0.33	0.36	1.08	0.31
K	0.00	0.00	0.00	0.00
Ba	0.00	0.00	0.00	0.00
X_{An}	0.83	0.83	0.46	0.84
X_{Ab}	0.16	0.17	0.54	0.15
X_{Or}	0.00	0.00	0.00	0.00

Table 4.16   WS995 plagioclase compostions. Stoichiometry recalculated from oxide
wt% on a 16 oxygen basis.

Label Locatio	P1a	P1c	P2a	P2b	P3a	P3b	P4a	P4c	P4b
n	core	rim	core	rim	core	rim	rim	rim	core
SiO_2	59.09	57.77	55.90	56.15	57.06	56.99	56.95	54.03	54.65
TiO_2	0.00	0.00	0.00	0.00	0.00	0.00	0.00	0.00	0.00
Al_2O_3	25.32	26.94	28.06	27.82	27.49	27.50	27.39	29.18	28.40
MgO	0.00	0.00	0.00	0.00	0.00	0.00	0.00	0.00	0.00
FeO	0.08	0.14	0.11	0.09	0.00	0.20	0.10	0.20	0.00
MnO	0.00	0.00	0.00	0.00	0.08	0.00	0.00	0.00	0.00
CaO	6.86	8.04	9.91	9.36	8.67	8.77	8.78	10.96	10.31
K_2O	0.07	0.07	0.06	0.04	0.05	0.06	0.04	0.00	0.05
Na_2O	7.21	6.73	6.24	6.34	6.30	6.59	5.68	5.61	5.89
BaO	0.00	0.00	0.00	0.00	0.00	0.00	0.00	0.00	0.00
Total	98.68	99.73	100.33	99.85	99.80	100.17	98.97	100.04	99.42
Si	5.33	5.18	5.02	5.05	5.12	5.10	5.14	4.88	4.96
Al	2.69	2.85	2.97	2.95	2.91	2.90	2.91	3.11	3.04
Ti	0.00	0.00	0.00	0.00	0.00	0.00	0.00	0.00	0.00
Fe	0.01	0.01	0.01	0.01	0.00	0.01	0.01	0.02	0.00
Mn	0.00	0.00	0.00	0.00	0.01	0.00	0.00	0.00	0.00
Mg	0.00	0.00	0.00	0.00	0.00	0.00	0.00	0.00	0.00
Ca	0.66	0.77	0.95	0.90	0.83	0.84	0.85	1.06	1.00
Na	1.26	1.17	1.09	1.11	1.10	1.14	0.99	0.98	1.04
K	0.01	0.01	0.01	0.01	0.01	0.01	0.00	0.00	0.01
Ba	0.00	0.00	0.00	0.00	0.00	0.00	0.00	0.00	0.00
X_{An}	0.34	0.40	0.47	0.45	0.43	0.42	0.46	0.52	0.49
X_{Ab}	0.65	0.60	0.53	0.55	0.57	0.57	0.54	0.48	0.51
X_{Or}	0.00	0.00	0.00	0.00	0.00	0.00	0.00	0.00	0.00

Table 4.17   H761 plagioclase compositions. Stoichiometry recalculated from oxide wt% on a 16 oxygen basis.

Label	P1a	P1b	P4a	P4b	P5	P6	P7a	P7b
Location	core	rim	rim	core	rim	rim	rim	core
SiO_2	48.45	47.26	53.51	46.86	56.99	47.42	46.99	46.69
TiO_2	0.00	0.00	0.00	0.00	0.10	0.00	0.00	0.00
Al_2O_3	33.63	34.33	29.45	33.52	27.36	33.97	33.90	34.47
MgO	0.00	0.00	0.00	0.00	0.00	0.00	0.00	0.00
FeO	0.18	0.13	0.17	0.00	0.14	0.17	0.12	0.00
MnO	0.00	0.09	0.00	0.00	0.10	0.00	0.00	0.00
CaO	15.46	16.08	11.91	16.82	9.26	16.91	17.05	17.28
K_2O	0.02	0.00	0.02	0.00	0.04	0.00	0.00	0.00
Na_2O	2.27	1.80	4.72	1.79	6.28	2.03	1.86	1.78
BaO	0.00	0.00	0.00	0.14	0.00	0.00	0.06	0.00
Total	100.02	99.70	99.82	99.15	100.33	100.54	100.03	100.36
Si	4.42	4.34	4.85	4.34	5.10	4.33	4.32	4.28
Al	3.62	3.71	3.14	3.66	2.89	3.66	3.67	3.72
Ti	0.00	0.00	0.00	0.00	0.01	0.00	0.00	0.00
Fe	0.01	0.01	0.01	0.00	0.01	0.01	0.01	0.01
Mn	0.00	0.01	0.00	0.00	0.01	0.00	0.00	0.00
Mg	0.00	0.00	0.00	0.00	0.00	0.00	0.00	0.00
Ca	1.51	1.58	1.16	1.67	0.89	1.66	1.68	1.70
Na	0.40	0.32	0.83	0.32	1.09	0.36	0.33	0.32
K	0.00	0.00	0.00	0.00	0.00	0.00	0.00	0.00
Ba	0.00	0.00	0.00	0.00	0.00	0.00	0.00	0.00
X_{An}	0.79	0.83	0.58	0.84	0.45	0.82	0.83	0.84
X_{Ab}	0.21	0.17	0.42	0.16	0.55	0.18	0.17	0.16
X_{Or}	0.00	0.00	0.00	0.00	0.00	0.00	0.00	0.00

Table 4.18   WS0011 amphibole compositons. Entries are blank for elements not analyzed. Stoichiometry recalculated from oxide wt% on a 23 oxygen basis with all Fe assumed to be Fe^{2+}.

Label	HBL1a	HBL2a	HBl2c	HBL3a	HBL1a-2	HBL1b-2	HBL5a	HBL6
Location	rim	rim	rim	core	core	rim	rim	rim
SiO_2	39.97	42.62	39.73	40.65	40.71	40.43	39.37	39.35
TiO_2	1.11	0.49	0.68	0.90	1.07	1.14	0.78	0.67
Al_2O_3	14.51	12.08	15.45	14.99	14.67	15.53	15.42	15.72
MgO	7.47	8.42	7.36	8.64	8.87	9.24	8.22	8.08
FeO	19.40	19.13	18.82	17.79	17.89	16.17	19.07	17.66
CaO	11.30	11.42	11.90	11.52	11.07	11.35	11.65	11.65
MnO	0.30	0.31	0.33	0.35	0.33	0.33	0.35	0.31
K_2O	1.09	0.78	0.96	1.07	0.93	0.79	0.99	0.99
Na_2O	1.29	0.93	1.31	1.44	1.29	1.35	1.41	1.38
BaO	0.10	0.00	0.00	0.00	0.00	0.00	0.00	0.00
F	0.24	0.13	0.13	0.16				
Cl	0.06	0.07	0.06	0.10				
Total	96.73	96.32	96.73	97.51	96.89	96.40	97.31	95.84
Si	6.17	6.58	6.13	6.28	6.29	6.24	6.08	6.08
Al^4	1.83	1.42	1.87	1.72	1.71	1.76	1.92	1.92
Al^6	0.81	0.78	0.95	1.00	0.96	1.07	0.88	0.94
Ti	0.13	0.06	0.08	0.11	0.12	0.13	0.09	0.08
Fe	2.50	2.47	2.43	2.30	2.31	2.09	2.46	2.28
Mn	0.04	0.04	0.04	0.05	0.04	0.04	0.05	0.04
Mg	1.72	1.94	1.69	1.99	2.04	2.13	1.89	1.86
Ca	1.87	1.89	1.97	1.91	1.83	1.88	1.93	1.93
Na	0.39	0.28	0.39	0.43	0.39	0.40	0.42	0.41
K	0.21	0.15	0.19	0.21	0.18	0.16	0.20	0.20
Ba	0.01	0.00	0.00	0.00	0.00	0.00	0.00	0.00

Table 4.18 continued

Label	HBL7	HBL8	HBL8a	HBL6a	HBL6b	HBL21a	HBL22a
Location	rim	rim	rim	rim	core	rim	
SiO_2	39.16	39.93	40.06	40.05	40.33	39.94	39.76
TiO_2	1.16	0.86	0.77	1.07	1.23	0.78	0.92
Al_2O_3	14.61	14.75	14.62	14.91	14.33	15.54	15.70
MgO	8.57	9.04	8.88	8.41	8.49	8.52	8.33
FeO	17.94	16.66	17.19	18.71	18.60	17.90	18.37
CaO	11.72	11.98	11.86	11.68	11.97	11.59	11.61
MnO	0.34	0.34	0.27	0.28	0.19	0.46	0.31
K_2O	1.24	1.03	1.06	1.39	1.19	1.03	0.94
Na_2O	1.17	1.27	1.30	1.19	1.23	1.33	1.49
BaO	0.13	0.00	0.00	0.13	0.00	0.14	0.00
F							
Cl							
Total	96.04	95.88	96.06	97.82	97.58	97.21	97.50
Si	6.05	6.17	6.19	6.18	6.23	6.17	6.14
Al^4	1.95	1.83	1.81	1.82	1.77	1.83	1.86
Al^6	0.70	0.85	0.85	0.90	0.83	0.99	1.00
Ti	0.13	0.10	0.09	0.12	0.14	0.09	0.11
Fe	2.32	2.15	2.22	2.42	2.40	2.31	2.37
Mn	0.04	0.04	0.04	0.04	0.02	0.06	0.04
Mg	1.97	2.08	2.04	1.94	1.95	1.96	1.92
Ca	1.94	1.98	1.96	1.93	1.98	1.92	1.92
Na	0.35	0.38	0.39	0.36	0.37	0.40	0.45
K	0.24	0.20	0.21	0.27	0.23	0.20	0.18
Ba	0.01	0.00	0.00	0.01	0.00	0.01	0.00

Table 4.19   WS995 amphibole compositions. Stoichiometry recalculated from oxide wt% on a 23 oxygen basis with all Fe assumed to be Fe^{2+}.

Pt#	HBL1a	HBL1b	HBL2a	HBL2b	HBL3c	HBL3d	HBL3a	HBL3b
Location	core	rim	core	rim	rim	core	rim	core
SiO_2	39.43	39.80	39.98	39.54	39.87	39.83	39.74	39.95
TiO_2	1.03	0.93	0.93	0.69	1.02	1.16	1.17	1.22
Al_2O_3	14.75	14.29	14.61	15.03	14.58	14.44	14.64	14.22
MgO	8.81	8.68	8.95	8.94	8.36	8.70	8.79	9.03
FeO	17.91	18.12	17.43	17.52	17.66	17.03	17.69	16.63
CaO	11.54	11.43	11.92	11.72	11.41	11.89	11.61	11.49
MnO	0.22	0.26	0.29	0.22	0.38	0.50	0.33	0.33
K_2O	1.14	1.08	0.96	0.87	0.85	1.05	1.11	1.08
Na_2O	1.46	1.40	1.38	1.62	1.52	1.36	1.48	1.42
BaO	0.00	0.00	0.00	0.00	0.00	0.11	0.00	0.00
Total	96.29	96.02	96.45	96.15	95.65	96.08	96.57	95.37
Si	6.07	6.13	6.16	6.09	6.14	6.14	6.12	6.15
Al^4	1.93	1.87	1.84	1.91	1.86	1.86	1.88	1.85
Al^6	0.75	0.73	0.81	0.82	0.79	0.76	0.78	0.74
Ti	0.12	0.11	0.11	0.08	0.12	0.13	0.14	0.14
Fe	2.31	2.33	2.25	2.26	2.28	2.19	2.28	2.14
Mn	0.03	0.03	0.04	0.03	0.05	0.07	0.04	0.04
Mg	2.02	1.99	2.06	2.05	1.92	2.00	2.02	2.07
Ca	1.90	1.89	1.97	1.93	1.88	1.96	1.92	1.90
Na	0.44	0.42	0.41	0.48	0.45	0.41	0.44	0.42
K	0.22	0.21	0.19	0.17	0.17	0.21	0.22	0.21
Ba	0.00	0.00	0.00	0.00	0.00	0.01	0.00	0.00

Table 4.19 continued

Pt#	HBL3c	HBL4a	HBL4b
Location	core	core	rim
SiO_2	39.42	39.31	40.57
TiO_2	1.12	1.05	0.71
Al_2O_3	14.06	14.65	14.64
MgO	8.85	8.55	8.71
FeO	17.16	17.53	17.82
CaO	11.81	11.77	11.66
MnO	0.35	0.37	0.19
K_2O	1.10	1.24	0.89
Na_2O	1.40	1.52	1.57
BaO	0.00	0.00	0.00
Total	95.28	95.98	96.83
Si	6.07	6.06	6.25
Al^4	1.93	1.94	1.75
Al^6	0.63	0.72	0.91
Ti	0.13	0.12	0.08
Fe	2.21	2.26	2.30
Mn	0.05	0.05	0.02
Mg	2.03	1.96	2.00
Ca	1.95	1.94	1.92
Na	0.42	0.45	0.47
K	0.22	0.24	0.18
Ba	0.00	0.00	0.00

Table 4.20   H761 amphibole compositions. Stoichiometry recalculated from oxide wt% on a 23 oxygen basis with all Fe assumed to be Fe^{2+}.

Label	HBL1a	HBL1b	HBL4a	HBL4b	HBL5a	HBL5a	HBL6a	HBL6b
Location	rim	core	rim	core	rim	rim	rim	core
SiO_2	41.66	42.75	41.07	41.64	41.14	40.81	41.90	43.23
TiO_2	0.69	0.71	0.68	0.62	0.66	0.76	0.64	1.19
Al_2O_3	14.19	13.03	14.86	14.23	14.27	15.12	14.56	12.39
MgO	10.06	10.53	9.75	9.96	9.91	9.49	9.70	10.93
FeO	16.10	16.18	16.83	16.53	16.15	15.55	15.32	15.88
CaO	11.05	11.27	11.69	11.77	11.82	12.01	11.97	11.85
MnO	0.27	0.31	0.26	0.32	0.34	0.26	0.24	0.28
K_2O	0.53	0.40	0.56	0.54	0.55	0.62	0.57	0.58
Na_2O	1.38	1.25	1.41	1.59	1.49	1.54	1.60	1.30
BaO	0.00	0.00	0.00	0.00	0.00	0.13	0.12	0.00
Total	95.94	96.43	97.14	97.30	96.36	96.29	96.62	97.71
Si	6.32	6.44	6.19	6.27	6.24	6.19	6.31	6.44
Al^4	1.68	1.56	1.81	1.73	1.76	1.81	1.69	1.56
Al^6	0.86	0.76	0.83	0.79	0.80	0.89	0.89	0.62
Ti	0.08	0.08	0.08	0.07	0.08	0.09	0.07	0.13
Fe	2.04	2.04	2.12	2.08	2.05	1.97	1.93	1.98
Mn	0.03	0.04	0.03	0.04	0.04	0.03	0.03	0.04
Mg	2.27	2.37	2.19	2.23	2.24	2.15	2.18	2.43
Ca	1.80	1.82	1.89	1.90	1.92	1.95	1.93	1.89
Na	0.41	0.37	0.41	0.46	0.44	0.45	0.47	0.38
K	0.10	0.08	0.11	0.10	0.11	0.12	0.11	0.11
Ba	0.00	0.00	0.00	0.00	0.00	0.01	0.01	0.00

Table 4.21   WS0011 zoisite compositions. Stoichiometry recalculated from oxide wt% on a 12.5 oxygen basis with all Fe assumed to be Fe^{2+}.

Label	EP5	EP9a	EP9b	EP10a
Location	rim	rim	rim	
SiO_2	37.37	37.64	37.52	38.06
TiO_2	0.02	0.09	0.05	0.14
Al_2O_3	21.40	25.53	25.77	25.90
MgO	2.61	0.02	0.02	0.02
FeO	25.37	9.57	9.64	9.07
MnO	3.99	0.30	0.15	0.19
CaO	10.28	23.56	23.89	23.75
K_2O	0.00	0.00	0.00	0.00
Na_2O	0.00	0.00	0.00	0.00
BaO	0.00	0.00	0.11	0.00
Total	101.05	96.73	97.16	97.17
Si	3.93	3.91	3.88	3.92
Al	2.65	3.12	3.14	3.14
Ti	0.00	0.01	0.00	0.01
Fe	2.23	0.83	0.83	0.78
Mn	0.36	0.03	0.01	0.02
Mg	0.41	0.00	0.00	0.00
Ca	1.16	2.62	2.65	2.62
Na	0.00	0.00	0.00	0.01
K	0.00	0.00	0.00	0.00
Ba	0.00	0.00	0.00	0.00

Table 4.22 WS995 zoisite compositions. Stoichiometry recalculated from oxide wt%
on a 12.5 oxygen basis with all Fe assumed to be Fe^{2+}.

Label	EP1a	EP1b
Location	core	rim
SiO_2	36.49	38.06
TiO_2	0.15	0.13
Al_2O_3	24.45	25.87
MgO	0.20	0.00
FeO	9.61	9.65
MnO	0.12	0.15
CaO	21.26	23.34
K_2O	0.00	0.00
Na_2O	0.00	0.00
BaO	0.00	0.00
Total	92.38	97.29
Si	3.09	3.06
Al	2.44	2.45
Ti	0.01	0.01
Fe	0.68	0.65
Mn	0.01	0.01
Mg	0.03	0.00
Ca	1.93	2.01
Na	0.01	0.00
K	0.00	0.00
Ba	0.00	0.00
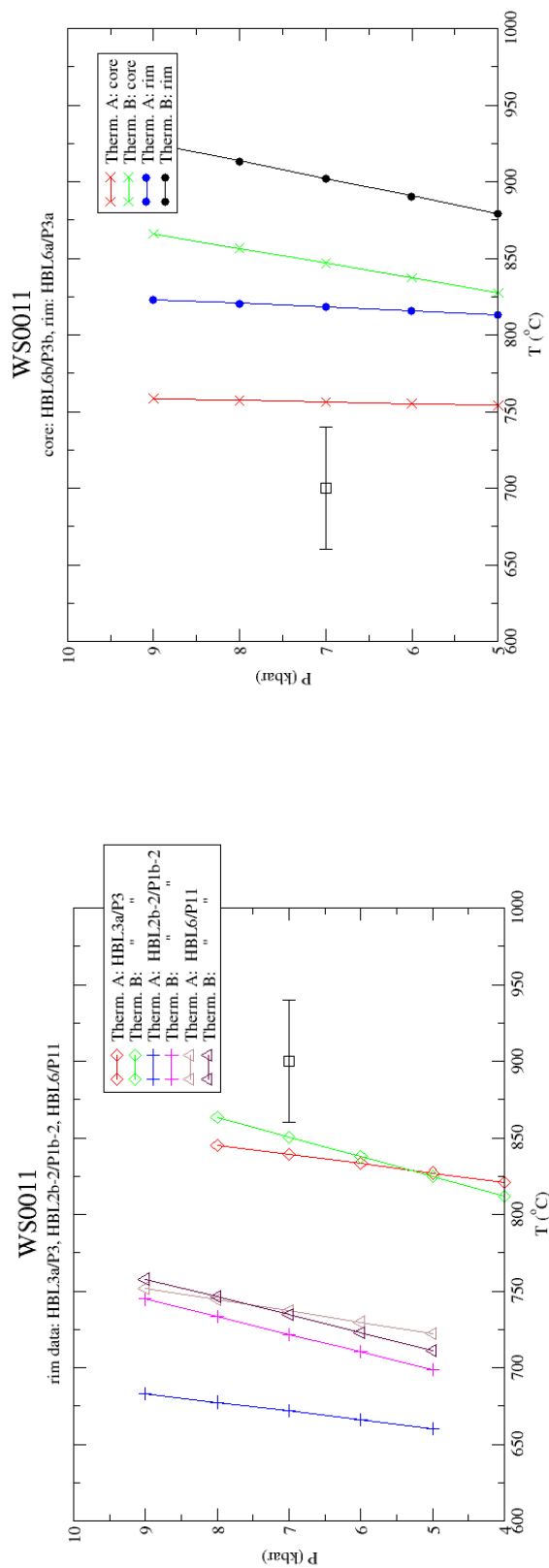
Figure 4.4   Thermometry results for sample WS0011. Thermometers A (Ed-Tr) and B (Ed-Rich) are from Holland and Blundy (1994). Right chart is for core and rim of one amphibole /plagioclase pair. Left plot is for rims of three different amph/plag pairs.
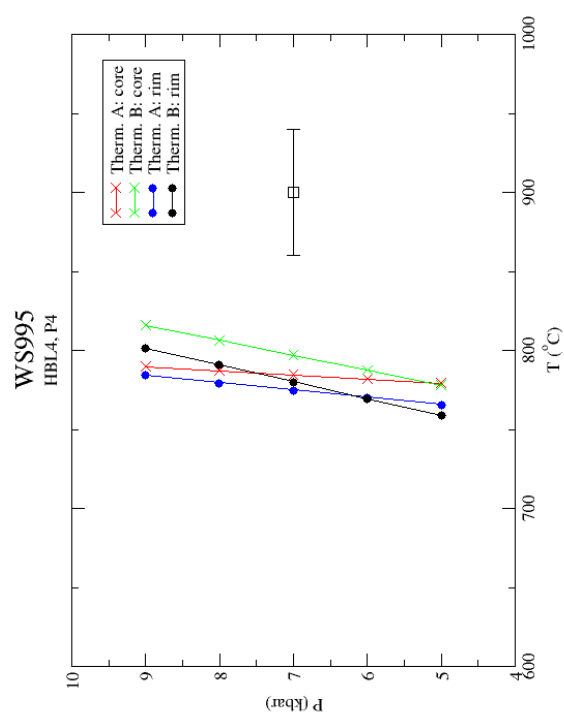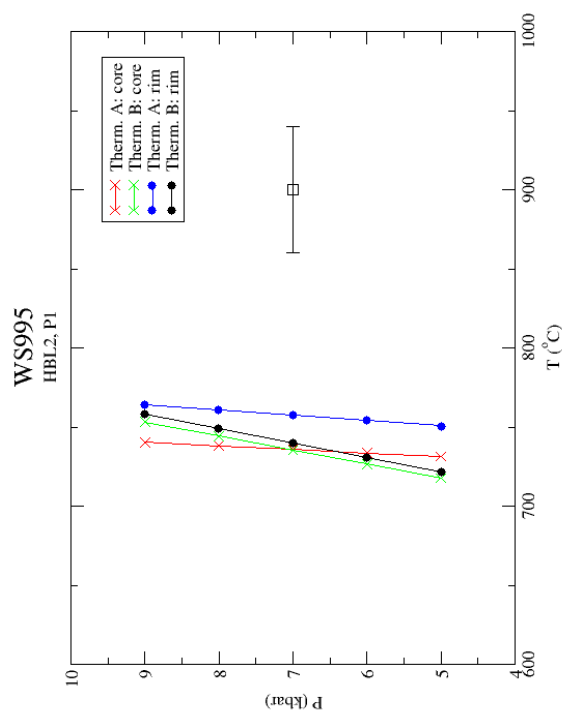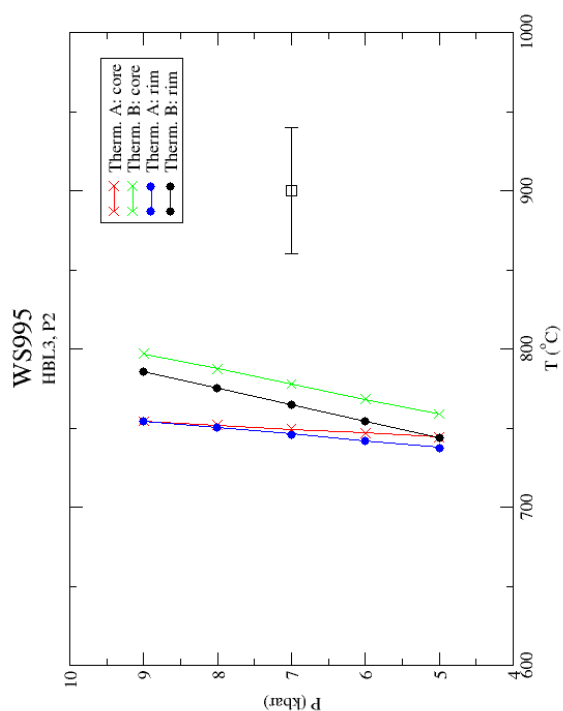
Figure 4.5   Thermometry results for WS995. Thermometers A (Ed-Tr) and B (Ed-Rich) from Holland and Blundy (1994). Each chart is for an individual amphibole/plagioclase core/rim pair.
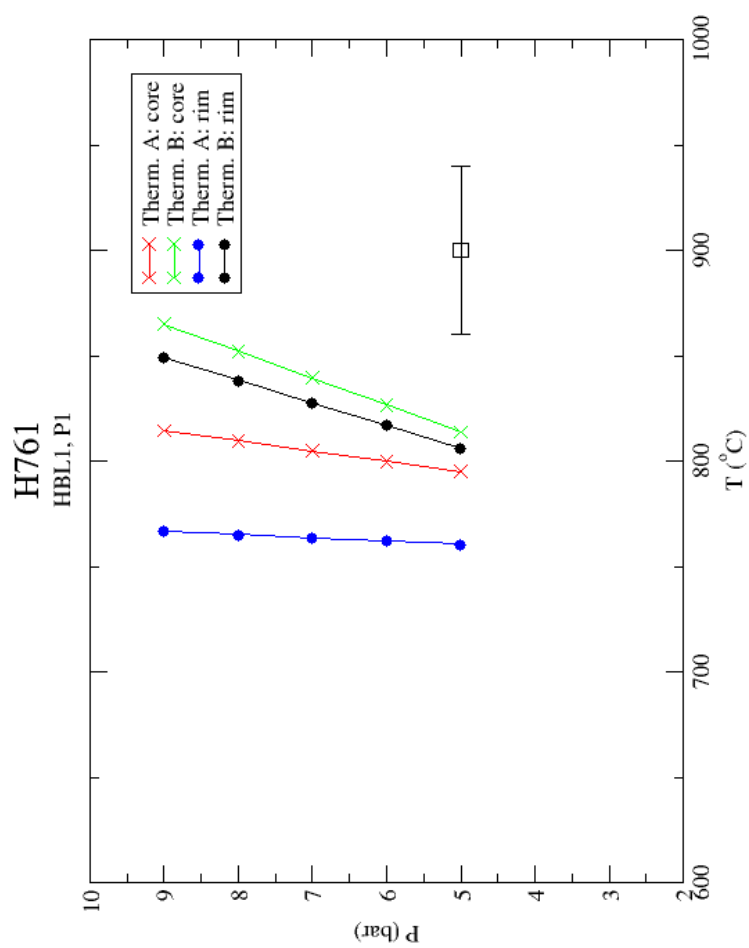
Figure 4.6   Thermometry results for H761. Thermometers A (Ed-Tr) and B (Ed-Rich) are from Holland and Blundy (1994).

of pressure by fixing temperature, which we get from the thermometry presented in the preceding sections. Next we find the standard the state fugacity of water (f^o_{H2O}) as a function of pressure at the temperature of interest by solving the Redlich-Kwong equation of state. The standard state fugacity of a fluid is the fugacity of the pure fluid at the P and T of interest and is the highest possible value for fugacity at that P and T. In a given mixture where $X_n < 1$ for any component n it follows that $f_n < f^o_n$ and that $f_n = f^o_n$ only in the case where $X_n = 1$. Therefore, any fugacity we calculate from mineral equilibria for a given P and T is only possible if it is less than or equal to the standard state fugacity at that P and T. When our two curves are plotted in $f - P$ space, the intersection point defines the minimum pressure for that system. Pressures lower than this are not possible since that would mean $f^{rxn}_{H2O} > f^o_{H2O}$, and f^{rxn}_{H2O} cannot be higher than that of the pure phase. With a temperature of 700^oC from previous thermometry, f^{rxn}_{H2O} was calculated over a range of pressure and plotted in $f - P$ space along with a curve for f^o_{H2O} obtained from the Redlich-Kwong equation (Figures 4.7 and 4.8). Three different f^{rxn}_{H2O} curves for zoisite activities ranging between a^{id} and 1 were plotted because an appropriate activity model for zoisite was unavailable. Without an activity model to estimate real activities, zoisite was considered to have an activity equal to or greater than its ideal activity. This assumption is justified in that the gamma term of a real activity model is almost always greater than 1 so that $a^{id} \leq \gamma a^{id} \leq 1$, where $\gamma a^{id} = a^{real}$.

4.5 SUMMARY OF PRESSURES AND TEMPERATURES

Sample WS009, a sillimanite-bearing bioite-garnet gneiss yielded temperatures between 625 and 725°C and pressures near 6 kbar. Biotite-amphibole-garnet gneisses, samples WS992 and WS996, had assemblages only appropriate for thermometry and yielded temperatures between 650 and 750°C. The amphibolite samples, WS0011, WS995, and H761, gave temperatures between 675 and 800°C with minimum pressures between 4.8 and 5.7 kbar.
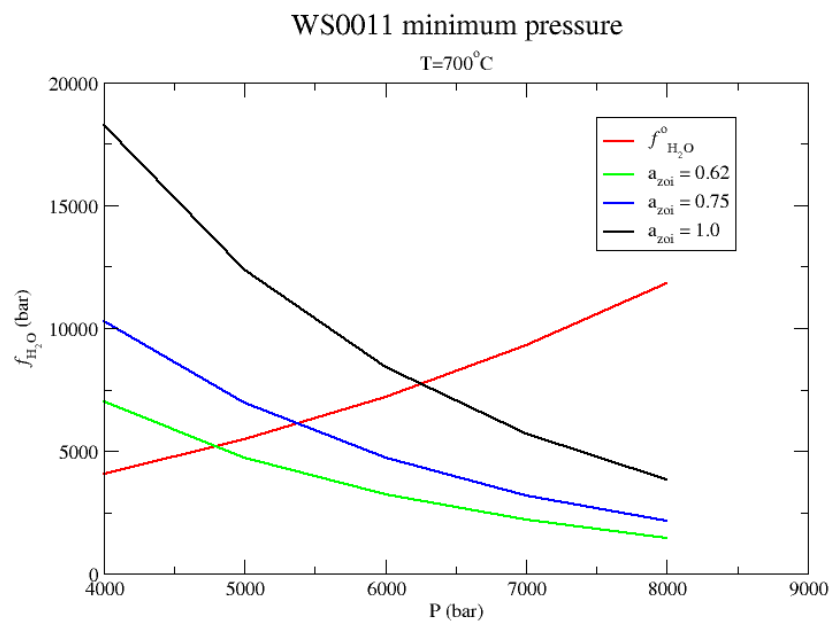
Figure 4.7   WS0011 minimum pressure. Temperature = 700ºC from thermometry. Ideal activity of zoisite = 0.62 = $(_{Xal})_{zoi}$. Water fugacities higher than the standard state fugacity are not real (see text).
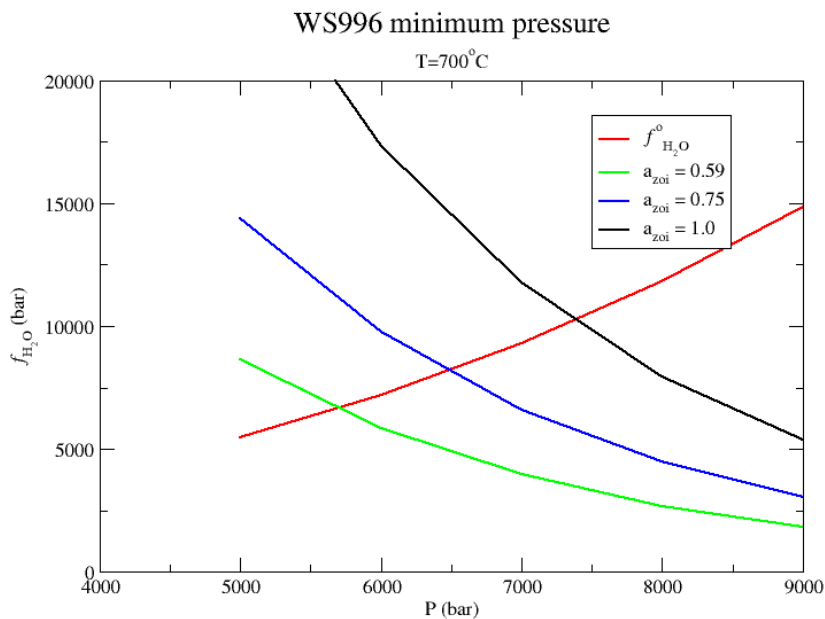
Figure 4.8   WS996 minimum pressure. Temperature = 700ºC from thermometry. Ideal activity of zoisite = 0.58 = $(_{Xal})_{zoi}$. Water fugacities higher than the standard state fugacity are not real (see text).

CHAPTER 5

CONCLUSIONS

5.1 THERMOBAROMETRY

As shown in the previous chapter, calculated pressures and temperatures are remarkably consistent across the study area. Moreover, temperatures from samples WS009, WS992, and WS996 are in very good agreement among themselves. The majority of temperatures from these samples fall into the 675°C to 750°C range (assuming a pressure of 6.25 kbar for the thermometer-only samples), with outliers at 630°C for sample WS009 (Fig. 4.1) and 780°C for sample WS992 (Fig. 4.5). Temperature data obtained from the amphibolites, WS0011, WS995, and H761 are generally higher and more scattered than data for the rest of the samples. The higher temperatures can be attributed to the Ca content of plagioclase (An$_{80-87}$) which approaches the limit of An$_{90}$ imposed by Holland and Blundy (1994) for use in their thermometers. Amphibolite temperatures range from 670 to 880°C with most temperatures near 750°C. The highest degree of scatter is in WS0011, as can be seen in Figure 4.4. A reasonable estimate for the equilibrium temperature for the samples in this study is 700°C ±50.

Pressure estimates were only directly available from WS009 and ranged from 5.75 kbar to 7 kbar. As alluded to in the previous chapter, WS009 is an important sample for this study because it contains an aluminosilicate which allowed for direct pressure calculation using well-calibrated equilibria and activity models. Based on margins of error reported in Patiño Douce *et al.* (1993) and the size of *P-T* regions from intersections of equilibria curves (Fig. 4.1) a value of 6.25 kbar is adopted as the pressure at equilibrium for this sample. This is in the acceptable range of minimum pressures obtained from samples WS0011 and WS996 (Figs. 4.7, 4.8). Due to their proximity, samples WS992, WS996, and WS995 are inferred to have equilibrated at this pressure as

76

well.   Although uncertainty increases with distance, WS0011 and H761 most likely equilibrated at pressures close to, if not the same as, the pressure obtained from the Woodall Shoals outcrop.

Water activities could not be directly computed because of uncertainties in zoisite activities . However, a range a water activities can be inferred using the 6.25 kbar pressure estimated from sample WS009 and the plots of P vs. f_{H2O}. The definition of activity for any fluid phase i is:

$$a_i \;=\; \frac{f_i^{rxn}}{f_i^{o}} \tag{5.1}$$

Where $f^{rxn}{}_i$ is the fugacity of component i as calculated from mineral equilibria at the P and T of interest and $f^{o}{}_i$ is the standard state fugacity of H_2O at that P and T. Applying Equation 5.1 to the results shown in Figure 4.8, it can be seen that calculated water activity is between ~0.65 and 1.0 at 6.25 kbar and 700°C, suggesting that H_2O made up the greatest portion of the vapor phase. The mineral assemblages do not allow us to know what, if any, other fluids were present, but a vapor phase of pure water ($a_{H2O} = 1$) would be highly unlikely since pelitic rocks evolve large amounts of both CO_2 *and* H_2O during prograde metamorphism (Miyashiro 1994). With the layering of pelitic and non-pelitic rocks at Woodall Shoals on the scale of centimeters, the fluid composition was most likely controlled by the pelitic assemblages and inundated all lithologies across the outcrop. The equilibrium:

$$\text{Ms} + \text{Qtz} \rightleftharpoons \text{Sill} + \text{Kfs} + H_2O \tag{5.2}$$

can be plotted as a function of X_{H2O} and T at constant pressure in order to test this estimate of a_{H2O}. In this case ideal mixing in the fluid phase is assumed so that $X_{H2O} = a_{H2O}$. Since there is no Kfs present in the assemblages, our conditions (T=700, a_{H2O}=0.65 at 6.25 kbar) should plot within the Ms+Qtz field of the phase diagram. Figure 5.1 shows that our conditions do indeed plot on the expected side of the phase boundary.
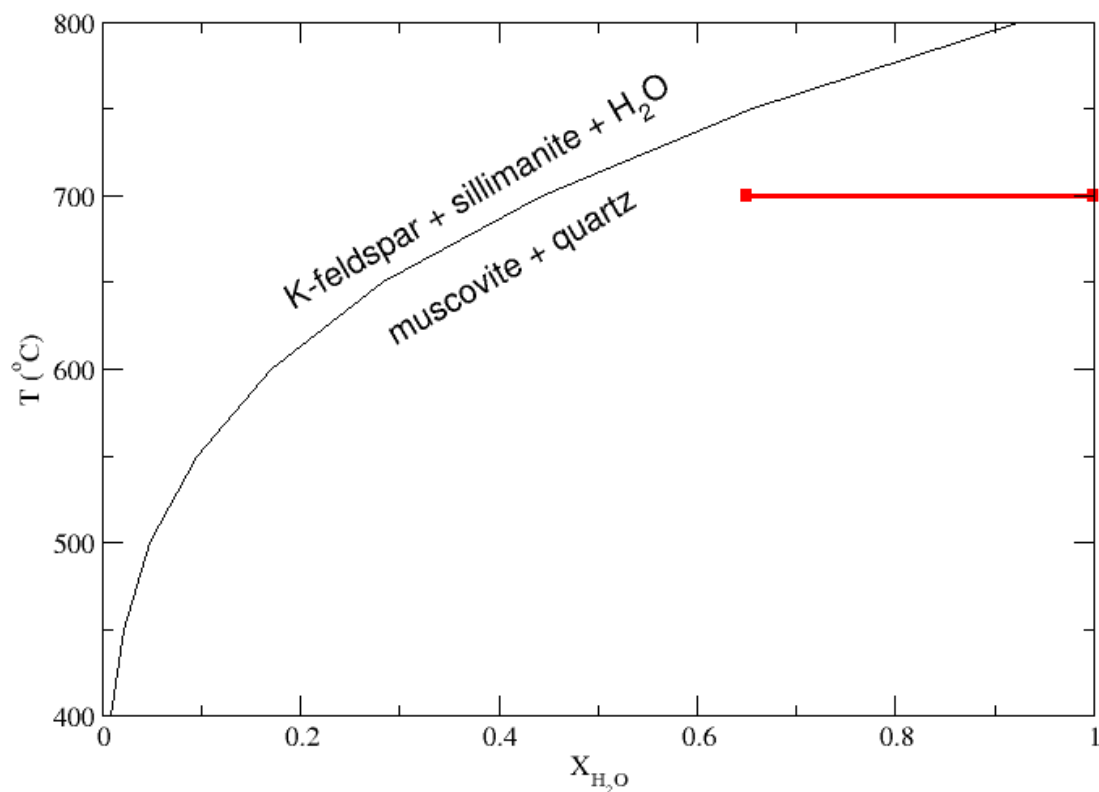
Figure 5.1   Ms+Qtz=Kfs+Sill+H$_2$O phase boundary in X_{H2O}–T space with P=6250bar. Red line shows conditions from this study, 700ºC, $0.65 \leq a$H2O≤ 1.0

5.2 REGIONAL GEOLOGY

The thermal-peak *P-T* conditions from this study indicate that rocks in the vicinity of Woodall Shoals underwent a high-grade Barrovian event (Miyashiro 1994) and equilibrated on the high temperature side of the kyanite-sillimanite phase boundary (Fig. 5.2). This *P-T* estimate at Woodall Shoals is consistent with the mapped kyanite-sillimanite isograd (Hatcher 1999) a short distance to the southeast of Woodall Shoals (Fig. 2.1) and with the general observation that the southeastern edge of the Tallulah Falls thrust sheet is of a lower metamorphic grade (Nelson 1998). Temperatures from this study are consistent with those of Bier *et al.*(2000) who found minimum temperatures between 625 and 725°C for the Tallulah Falls Formation of North Carolina.

Petrologic evidence shows that the S_2 foliation recognized by Hopson *et al.* (1989) was the last major metamorphic event at Woodall Shoals and is the event that is quantified in this study. The absolute age of this event is uncertain. Dallmeyer (1988) obtained amphibole $^{40}Ar/^{39}Ar$ plateau dates between 322Ma and 328Ma for the Tallulah Falls thrust sheet which dates postmetamorphic cooling through ~500°C, suggesting that the last metamorphic event at Woodall Shoals is Acadian. Stewart *et al.* (1997) put forth model involving the Ashe Metamorphic Suite of western North Carolina, a correlative unit to the Tallulah Falls Formation, that fits with Hatcher's (1999) assertion that the Tallulah Falls thrust sheet is a remnant from the Inner Piedmont that was dismembered and deflected dextrally by the Brevard fault during the Acadian. Stewart *et al.*'s (1997) model is a crustal thickening model such that the rocks involved would exhibit a Barrovian *P/T* ratio as is seen in both the Ashe Metamorphic Suite (AMS) and this study. In Stewart *et al.*'s (1997) model the AMS (used here as a proxy for the Tallulah Falls Formation of the Tallulah Falls thrust sheet) is believed to be the metamorphosed accretionary wedge on the leading edge of the Piedmont when it collides with Laurentia in the Ordovician (Taconic). This event metamorphosed rocks in both Laurentia and the AMS to amphibolite grade. With continued thrusting the Taconic suture evolves into a dextral strike slip fault, but with uncertainties in absolute timing. Stewart *et al.* (1997)

speculate that the strike-slip faulting in their model may be Taconic-aged, but is possibly a discrete event during the Acadian. This could be a mechanism by which the eastern Blue Ridge is dismembered from the inner piedmont as Hatcher (1999) asserts and is re-metamorphosed to give the Acadian ages seen by Dallmeyer (1988). Moreover, the model of Stewart *et al.* (1997) is consistent with the conditions observed in this study becasue it shows how a single Barrovian metamorphic event can be preserved in the mineral assemblages at Woodall Shoals. In addition, Adams and Trupe (1997) propose a retrograde *P-T* path for the AMS (Fig 5.2) that passes close to the *P-T* estimate from this study. Adam and Trupe's (1997) *P-T* path is based on the *P-T* estimates of eclogite, eclogite retrograded to amphibolite facies, and adjacent schists (Willard and Adams 1994). Although the *P-T* estimate from this study falls close to the *P-T* estimates for the AMS, there is no higher grade event preserved in the rocks at Woodall Shoals that could suggest a retrograde *P-T* path for the Tallulah Falls Formation as put forth for the AMS.

Work on the nature and history of metamorphism in the southern Appalachians remains to be done. Although the aluminous schist of the Tallulah Falls Formation in which Woodall Shoals lies has been recognized for its usefulness in tracing structure through the eastern Blue Ridge and western Inner Piedmont (Hatcher 1999), this is the only work to examine the metamorphic conditions of this important unit. With the sketchy picture we have of the Acadian orogen in the southern Appalachians almost any conclusions drawn with the data presented here would be premature and tenuous at best.
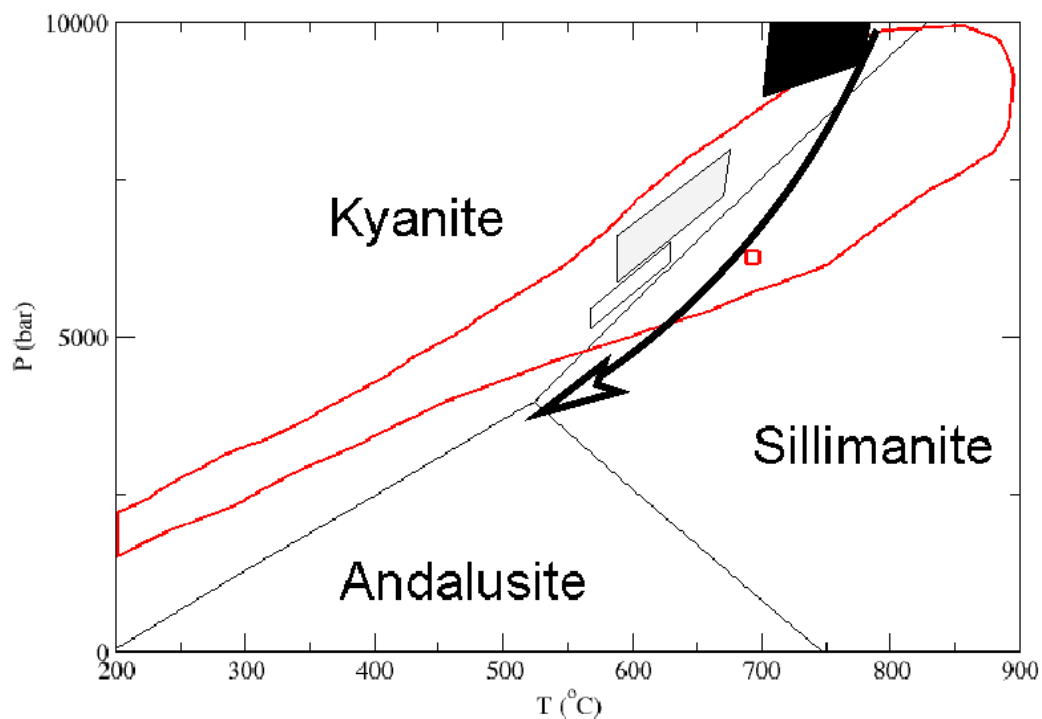
Figure 5.2   Region outlined in red shows Barrovian conditions
(Miyashiro 1994) and red square shows conditions
found in this study at Woodall Shoals. Conditions for
the Ashe Metamorphic Suite from Willard and Adams
(1995) are shown in the boxes: white- final conditions
in schist, grey- peak conditions in schist, black (box
continues just outside area of view to ~11kbar)-
retrograde amphibolite facies. Arrow is a possible P-T
path proposed by Adams and Trupe (1997).

REFERENCES

Absher, B.S.; McSween, H.Y., 1985, Granulites at Winding Stair Gap, North Carolina: The thermal axis of Paleozoic metamorphism in the southern Appalachians: GSA Bulletin, v. 96, p. 588-599.

Adams, M.G., Trupe, C.H., 1997, Conditions and timing of metamorphism in the Blue Ridge thrust complex, northwestern North Carolina and eastern Tennessee, *in* Stewart, K.G., Adams, M.G., Trupe, C.H., *eds.*, Paleozoic structure, metamorphism, and tectonics of the Blue Ridge of western North Carolina: Carolina Geological Society, 1997 Field Trip Guidebook

Allard, G.O.; Witney, J.A., 1994, Geology of the Inner Piedmont, Carolina terrane, and Modoc Zone in Northeast Georgia: Project Report 20, Georgia Geologic Survey.

Berman, R.G., 1988, Internally-Consistent Thermodynamic Data for Minerals in the System Na2O-K2O-CaO-MgO-FeO-Fe2O3-Al2O3-SiO2-TiO2-H2O-CO2: Journal of Petrology, v. 29, part 2, p. 445-522.

Berman, R.G., 1990, Mixing properties of Ca-Mg-Fe-Mn garnets: American Mineralogist, v. 75, p. 328-344

Bier, S.E.; Giorgis, S.D.; Bream, B.R.; Williams, S.T.; and Hatcher, R.D., Jr., 2000,, Temperature and Pressure Estimates of Acadian Metamorphism in the Inner Piedmont, North Carolina: GSA Abstracts with Programs, SE section, v. 32, p. A-6.

Butler, J.R., 1972, Age of Paleozoic regional metamorphism in the Carolinas, Georgia, and Tennessee southern Appalachians: American Journal of Science, v. 272, no. 4, p. 319-333.

Dallmeyer, R.D., 1988, Later Paleozoic tectonothermal evolution of the western Piedmont and eastern Blue Ridge, Georgia: Controls on the chronology of terrane accretion and transport in the southern Appalachian orogen: GSA Bulletin, v. 100, p. 702-713.

Deer, W.A., Howie, R.A., Zussman, J, 1992, An Introduction to the Rock-Forming Minerals: Addison Wesley Longman, Essex.

Drake, A.D., Jr.; Sinha, A.K.; Laird, J.; Guy, R.E., 1989, The Taconic orogen *in* Hatcher, R.D., Jr.; Thomas, W.A.; Viele, G.W., *eds.*, The Appalachian—Ouchita Orogen in the United States: Boulder, Colorado, Geological Society of America, The Geology of North America, v. F-2.

Eckert, J.O., Jr.; Hatcher, R.D., Jr.; and Mohr, D.W., 1989, The Wayah granulite-facies metamorphic core, southwestern North Carolina: High-grade culmination of Taconic metamorphism in the southern Blue Ridge: Geological Society of America Bulletin, v. 101, p. 1434-1447.

Fuhrman, M.L.; Lindsley, D.H., 1988, Ternary-feldspar modeling and thermometry: American Mineralogist, v. 73, p. 201-215.

Gillon, K.A., 1982, Stratigraphic, structural and metamorphic geology of portions of the Cowrock and Helen, Georgia quadrangles [M.S. thesis]: University of Georgia.

Guidotti, C.V., 1984, Micas in Metamorphic Rocks, *in* Bailey, S.W., *ed.*, Micas: Reviews in Mineralogy, v. 13.

Hatcher, R.D., Jr.; and Butler, J.R., 1979, Guidebook for southern Appalachian field trip in the Carolinas, Tennessee and northeastern Georgia: International geologic Correlation program—Caledonide orogen project 27, University of North Carolina, Chapel Hill, 117 p.

Hatcher, R.D., Jr., 1999, Geotraverse across part of the Acadian orogen the southern Appalachians, in SE-GSA 1999 section meeting field guide.

Hatcher, R.D., Jr, 1989, Georgia Geological Society Field Trip Stops for 1989, *in* Fritz, W.J.; Hatcher, R.D., Jr.; Hopson, J.L., *eds*, Geology of the eastern Blue Ridge of northeastern Georgia and the adjacent Carolinas: Georgia Geological Society Guidebooks, v. 9, no. 3.

Hatcher, R.D., Jr., 1978, Tectonics of the western piedmont and Blue Ridge, southern Appalachians: Review and speculation: American Journal of Science, v. 278, p. 276-304.

Hatcher, R.D., Jr., 1971, Geology of Rabun and Habersham Counties, Georgia: A reconnaissance study: Georgia Geological Survey Bulletin 83, p. 43.

Hatcher, R.D., Jr.; Horkowitz, J.P.; Wynne, D.B.; Burns, A.C.; and Poe, S.H, 1983, Geologic Map of Woodall Shoals, South Carolina-Georgia.

Holland, T.J.B.,Blundy, J.D., 1994, Non-ideal interactions in calcic amphiboles and their bearing on amphibole-plagioclase thermometry: Contrib. Mineral Petrol., v. 116, p. 432-437..

Hopson, J.L.; Hatcher, R.D., Jr.; Stieve, A.L., 1989, Geology of the eastern Blue Ridge, northeastern Georgia and the adjacent Carolinas, *in* Fritz, W.J.; Hatcher, R.D., Jr.; and Hopson, J.L., *eds*., Geology of the eastern Blue Ridge of northeastern Georgia and the adjacent Carolinas: Georgia Geological Society Guidebooks, v. 9, n. 3, p. 1-38.

McSween, H.Y., Jr.; Abbott, R.N.; and Raymond, L.A., 1989, Metamorphic conditions in the Ashe Metamorphic Suite, North Carolina Blue Ridge: Geology, v. 17, p. 1140-1143.

Miyashiro, A., 1994, Metamorphic Petrology, Oxford University Press: New York,

Moecher, D.P, 2000, P-T conditions and timing of peak Taconian granulite facies metamorphism in the southern Blue Ridge: GSA Abstracts with Programs, v. 32, p. A113

Nelson, A.E.; Horton, J.W.; and Clarke, J.W., 1998, Geologic map of the Greenville 1˚x 2˚ quadrangle, South Carolina, Georgia, and North Carolina: U.S. Geological Survey Map I-2175, scale 1/250,000.

Patiño-Douce, A.E.; Johnston, A.D.; and Rice, J.M., 1993 Octahedral excess mixing properties in biotite: A working model with applications to geobarometry and geothermometry: American Mineralogist, v. 78, p. 113-131.

Rankin, D.W., 1970, Stratigraphy and structure of Precambrian rocks in northwestern North Carolina, *in* Fisher, G.W.; Pettijohn, F.J.; Reed, J.C., Jr.; and Weaver, K.N., *eds*., Studies in Appalachian Geology: Central and Southern: New York, Wiley-Interscience, p. 227-245.

Stewart, K.G., Adams, M.G., Trupe, C.H., 1997,Paleozoic structural evolution of the Blue Ridge thrust complex, western North Carolina, *in* Stewart, K.G., Adams, M.G., Trupe, C.H., *eds.*, Paleozoic structure, metamorphism, and tectonics of the Blue Ridge of western North Carolina: Carolina Geological Society, 1997 Field Trip Guidebook

PETROGRAPHIC DESCRIPTIONS

A.1   WS0011

Sample WS0011 is an amphibolite with the assemblage amph + qtz + plag + zoi + ep + gar + ms + sph + il + py. A moderately developed non-penetrative fabric is definded by aligned amphibole grains. No evidence of secondary foliations is present. Amphiboles range in size from 5mm to 0.5mm, are generally subhedral and possess small quartz and epidote inclusions. Quartz and feldspar are closely associated and are present together throughout the thin section with interlobate grain boundaries. Both minerals range in size from 2mm - 0.1mm, but small grains (>1mm) are the norm. Large feldspar grains are polysynthetically twinned, have small quartz inclusions, and are commonly partially altered to muscovite. Although some areas are slightly richer in feldspar and quartz, no distinct banding is present. Zoisite is present as euhedral crystals ranging in size from 1.5mm to 0.2mm with sharp grain boundaries. Distinct cores are most common in the smaller grains. Epidote is distinguished by its clear to yellow-green pleochoism and ragged grain boundaries and occurs in small patches. Although rare, garnet is present as anhedral crystals with many quartz, feldspar, and epidote inclusions. Sphene occurs as aggregates of subhedral to anhedral 0.45mm to 0.1mm-sized grains that are usually found with ilmentite. Large sphene grains are commonly twinned. Pyrite is disseminated throughout the sample. Ilmenite is closely associate with sphene and in one instance was found mantled by sphene.

A.2 H761

Sample H761 is an amphibolite containing amph + plag + qtz + zoi + il. A
well-developed non-penetrative fabric is defined by amphibole alignment and quartz
ribbons.Amphibole predominates in H76-1 as subhedral grains with straight grain
boundaries ranging in size from 4mm to 0.3mm. Quartz occurs in small grains
throughout the sample and as ribbons approximately 0.4mm wide with polygonal to
interlobate grain boundaries. Subgrains are visible in some ribbons. Plagioclase occurs
in distinct grains between 0.5mm and 0.75 mm diameter and is not closely associated
with quartz as in other samples. Most plagioclase grains are polysynthetically twinned
and have an internal network of cracks. Some crack networks are completely lined with
epidote while others are free of any alteration material. Primary epidote occurs as small,
1mm to 0.2mm euhedral grains distributed throughout the sample. Ilmenite is distributed
as blobs across H76-1.

A.3 WS995

Sample WS995 is an amphibolite containing amph + plag + qtz + bt + zoi + ep + il + chl
+ sph and two non-penetrative fabrics: a well-developed fabric defined by amphiboles
and a weak fabric defined by cross-cutting biotite. Amphibole grains are subhedral,
ranging in size from 5mm to 0.2mm. Biotite ranges in size from 2.5mm to 0.4mm and
chlorite replacement, from partial to complete replacement, is common. With a single
exception, the biotite grains cut across the amphibole fabric at a high (>40) angle.
Zoisite is spread across the sample as small (<1mm), euhedral to subhedral grains.
Epidote is associated with chlorite replacement of biotite. Sphene is always associated
with ilmenite, either forming total or partial mantles around anhedral ilmenite grains.

A.4 WS009

WS009 is a garnet-biotite gneiss with the assemblage qtz + plag + bt + gar + sill + ms + zoi + il. Both primary and secondary fabrics are defined by fine-grained (1mm and smaller), red pleochroic biotite. The weak secondary fabric is defined by cross-cutting biotite grains approximately 50° from the primary fabric. There is no grain-size distinction between the two fabrics. Inequigranular quartz grains from 0.75mm to 0.01mm are dispersed throughout the sample as single crystals and as elongated aggregates, but ribbons are not present. Lobate grain boundaries, subgrains, and sweeping extinction are common among quartz grains in this sample. Size distribution of plagioclase varies greatly, from 2mm to less than 0.01mm. Many crystals are twinned and have sweeping extinction. Alteration is uncommon, but a few plagioclase crystals have fine-grained epidote and/or muscovite growths around their rims. Garnet is present as euhedral to subhedral crystals between 1mm and 0.2mm in size. Inclusions are not found in all garnets, but when present are mainly quartz and feldspar. Biotite inclusions are frustratingly rare. The lack of passive inclusions (i.e., biotite) makes exact determination of garnet growth difficult, but since they show no signs of post-growth strain they are taken to be post-tectonic. Sillimanite in WS009 is found as 0.75mm to <0.01mm euhedral crystals.

A.5 WS996

WS996 is a hornblende-garnet-biotite gneiss with the assemblage Qtz + bt + plag + gar + zoi + ms + chl containing two fabrics. The primary fabric is defined by biotite and to a lesser extent by amphibole. Cross-cutting biotite crystals show the weaker secondary fabric at $\geq40^{o}$ from the primary foliation. Amphiboles range in size from 2.75mm to 0.2mm, are subhedral to anhedral, and inclusions are uncommon. Biotite crystals are no larger than approximately 1mm and show dark brown pleochroism, with some chlorite

replacement along cleavage planes. Anhedral garnets between 4mm and 0.3mm have many inclusions, mainly of quartz and feldspar and lesser amounts of amphibole, bt, and ilmenite. The primary fabric is deflected around and is preserved by inclusions in some garnets, so they are believed to be syntectonic with respect to the primary foliation. Due to the weak nature of the secondary fabric, the relationship of the garnets to it could not be determined. However, no deformation took place after garnet growth as they show no signs of anisotropy. The matrix is chiefly composed of inequigranular quartz and plagioclase. Quartz occurs as crystals up to 2mm with rounded polygonal to lobate boundaries and undulatory in the larger crystals. Plagioclase crystals are small, <1mm, subhedral with some twinning. Few crystals exhibit partial seritization. Zoisite is spread across the sample as small, 0.5mm to <0.3mm, euhedral to subhedral grains. Pyrite occurs as euhedral grains generally 0.8mm and smaller. Ilmentite crystals are elongate blobs <0.75mm.

A.6   WS992

The amphibole-biotite gneiss WS992 is composed of amph + bt + plag + qtz + gar + ep + il. A strong non-penetrative fabric is defined by amphibole, biotite, and quartz ribbons. Amphibole ranges from euhedral to subhedral with grain sizes from 5mm to <0.1mm. Few inclusions are present. All biotite has a dark brown pleochroic scheme, is 3mm and smaller, and has been slightly chloritized along cleavage planes. Plagioclase occurs in the matrix as equigranular crystals between 0.7mm and 0.1mm. Many are twinned and have sweeping extinctions. Seritization is present, but very minimal. Quartz is found in both the matrix and in ribbons approximately 0.45mm wide. Quartz in both occurances is inequigranular with polygonal to rounded polygonal boundaries. Subgrains have developed in some larger grains. Syntectonic garnet is present in the sample as a singe, 5mm, anhedral crystal with abundant inclusions of quartz, plagioclase, and biotite. The

fabric is deflected around the garnet and is preserved within by biotite inclusions. Epidote is found throughout the sample in small (≤0.3mm) euhedral to subhedral crystals. Ilmenite occurs as acicular to irregularly shaped crystals 0.5mm and smaller dispersed across the sample.

AMPHIBOLE–PLAGIOCLASE THERMOMETERS

The amphibole–plagioclase thermometers used in this study are from Holland and Blundy (1994). Temperatures for each thermometer (see Chapter 4) are given by:

Thermometer A:

$$T_A = \frac{-76.95 + 0.79P + Y_{ab} + 39.4X_{Na}^A + 22.4X_K^A + (41.5 - 2.89P) \cdot X_{Al}^{M2}}{-0.0650 - R\ln\left(\frac{27 \cdot X_{\square}^A \cdot X_{Si}^{T1} X_{Ab}^{plag}}{256 \cdot X_{Na}^A \cdot X_{Al}^{T1}}\right)}$$

$$\text{where } Y_{ab} = \begin{cases} 0 & \text{if } X_{Ab}^{plag} > 0.5 \\ 12.0\left(1 - X_{Ab}^{plag}\right)^2 - 3\text{kJ} & \text{if } X_{Ab}^{plag} < 0.5 \end{cases}$$

Thermometer B:

$$T_B = \frac{78.44 + Y_{ab-an} + 33.6X_{Na}^{M4} - (66.8 - 2.92P) \cdot X_{Al}^{M2} + 78.5X_{Al}^{T1} + 9.4X_{Na}^A}{0.0721 - R\ln\left(\frac{27 \cdot X_{Na}^{M4} \cdot X_{Si}^{T1} X_{An}^{plag}}{64 \cdot X_{Ca}^{M4} \cdot X_{Al}^{T1} \cdot X_{Ab}^{plag}}\right)}$$

$$\text{where } Y_{ab-an} = \begin{cases} 3.0\text{kJ} & \text{if } X_{Ab}^{plag} > 0.5 \\ 12.0(2X_{Ab}^{plag} - 1) + 3\text{kJ} & \text{if } X_{Ab}^{plag} < 0.5 \end{cases}$$

Amphiboles must be recalculated on a 23 oxygen basis. To begin recalculating the ferric iron content, calculate all f values below:

Group A	Group B

$$f_1 = \frac{16}{\Sigma} \qquad f_6 = \frac{8}{\text{Si}+\text{Al}^{total}}$$

$$f_2 = \frac{8}{\text{Si}} \qquad f_7 = \frac{15}{\Sigma-\text{K}}$$

$$f_3 = \frac{15}{\Sigma-\text{Na}-\text{K}} \qquad f_8 = \frac{12.9}{\Sigma-\text{Na}-\text{K}-\text{Ca}}$$

$$f_4 = \frac{2}{\text{Ca}} \qquad f_9 = \frac{36}{46+\text{Al}^{total}+\text{Si}+\text{Ti}}$$

$$f_5 = 1.00 \qquad f_{10} = 1 - \left(\frac{\text{Fe}^{total}}{46}\right)$$

Σ is the sum of cations. If any value from Group B is larger than 1.00 then the amphibole cannot be used. Set any Group A value greater than 1.00 equal to 1.00. Take the smallest Group A value and largest Group B value and average them (f_{av}). Renormalize *all* cations by multiplying each cation by the average obtained from the Group A and B values. Amounts of ferric and ferrous iron are given by:

$\text{Fe}^{3+} = 46(1 - f_{av})$ and $\text{Fe}^{2+} = \text{Fe}^{total} - \text{Fe}^{3+}$.

Site allocations are made by first determining the "cummingtonite" substitution using the final recalculated amphibole analysis:

$$\text{cm} = \text{Si} + \text{Al} + \text{Fe}^{2+} + \text{Fe}^{3+} + \text{Mg} + \text{Mn} - 13.0$$

Then the sites are assigned:

$$X_{\text{Si}}^{T1} = \frac{\text{Si}-4}{4}$$

$$X_{\text{Al}}^{T1} = \frac{8-\text{Si}}{4}$$

$$X_{\text{Al}}^{M2} = \frac{\text{Si}+\text{Al}-8}{2}$$

$$X_{\text{K}}^{A} = \text{K}$$

$$X_{\square}^{A} = 3 - \text{K} - \text{Ca} - \text{Na} - \text{K} - \text{cm}$$

$$X_{\text{Na}}^{A} = \text{Ca} + \text{Na} + \text{cm} - 2$$

$$X_{\text{Na}}^{M4} = \frac{2-\text{Ca}-\text{cm}}{4}$$

$$X_{\text{Ca}}^{M4} = \frac{\text{Ca}}{2}$$

C.1   GARNET

All garnet activities in this work are calculated following the methodology of Berman (1990). When only nonzero terms are included, expansion of Equation 4.2 gives:

$$3RT \ln \gamma_{grs}$$

$$= W_{112}(2X_1X_2 - 2X_1^2X_2) + W_{122}(X_2^2 - 2X_1X_2^2)$$

$$+ W_{113}(2X_1X_3 - 2X_1^2X_3) + W_{123}(X_3^2 - 2X_1X_3^2)$$

$$+ W_{223}(-2X_2^2X_3) + W_{233}(-2X_2X_2^3)$$

$$+ W_{123}(X_2X_3 - 2X_1X_2X_3) + W_{124}(X_2X_4 - 2X_1X_2X_4)$$

$$+ W_{134}(X_3X_4 - 2X_1X_3X_4) + W_{234}(-2X_2X_3X_4)$$

$$3RT \ln \gamma_{pyr}$$

$$= W_{112}(X_1^2 - 2X_1^2X_2) + W_{122}(2X_1X_2 - 2X_1X_2^2)$$

$$+ W_{133}(-2X_1^2X_3) + W_{133}(-2X_1X_3^2)$$

$$+ W_{223}(2X_2X_3 - 2X_2^2X_3) + W_{233}(X_3^2 - 2X_2X_3^2)$$

$$+ W_{123}(X_1X_3 - 2X_1X_2X_3) + W_{124}(X_1X_4 - 2X_1X_2X_4)$$

$$+ W_{134}(-2X_1X_3X_4) + W_{234}(X_3X_4 - 2X_2X_3X_4)$$

$3RT \ln \gamma_{alm}$

$= W_{122}(-2X_1^2 X_2) + W_{122}(-2X_1 X_2^2)$

$+ W_{113}(X_1^2 - 2X_1^2 X_3) + W_{133}(2X_1 X_3 - 2X_1 X_3^2)$

$+ W_{223}(X_2^2 - 2X_2^2 X_3) + W_{233}(2X_2 X_3 - 2X_2 X_3^2)$

$+ W_{123}(X_2 X_3 - 2X_1 X_2 X_3) + W_{124}(-2X_1 X_2 X_4)$

$+ W_{134}(X_1 X_4 - 2X_1 X_3 X_4) + W_{234}(X_2 X_4 - 2X_2 X_3 X_4)$

$3RT \ln \gamma_{sps}$

$= W_{112}(-2X_1^2 X_2) + W_{122}(-2X_1 X_2^2)$

$+ W_{113}(-2X_1^2 X_3) + W_{133}(-2X_1 X_3^2)$

$+ W_{223}(-2X_2^2 X_3) + W_{233}(-2X_2 X_3^2)$

$+ W_{123}(-2X_1 X_2 X_3) + W_{124}(X_1 X_2 - 2X_1 X_2 X_4)$

$+ W_{134}(X_1 X_3 - 2X_1 X_3 X_4) + W_{234}(X_2 X_3 - 2X_2 X_3 X_4)$

Where 1 = Grs, 2 = Pyr, 3 = Alm, 4 = Sps. W_G terms in the above equations are found from $W_G = W_H - TW_S + PW_V$

C.2 FELDSPAR

The feldspar activity model in this study is from Fuhrman and Lindsley (1988). Activites of the Albite (Ab), Anorthite (An), and Orthoclase (Or) endmembers are given by:

$$a_{Ab} = X_{Ab}(1 - X_{An}^2)$$

$$\cdot \exp \left\{ (W_{OrAb} \left[2X_{Ab}X_{Or} \left(1 - X_{Ab} \right) + X_{Or}X_{An} \left(0.5 - X_{Ab} \right) \right] \right.$$

$$+ W_{AbOr} \left[X_{Or}^2 \left(1 - 2X_{Ab} \right) + X_{Or}X_{An} \left(0.5 - X_{Ab} \right) \right]$$

$$+ W_{OrAn} \left[X_{Or}X_{An} \left(0.5 - X_{Ab} - 2X_{An} \right) \right]$$

$$+ W_{AnOr} \left[X_{Or}X_{An} \left(0.5 - X_{Ab} - 2X_{Or} \right) \right]$$

$$+ W_{AbAn} \left[X_{An}^2 \left(1 - 2X_{Ab} \right) + X_{Or}X_{An} \left(0.5 - X_{Ab} \right) \right]$$

$$+ W_{AnAb} \left[2X_{Ab}X_{An} \left(1 - X_{Ab} \right) + X_{Or}X_{An} \left(0.5 - X_{Ab} \right) \right]$$

$$\left. + W_{OrAbAn} \left[X_{Or}X_{An} \left(1 - 2X_{Ab} \right) \right] \right) / RT \right\}$$

$$a_{Or} = X_{Or}(1 - X_{An}^2)$$

$$\cdot \exp \left\{ (W_{OrAb} \left[X_{Ab}^2 \left(1 - 2X_{Or} \right) + X_{Ab}X_{An} \left(0.5 - X_{Or} \right) \right] \right.$$

$$+ W_{AbOr} \left[2X_{Ab}X_{Or} \left(1 - X_{Or} \right) + X_{Ab}X_{An} \left(0.5 - X_{Or} \right) \right]$$

$$+ W_{OrAn} \left[X_{An}^2 \left(1 - 2X_{Or} \right) + X_{Ab}X_{An} \left(0.5 - X_{Or} \right) \right]$$

$$+ W_{AnOr} \left[2X_{Or}X_{An} \left(1 - X_{Or} \right) + X_{Ab}X_{An} \left(0.5 - X_{Or} \right) \right]$$

$$+ W_{AbAn} \left[X_{Ab}X_{An} \left(0.5 - X_{Or} - 2X_{An} \right) \right]$$

$$+ W_{AnAb} \left[X_{Ab}X_{An} \left(0.5 - X_{Or} - 2X_{Ab} \right) \right]$$

$$\left. + W_{OrAbAn} \left[X_{Ab}X_{An} \left(1 - 2X_{Or} \right) \right] \right) / RT \right\}$$

$$a_{An} = \left[X_{An} \left(1 + X_{An} \right)^2 / 4 \right]$$

$$\cdot \exp \left\{ \left(W_{OrAb} \left[X_{Ab} X_{Or} \left(0.5 - X_{An} - 2X_{Ab} \right) \right] \right. \right.$$

$$+ W_{AbOr} \left[X_{Ab} X_{Or} \left(0.5 - X_{An} - 2X_{Or} \right) \right]$$

$$+ W_{OrAn} \left[2X_{Or} X_{An} \left(1 - X_{An} \right) + X_{Ab} X_{Or} \left(0.5 - X_{An} \right) \right]$$

$$+ W_{AnOr} \left[X_{Or}^2 \left(1 - X_{An} \right) + X_{Ab} X_{Or} \left(0.5 - X_{An} \right) \right]$$

$$+ W_{AbAn} \left[2X_{Ab} X_{An} \left(1 - X_{An} \right) + X_{Ab} X_{Or} \left(0.5 - X_{An} \right) \right]$$

$$+ W_{AnAb} \left[X_{Ab}^2 \left(1 - 2X_{An} \right) + X_{Ab} X_{Or} \left(0.5 - X_{An} \right) \right]$$

$$\left. \left. + W_{OrAbAn} \left[X_{Or} X_{Ab} \left(1 - 2X_{An} \right) \right] \right) / RT \right\}$$

W_G terms in the above equations are from $W_G = W_H - TW_S + PW_V$:

Parameter (W_G)	W_H (J/mol)	W_S [J/(mol K)]	W_V (J/bar)
W_{AbOr}	18810	10.3	0.394
W_{OrAb}	27320	10.3	0.394
W_{AbAn}	28226		
W_{AnAb}	8471		
W_{AnOr}	52468		-0.120
W_{OrAn}	47396		
W_{OrAbAn}	8700		-1.094

C.3 BIOTITE

Biotite exchange component activities used in this study were calculated with the model of Patiño-Douce *et al.* (1993). All biotite stoichiometries must be on a 12-anion basis.

Tetrahedral sites
$X_{\text{Si}} = \frac{\text{Si}}{4}$
$X_{\text{Al}} = \frac{\text{Al}^{iv}}{4}$
M1 Octahedral site
$X_{Mg}^{M1} = \frac{Mg}{Mg + Fe^{2+}} \cdot (\Sigma - 6)$
$X_{Fe}^{M1} = \frac{Fe^{2+}}{Mg + Fe^{2+}} \cdot (\Sigma - 6)$
$X_{\square} = 7 - \Sigma$
M2 Ocathedral sites
$X_{Mg}^{M2} = \frac{Mg}{Mg + Fe^{2+}} \cdot \frac{2 - Al^{[6]} - Ti - Fe^{3+}}{2}$
$X_{Fe}^{M2} = \frac{Fe^{2+}}{Mg + Fe^{2+}} \cdot \frac{2 - Al^{[6]} - Ti - Fe^{3+}}{2}$
$X_{Al}^{M2} = \frac{Al^{[6]}}{2}$
$X_{Ti}^{M2} = \frac{Ti}{2}$
$X_{\square}$ denotes mol fraction of vacancies;
Σ = sum of octahedral plus tetrahedral cations

The general form for the activity expression for each exchange component, *i*, is given by $a_i^{real} = a_i^{ideal} \cdot \gamma_i$ where the ideal activities for the exchange components are:

$$a_{\text{Mg-dic}}^{ideal} = \frac{\left(X_{\text{Al}}^{M2}\right)^2 X_{\square}}{\left(X_{\text{Mg}}^{M2}\right)^2 X_{\text{Mg}}^{M1}}$$

$$a_{\text{Fe-dic}}^{ideal} = \frac{\left(X_{\text{Al}}^{M2}\right)^2 X_{\square}}{\left(X_{\text{Fe}^{2+}}^{M2}\right)^2 X_{\text{Fe}^{2+}}^{M1}}$$

$$a_{\text{FeMg}_{-1}}^{ideal} = \left(\frac{X_{\text{Fe}}^{M2}}{X_{\text{Mg}}^{M2}}\right)^3$$

Parameter (W_G)	W_H (J/mol)	W_S [J/(mol K)]	W_V (J/bar)
112	21560	18.79	0.10
122	69200	18.79	0.10
113	20320	5.08	0.17
133	2620	5.08	0.09
223	230		0.01
233	3720		0.06
123	58825	23.87	0.265
124	45424	18.79	0.100
134	11470	5.08	0.130
234	1975		0.035

Activities are computed with:

$$a_{Grs} = (X_{Grs} \cdot \gamma_{Grs})^3$$

$$a_{Pyr} = (X_{Pyr} \cdot \gamma_{Pyr})^3$$

$$a_{Alm} = (X_{Alm} \cdot \gamma_{Alm})^3$$

$$a_{Sps} = (X_{Sps} \cdot \gamma_{Sps})^3$$

where the Mg diocatahedral component (Al_2Mg_{-3}) is denoted with the Mg-dic subscript, the Fe dioctahedral component (Al_2Fe_{-3}) is denoted with the Fe-dic subscript, and the FeMg exchange component ($FeMg_{-1}$) is denoted with the $FeMg_{-1}$ subscript. Expressions of γ for each exchange component:

$$RT \ln \gamma_{\text{Mg-dic}}$$
$$= (X_{\text{Mg}} - X_{\text{Al}}) W_{\text{MgAl}} + X_{\text{Fe}} W_{\text{FeAl}} + X_{\text{Ti}} (W_{\text{AlTi}} - W_{\text{MgTi}})$$

$$RT \ln \gamma_{\text{Fe-dic}}$$
$$= (X_{\text{Fe}} - X_{\text{Al}}) W_{\text{FeAl}} + X_{\text{Mg}} W_{\text{MgAl}} + X_{\text{Ti}} (W_{\text{AlTi}} - W_{\text{FeTi}})$$

$$RT \ln \gamma_{\text{FeMg}}$$
$$= X_{\text{Al}} (W_{\text{FeAl}} - W_{\text{MgAl}}) + X_{\text{Ti}} (W_{\text{FeTi}} - W_{\text{MgTi}})$$

If all Fe is assumed to be Fe^{2+} the excess mixing parameters (W_G) are:

$$W_{\text{MgAl}} = 54.7$$

$$W_{\text{FeAl}} = 57.4$$

$$W_{\text{AlTi}} - W_{\text{MgTi}} = 65.1$$

$$W_{\text{AlTi}} - W_{\text{FeTi}} = 75.1$$

and $\qquad W_{\text{FeTi}} - W_{\text{MgTi}} = (W_{\text{AlTi}} - W_{\text{MgTi}}) - (W_{\text{AlTi}} - W_{\text{FeTi}})$